MODELLING DYNAMIC ICE-STRUCTURE INTERACTION BASED ON HIGH-PRESSURE ZONES' BEHAVIOUR AT MEDIUM-SCALE

by

©Ridwan Hossain

A thesis submitted to the School of Graduate Studies in
partial fulfillment of the requirement of
Doctor of Philosophy

Faculty of Engineering and Applied Science
Memorial University

February 2021

St.John's, Newfoundland, Canada

Abstract

Although ice-induced vibrations (IIV) resulting from dynamic ice-structure interaction have been reported as infrequent occurrences in nature, the catastrophic consequences of these events makes them a fundamental design consideration for structures in ice-prone regions. Over the last 50 years, these events have affected a wide range of structures, including bottom founded lighthouses, channel markers, jacket and caisson retained structures, and have led to operational shutdowns, human discomfort, and even complete collapse of the structure in some cases. Rigorous experimental investigations and theoretical modeling approaches over the years have provided valuable insight into the physical mechanism of the process; however, a significant amount of uncertainty in identifying the conditions associated with IIV and its severity still exists. The primary source of the uncertainty comes from the complexity of the ice failure process, since it is highly influenced by the interplay of different competing mechanisms, such as fracture, damage and microstructural changes. One of the fundamental components of compressive ice failure is the development of 'high-pressure zones (*hpz*s),' which are responsible for transmitting the majority of the loads in ice-structure interactions. As the properties and dynamic behaviour of *hpz*s exhibit similar characteristics over a wide range of scales, efforts to link *hpz* mechanics with the occurrence of dynamic ice-structure interactions is seen as a promising approach.

During ice-structure interaction, the ice failure process is highly influenced by different interaction parameters. An uncertainty analysis with self-excited vibration modeling approaches was performed first to identify the critical parameters and how their effects can propagate through the dynamic ice-structure interaction process. Based on the simulations, ice temperature, interaction speed, and interaction area were identified as the key parameters affecting the dynamic ice-

structure interaction process. A medium-scale ice crushing dynamics test program was then carried out to study the influence of these parameters on the dynamics of *hpz*s under controlled conditions with variable structural compliance. In general, more severe dynamics associated with failure behaviour were observed to be more pronounced for colder ice, smaller interaction areas, higher interaction speed, and lower structural compliances.

The observed dynamics of a single *hpz* was then used to develop a simplified ice-structure interaction model. The behaviour of the *hpz* was estimated using results from previous triaxial tests, which showed a non-linear relationship between *hpz* stiffness and the nominal strain, with the degree of softening depending on the average strain-rate. Two distinct failure processes were assessed in the context of the periodic sinusoidal response of the structure using the model. First, such responses can result from the vibration within the layer of damaged ice when the formation of the damaged layer and the extrusion process become cyclical in pure crushing. Theoretical calculation from a previous study was adopted to estimate the equilibrium layer thickness that can result in such vibrations, and the model showed reasonably good agreement with the calculations. The other failure process considered was for spall-dominated interactions with occasional crushing events. Such a failure process can result in frequency lock-in of the structure; however, these responses were observed to be highly sensitive to interaction speed and structural parameters. This was identified as the primary reason for the infrequent observation of frequency lock-in in full-scale interactions. Although the simplified modeling framework presented here shows promising results, further experimental investigation and modeling refinement are required for a full-scale implementation.

Acknowledgements

For most PhDs, the thesis only contains a very small portion of the overall experience. For the last five years, I have studied this very specific topic of dynamic ice-structure interaction; however, the experiences I gained were certainly much broader. Now, when I look back, I feel really glad about how these experiences have shaped me as a person.

I would like to express my sincere gratitude to my supervisor, Dr. Rocky Taylor, for his earnest guidance and support. I am very fortunate to have him as my supervisor who always provided me with valuable feedback and useful insights. I would also like to thank my co-supervisors, Dr. Lorenzo Moro and Dr. Bruce Quinton, for their suggestions and guidance throughout this work.

I would like to thank C-CORE for generously allowing me to use their facilities, and its employees, Rob Pritchett, Karl Kuehnemand and Karl Tuff, for their help and support in the experimental program. I also want to thank my colleagues: Igor Gribanov, Marjan Boorojerdi, Pranav Birajdar and Kashfi Habib; discussions with whom were always insightful.

Finally, I would thank my wife who shared a significant portion of the burden during these years and made it possible for me to focus on my thesis. I also want to thank my parents who supported my efforts over the years.

The financial support was made available by Memorial University, the Natural Sciences and Engineering Research Council (NSERC) of Canada, the Research Development Corporation of Newfoundland and Labrador (RDC), Hibernia Management and Development Company, Ltd. (HMDC), Terra Nova Development (Suncor Energy Inc. - Operator) and InnovateNL.

Table of Contents

List of Abbreviations

API	American Petroleum Institute
ISO	International Organization for Standardization
IIV	Ice-Induced Vibration
hpz	High-Pressure Zone
SDOF	Single-Degree of Freedom
PVDF	Polyvinylidene Fluoride
MTS	Material Testing System
SEM	Self-Excited Model
JIP	Joint Industry Project
SS-IIV	Steady State Ice-Induced Vibrations
D-IIV	Damped Ice-Induced Vibrations
HPU	Hydraulic Power Unit
LVDT	Linear Variable Displacement Transducer
RTD	Resistance Temperature Detector
ICD	Ice Crushing Dynamics
GEV	Generalized Extreme Value
FFT	Fast Fourier Transform

Nomenclature

ζ_n	Damping ratio of the eigenmode
$\emptyset_{nC}$	Non-normalized modal amplitude at the ice action point
M_n	Modal Mass
f_n	Natural frequency of the eigenmode
h	Ice thickness
v	Ice velocity
σ	Uniaxial stress (Force/Area)
σ_c	Compressive strength
a	Radius of the structure
t	Time (sec)
T	Temperature
K_s	Stiffness of the structure/beam
C_s	Damping coefficient of the structure/beam
m_s	Mass of the structure/beam
y	Displacement of the hydraulic cylinder
$\dot{y}$	Speed of the ram
x_s	Displacement of the indenter
x_{ice}	Displacement of the *hpz* boundary
K_{hpz}	Stiffness of the *hpz*
C_{hpz}	Damping coefficient of the *hpz*

K_{ice}	Stiffness of the ice
C_{ice}	Damping coefficient of the ice
$f_{L,tot}$	Accumulation of the failure length after each failure event
D_i	Diameter of the indenter
ε	Nominal strain $\left(\frac{y-f_{L,tot}}{D_i}\right)$
$\dot{\varepsilon}$	Strain-rate

List of Figures

List of Tables

Chapter: 1 Introduction

1.1 Background

Ice loads are fundamental design considerations for fixed structures operating in the Arctic and sub-Arctic regions, as the extreme forces in some cases can exceed 100-year wave loads (API, 1995). Historically, the lighthouses and channel markers for ship navigations, and platforms for hydrocarbon explorations and productions were the primary types of structures prone to dynamic ice-structure interactions. However, as the offshore wind farm developments expand into ice covered waters, wind turbine towers designed for the sub-arctic region will need to withstand ice loads during an event of ice-structure interaction. Continuous failure of ice against a structure, primarily in the form of crushing, can generate a condition of dynamic ice-structure interaction leading to severe vibration of the structure. This is known as ice-induced vibrations (IIV), and such events are widely discussed in the literature. The types of structures affected by IIV include lighthouses (Määttänen, 1978), channel markers (Nordlund et al., 1988), jacket structures (Xu and Bernt, 1981) and even caisson retained structures (Jefferies and Wright, 1988; Frederking and Sudom, 2006). The International Standard for Petroleum and Natural Gas Industries – Arctic Offshore Structures (ISO 19906, 2010) classifies the dynamic ice actions on structures into three categories, as shown in Figure 1.1.

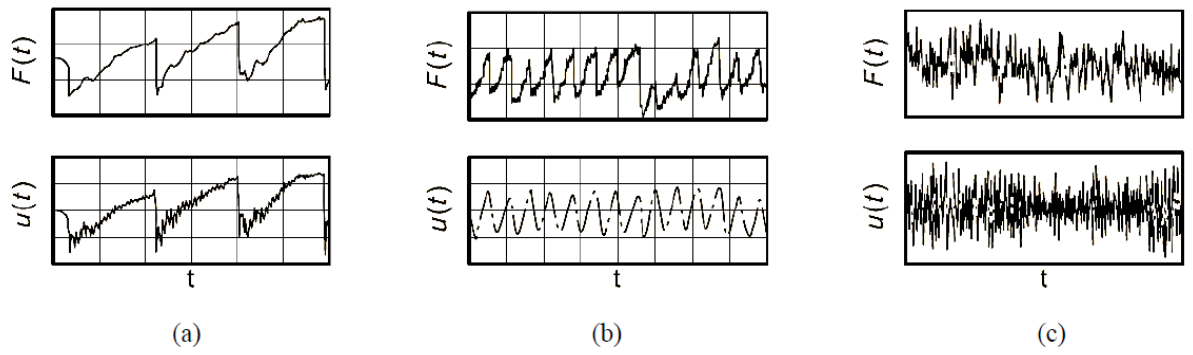

Figure 1.1 Modes of dynamic ice-structure interaction showing force and structural response (ISO 19906); (a) Intermittent crushing; (b) Frequency lock-in; (c) Continuous brittle crushing

Among these three, the frequency lock-in receives particular attention when the response of the structure becomes periodic and more sinusoidal in nature. If this periodic motion occurs at a frequency closer to the natural frequency of the structure, it can result in a dynamic amplification due to resonance. Also, the periodic motion can cause fatigue failure of different components and discomfort for the operating personnel (Yue and Li, 2003). The primary challenge in mitigating such conditions comes from the lack of data and uncertainty associated with compressive ice failure. The guidelines provided by the current design standards consider a simplified 'sawtooth' force time-trace at a frequency equal to the natural frequency of the structure for the mode 'most susceptible' to IIV, irrespective of the interaction conditions. However, during a nine-month monitoring period in Molikpaq, for a caisson retained structure operating in the Beaufort Sea, crushing was found to occur only about 1% of the time, and associated vibrations were often of relatively short duration, typically lasting about four minutes (Wright and Timco, 1994; Timco and Wright, 2005). Thus, the simplified assumption of the 'sawtooth' forcing function produces a conservative design assumption and since the mechanics are highly simplified, this approach offers

engineers with limited insight into strategies for improving their designs. New design approaches are needed to better model the conditions under which IIV occur and their associated severity.

Design codes are often based on simplified assumptions which are complemented by certain empirical constants or safety factors. The goal of this research, on the other hand, is to provide more insight into the physical mechanism of the process. While the current design code and dynamic ice-structure interaction models show acceptable agreement to certain full-scale events, the different empirical factors used in the models are often difficult to translate for unknown conditions. Results from a recent Joint Industry Project show that when tested against different conditions, none of the widely studied models are capable of capturing the characteristics of IIV for different ice conditions and structural configurations (Kärnä et al., 2013). The compressive failure of ice is a complex process involving the interplay of different mechanisms, such as fracture, damage, and microstructural changes, which are fundamental components of ice mechanics. To improve the reliability of the current and future design codes, these physical mechanisms need to be incorporated into the modelling framework, at least to an acceptable extent.

1.2 Knowledge Gaps

Over the last 50 years, a number of dynamic ice-structure interaction models have been proposed in the literature (discussed in detail in Chapter 2). However, a significant knowledge gaps still exist, as highlighted below:

- One of the primary disputes in the literature is whether to model IIV as forced vibration or self-excited vibration. From the ice point of view, ice has its own failure characteristics irrespective of structural properties, thus suggesting a forced vibration approach. However,

during an interaction, ice force is controlled not only by the ice itself but also structural responses. The key issue here is to identify how to incorporate the structural behavior into the original ice failure characteristics.

- Most of the models use some kind of empirical constants validated against certain interaction scenarios. But without understanding the physical mechanism for using these constants, their applicability to unknown conditions remains limited.
- Ice force is limited by the crushing strength and failure behaviour of ice. Although the process is highly complex, fundamental components of ice mechanics need to be identified and incorporated in the modelling approach.
- All models require some simplified assumptions. However, to ensure the robustness of the model, such assumptions should be linked to some physical process that is easily interpretable.
- Experimental observations from both field and laboratory suggest that the dynamic response of the structure is associated with the periodic extrusion process of crushed ice from the damage layer. According to the knowledge of the author, none of the current modelling approaches address this issue.

1.3 Scope of Thesis

During ice-structure interaction, the majority of the loads are transmitted to the structure through localized regions of high pressure, termed 'high-pressure zones (*hpz*s)' (Johnston et al., 1998; Dempsey et al., 2001). *Hpz*s have been found at a wide range of scales, and their physical characteristics are found to be similar in nature (details in Chapter 2). However, continuous spalling only allows them to possess a minor fraction of the global interaction area (Frederking,

2004; Taylor et al., 2008); hence, they are a major consideration for the design of the local area of the structure. Results from small-scale experiments suggest that the mechanics of *hpz*s can be highly influenced by interaction speed, *hpz* area, ice temperature, and the compliance of the tests' apparatus (Barrette et al., 2002; Mackey et al., 2007; Wells et al., 2011; Browne et al., 2013; O'Rourke et al., 2016b). To understand how the influence of these parameters can propagate through the interaction process and affect the vibration response, a sensitivity analysis of these parameters on the self-excited vibration model was performed. The results were used to identify the most significant parameters affecting the dynamic ice-structure interactions.

Another important consideration for modelling dynamic ice-structure interaction is the scale-dependence of ice. Although the failure behaviour and the microstructural changes for *hpz*s have been compared for different scales, the study of their dynamics has so far been very limited beyond small-scales. To identify whether the dynamic behaviour of *hpz*s and the effect of different parameters on their dynamics translate to larger scales, a medium-scale ice crushing dynamics test program was carried out. The effect of interaction speed, *hpz* area, ice temperature and structural compliance on the dynamics and failure behaviour of the *hpz*s were studied in detail. Based on the observed failure behaviour and the mechanics of *hpz*s, a simple mechanical ice-structure interaction model was developed for a single-degree of freedom (SDOF) structure. The stiffness of the *hpz* was modelled as a non-linear function of the applied nominal strain, and results from triaxial experiments were used to validate the assumption. Two distinct processes, namely, spalling and crushing, were linked to the dynamic ice-structure interaction, and the failure of ice was considered to be influenced by the competition between these two processes.

The model was calibrated using the experimental results and was able to reproduce the intermittent crushing behaviour observed in the test program. Theoretical calculations from previous study were used to identify the equilibrium layer thickness at which periodic vibration within the layer can exist, and the model showed reasonably good agreement with the calculations. Signatures of frequency lock-in, similar to the one observed for operational structures, were reproduced by the model for spall dominated failures; however, as discussed in the literature, such vibrations were found to exist for very specific conditions. The effect of speed, shown in Figure 1.1, was also observed with the dynamic amplification occurring at some intermediate speed for certain conditions. The model is a simplified first-order approximation of dynamic ice-structure interaction process; however, the incorporation of fundamental elements of ice mechanics presents a promising step toward a complete framework.

1.4 Thesis Outline

The thesis is written in manuscript format and the title of the manuscripts are used as chapter titles (where applicable). The outline of the thesis is summarized as follows:

- Chapter 1 gives a brief overview of the ice-induced vibration problem for offshore structures in ice prone regions. By highlighting the limitations of the current design guidelines, the scope of the thesis is discussed to address some of the current knowledge gaps.
- Chapter 2 provides a comprehensive literature review of the full-scale dynamic ice-structure interaction events leading to ice-induced vibrations and the different modelling approaches explaining these events. A brief review of compressive ice failure is then presented, providing the theoretical basis of the *hpz*s. The chapter ends with a review of

the different ice indentation test programs, highlighting the characteristics of *hpz* dynamics under controlled conditions and their influence on the overall interaction process.

- Chapter 3 presents an uncertainty analysis of the effects of ice temperature and the scale of interaction on ice-induced vibrations using the self-excited vibration model. The goal of the chapter is to identify the important parameters of dynamic ice structure interaction through uncertainty analysis and assess how the influence of such parameters can propagate in a modelling approach.
- Chapter 4 presents the results from the medium-scale ice crushing dynamics tests which were used to study the dynamics of *hpz*s at a larger scale than in any previous studies. The effect of ice temperature, *hpz* area, interaction speed and structural compliance on *hpz* dynamics and the overall interaction process are discussed.
- Chapter 5 presents the failure characteristics of the *hpz*s and how these characteristics are influenced by interaction parameters, and especially the compliance of the structure. Results suggest that the structural feedback plays a major role in the extrusion of the crushed ice layer adjacent to the indenter, which can contribute to the cyclical hardening and extrusion process, leading to ice-induced vibrations.
- Chapter 6 presents a simplified modelling framework for dynamic ice-structure interaction based on the mechanics of high-pressure zones (*hpz*s). Two different failure criteria were defined for *hpz* failure, and the stiffness of a single *hpz* was modelled as a function of nominal strain and strain-rate. Results from the test series presented in the previous two chapters were used to estimate the modelling parameters, and the conditions for periodic vibration for both pure crushing and spall dominated failure were evaluated.
- Chapter 7 provides a summary, discussion and recommendations for future work.

References

API, 1995. Recommended Practice 2N – Planning, Designing and Constructing Structures and Pipelines for Arctic Conditions. Am. Pet. Inst.

Barrette, P., Pond, J., Jordaan, I., 2002. Ice damage and layer formation in small-scale indentation experiments, in: Proceedings of the 16th IAHR International Symposium on Ice. International Association for Hydraulic Research, Dunedin, New Zealand, vol. 3 pp. 246–253.

Browne, T., Taylor, R., Jordaan, I., Gürtner, A., 2013. Small-scale ice indentation tests with variable structural compliance. Cold Reg. Sci. Technol. 88, 2–9. https://doi.org/10.1016/j.coldregions.2012.12.006

Dempsey, J., Palmer, A., Sodhi, D., 2001. High pressure zone formation during compressive ice failure. Fract. Ice 68, 1961–1974. https://doi.org/10.1016/S0013-7944(01)00033-9

Frederking, R., 2004. Ice pressure variations during indentation, in: Proceeding of the 17th IAHR International Symposium on Ice. International Association for Hydraulic Research, Saint Petersburg, Russia, vol. 2 pp. 307–314.

Frederking, R., Sudom, D., 2006. Maximum ice force on the Molikpaq during the April 12, 1986 event. Cold Reg. Sci. Technol. 46, 147–166. https://doi.org/10.1016/j.coldregions.2006.08.019

ISO 19906, 2010. Petroleum and natural gas industries — Arctic offshore structures. Int. Organ. Stand.

Jefferies, M., Wright, W., 1988. Dynamic response of “Molikpaq” to ice structure interaction, in:

Proceedings of the International Offshore Mechanics and Arctic Engineering Symposium. Houston, Texas, USA, vol. 4 pp. 201–220.

Johnston, M.E., Croasdale, K.R., Jordaan, I.J., 1998. Localized pressures during ice-structure interaction: relevance to design criteria. Cold Reg. Sci. Technol. 27, 105–117. https://doi.org/10.1016/S0165-232X(97)00026-8

Kärnä, T., Andersen, H., Gürtner, A., Metrikine, A., Sodhi, D., Loo, M., Kuiper, G., Gibson, R., Fenz, D., Muggeridge, K., Wallenburg, C., Wu, J.-F., Jefferies, M., 2013. Ice- induced vibrations of offshore structures - Looking beyond ISO 19906, in: Proceedings of the 22nd International Conference on Port and Ocean Engineering under Arctic Conditions, (POAC'13). Espoo, Finland.

Määttänen, M., 1978. On conditions for the rise of self-excited ice-induced autonomous oscillations in slender marine pile structures. Winter Navigation Research Board.

Mackey, T., Wells, J., Jordaan, I., Derradji-Aouat, A., 2007. Experiments on the fracture of polycrystalline ice, in: Proceedings of the 19th International Conference on Port and Ocean Engineering under Arctic Conditions (POAC'07). Dalian, China, vol. 1 pp. 339–349.

Nordlund, O.P., Kärnä, T., Järvinen, E., 1988. Measurements of ice-induced vibrations of channel markers, in: Proceedings of the 9th IAHR International Symposium on Ice. International Association for Hydraulic Research, Sapporo, Japan, vol. 1 pp. 537–548.

O'Rourke, B.J., Jordaan, I.J., Taylor, R.S., Gürtner, A., 2016. Experimental investigation of oscillation of loads in ice high-pressure zones, part 1: Single indentor system. Cold Reg. Sci. Technol. 124, 25–39. https://doi.org/10.1016/j.coldregions.2015.12.005

Taylor, R., Frederking, R., Jordaan, I., 2008. The nature of high pressure zones in compressive ice failure, in: Proceeding the 19th IAHR International Symposium on Ice. International Association for Hydraulic Research, Vancouver, BC, Canada., vol. 2 pp. 1001–1010.

Timco, G., Wright, B., 2005. Multi-Year Ice Loads on the Molikpaq: May 12, 1986 Event;, in: Proceedings 18th International Conference on Port and Ocean Engineering under Arctic Conditions (POAC ’05). Postdam, NY, vol. 1 pp. 453–462.

Wells, J., Jordaan, I., Derradji-Aouat, A., Taylor, R., 2011. Small-scale laboratory experiments on the indentation failure of polycrystalline ice in compression: Main results and pressure distribution. Cold Reg. Sci. Technol. 65, 314–325. https://doi.org/10.1016/j.coldregions.2010.11.002

Wright, B., Timco, G., 1994. A Review of Ice Forces and Failure Modes on the Molikpaq, in: Proceedings of the 12th IAHR International Symposium on Ice. International Association for Hydraulic Research, Trondheim, Norway, vol. 2 pp. 816–825.

Xu, J., Bernt, J.L., 1981. Dynamic response of a jacket platform subjected to ice loads, in: Proceedings of the 6th International Conference on Port and Ocean Engineering under Arctic Conditions (POAC’81). Quebec, Canada, vol. 1 pp. 502–516.

Yue, Q., Li, L., 2003. Ice problems in Bohai Sea oil exploitation, in: Proceedings of the 17th International Conference on Port and Ocean Engineering under Arctic Conditions (POAC’03). Trondheim, Norway, vol. 1 pp. 151–164.

Chapter: 2 Literature Review

Preface

The chapter aims to provide a comprehensive literature review related to the topics presented in the thesis. Since the primary focus of the thesis is the dynamic ice-structure interaction events leading to ice-induced vibrations (IIV), the chapter begins with the review of the observations of such events. The next section discusses the different modeling approaches of the observed behaviour and their limitations. One of the primary reasons for the limitations is the complexity of the compressive ice failure process, which is highlighted in the following section. This section also presents the mechanisms for the development of high-pressure zones (*hpz*s) during dynamic ice-structure interaction, which is found to be independent of scales. In the next section, a series of indentation tests is reviewed showing the existence of *hpz*s during different types of tests and providing some insights about the dynamics of *hpz*s.

2.1 Dynamic Ice-Structure Interaction in Full-Scale

2.1.1 Cook Inlet, Alaska

Subsequent to drilling of the first discovery wells in 1962, the upper segment of Cook Inlet, Alaska had been the site of an intensive offshore oil development activity. In the absence of design information applicable to the conditions, an extensive effort was devoted to study the region and determine the ice force (Peyton, 1968; Blenkarn, 1970). From 1963-1969, a number of test structures were constructed and instrumented to measure ice force exerted on the structures.

However, the instrumentation of the platforms and the documentation of the data were very limited. Based on the available measurements, both authors concluded that a moving ice field could induce severe vibrations to slender offshore structures; however, the explanations offered by the authors regarding the cause of these IIV differed significantly. Results from the test beam attached to the temporary drilling platform showed that a sharp, ratcheting force oscillation was caused by a slowly moving ice sheet and the frequency of oscillation was about one cycle per second. Comparing his observations to his laboratory test pile data, Peyton (1968) concluded that ice has a "characteristic failure frequency" of $1Hz$. However, Blenkarn (1970) argued that the ratcheting frequency is governed by ice sheet velocity, structural flexibility and the strength vs loading rate characteristics of ice. The author suggested that the transient decay of the recorded vibration can be attributed to the damping offered by ice moving past the structure. The term 'damping' in this context refers to the increase in ice force with increasing ice velocity; however, as the strength vs. stress rate data form Peyton's measurement shows, such 'damping' might not be always positive. With an example of how to calculate the instability, conditions under which vibrations arise, the author was the first to suggest that IIV are self-excited by nature. Although the lack of available data makes it very difficult to gain insight about the vibration events, the proposed mechanisms have been explored in detail by the ice research community over the last 50 years.

2.1.2 Norströmsgrund, Gulf of Bothnia

About fifty caisson type offshore lighthouses were constructed along the Swedish coast in the 1970s to facilitate ship navigation. Norströmsgrund was constructed in 1971 in the Gulf of Bothnia, which is located in the northern part of the Baltic Sea (Figure 2.1). The structure was

located at a water depth of 16.15*m* with a waterline diameter of 7.58*m* and a stiffness of 1.7*GN/m* (Kärnä et al., 2006). During the winter of 1972-73, the structure experienced heavy vibration when crushing through drifting ice with a frequency very close to the calculated natural frequency of approximately 2.8*Hz* (Engelbrektson, 1977). The ice thickness was reported to be in the range of 0.5-1*m* during this event, with a drift velocity of approximately 1*m/min* (Løset et al., 2006). Results from the accelerometer data located 16.5*m* above the seabed showed acceleration close to 0.2*g*, which lasted for about 10 seconds.

Figure 2.1 Norströmsgrund Lighthouse (Bjerkås and Skiple, 2005)

The structure was also instrumented during two major full-scale ice force measurement projects, titled "LOw LEvel Ice Forces" (LOLEIF) and "STRuctures in ICE" (STRICE). While the full datasets and reports for the LOLEIF and STRICE projects are not readily accessible, brief descriptions of the tests' setups can be found in the literature (Schwarz and Jochmann, 2001; Bjerkås et al., 2013a). The STRICE data have been extensively analyzed by Bjerkås to study the

dynamics of ice structure interactions and associated ice-induced vibrations (Bjerkås and Skiple, 2005; Bjerkås et al., 2013a, 2013b). From these analyses, three different interaction modes, namely intermittent crushing, frequency lock-in and continuous crushing were observed. Intermittent crushing was observed at speeds between $0.02 m/s$ to $0.08 m/s$ and was associated primarily with circumferential cracking events or simultaneous high crushing loads on several panels. While rare, frequency lock-in was observed to occur occasionally, and during one reported event, steady state vibration persisted for about 190 cycles (Bjerkås et al., 2013a). Associated with this particular event was the observation that it was preceded by a circumferential crack that produced a smooth contact surface, which helped to synchronize contact during the ice crushing process. According to the authors, during the first phase of this event, as the force built up, the structure exhibited lateral displacement and then sprang back when the load dropped following ice failure, creating contact conditions that allowed the next phase of synchronized load build up. During this event there were several intervals, each having 8-10 cycles, in which the local load progressively increased during each cycle, due to synchronization of the ice failure with the structural response, ultimately displacing the structure up to 24-30mm (Bjerkås et al., 2013a). Since this displacement was associated with dynamic amplification, system damping was an important factor in influencing this response. After many failure cycles, the mass of accumulated broken ice caused a local collapse in a sector of the ice, triggering flooding of the ice cover, causing it to bend and fail. For speeds greater than $0.1 m/s$, continuous crushing was observed, which generally produced loads that were significantly lower than either intermittent or 'lock-in' modes. It should be noted here that the critical speed above which continuous crushing occurred was found to vary with ice thickness and temperature.

2.1.3 Bohai Bay, China

In the Bohai Gulf of Northern China, offshore engineering activities for oil and gas exploration started in the late 1960s. Due to the soft sea bed, the primary choice for the platforms in the area was multi-piled (jacket) structures; however, two such structures collapsed during their operation because of ice force (Xu and Bernt, 1981). After some research and a survey of ice force, a new jacket structure, JZ202 MS, was erected in 1988 and was used for measuring ice force for three years before being put into operation. The joint project, conducted by the Hamburg Ship Model Basin (HSVA), found that the structure experienced severe ice vibrations with amplitudes as high as 0.2g (Yue and Li, 2003).

Another platform, JZ202 MSW, a three-leg wellhead platform, was put into operation in 1997 and was instrumented to measure ice forces and structural responses during the winter of 1999-2000 (Figure 2.2). The structural response was recorded using six accelerometers and several strain gauges and the load was measured using load panels mounted in one vertical leg. This structure also faced severe vibrations, which caused a failure of the pipeline on January 28, 2000 (Yue and Li, 2003). From the recorded data, two types of vibration were identified: steady state vibration and random vibration. For a similar ice thickness range, steady state vibration was found to occur at a speed of about 2-4cm/s, whereas faster speed caused random vibrations of the structure (Figure 2.3). It should be noted here that since the MSW is an unmanned platform, considerable uncertainty exists regarding the accuracy of the ice thickness measurement; however, a general overview of the ice conditions of the Bohai Bay can be found in the work of Yang (2000).

Figure 2.2 JZ202 MSW Platform (Yue and Li, 2003)

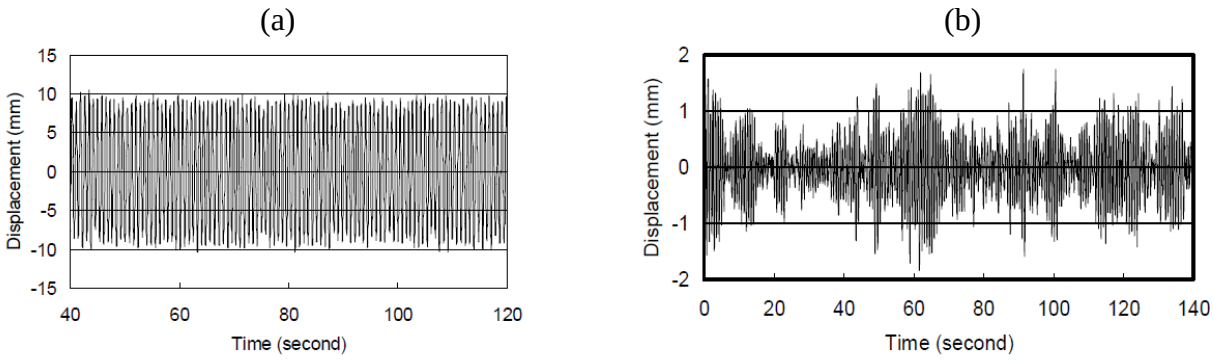

Figure 2.3 (a) Steady-state vibration and (b) random vibration of MSW platform at 15 cm ice thickness (Yue et al., 2001)

2.1.4 Molikpaq, Beaufort Sea

In the early 1970s, exploration for hydrocarbon reserves began on the Canadian Beaufort Shelf with the construction of artificial islands in shallow, near shore locations. But as the exploration moved to deeper waters, island costs increased almost exponentially, due to the increase in fill volumes. The solution adopted by the industries was to use caisson structures, which would reduce

the fill volume significantly while retaining sufficient mass to resist ice loads. The Molikpaq was one of those structures deployed at four sites in the Canadian Beaufort shelf: Tarsiut P-45, during 1984-85; Amauligak I-65, during 1985-86; Amauligak F-24, during 1986-87 and Isserk I-15, during 1988-89 (Jefferies et al., 2008). It is an octagon shaped annular caisson with near vertical sides, with waterline dimensions of $89m \times 89m$ and base dimensions of $111m \times 111m$ (Jefferies and Wright, 1988). The structure was ballasted down onto a sand berm which was constructed using hydraulically placed sands. The sand core provided the majority of the resistance to ice loads, while the use of the caisson reduced the volume of sand providing a convenient self-contained unit for the entire drilling and support systems (Figure 2.4). The structure was extensively instrumented with MEDOF panels, strain gauges, extensometers, accelerometers, inclinometers and soil pressure cells. Ice loading events and uncertainties associated with the measured data have been broadly discussed in the ice mechanics community (Jefferies and Wright, 1988; Timco and Wright, 2005; Frederking and Sudom, 2006; Jefferies et al., 2008; Jordaan et al., 2011; Taylor and Jordaan, 2011a). Two specific events are discussed here in the context of ice-induced vibrations.

Figure 2.4 Photograph of Molikpaq in moving first year ice (Jefferies et al., 2008)

On April 12, 1986, while operating in Amauligak I-65 (located approximately 75*km* offshore and in 32*m* water depth), a multi-year ice floe followed by a hummock crushed against Molikpaq's east and southeast outer walls at a velocity of approximately 0.06*m/s* (Frederking and Sudom, 2006). The peak face load during the interaction with the hummock was reported to be 380*MN* and the interaction resulted in severe structural vibration. Based on the extensometer data, the frequency of the vibration was found to be 1.3*Hz*. The values obtained from the strain gauge and the video were also in a similar range, suggesting that the platform was vibrating close to its natural frequency, which was reported to be 1.3*Hz* when the platform moved in the horizontal direction (Jefferies and Wright, 1988).

On May 12, 1986, Molikpaq again experienced severe vibration when a 7*km* by 15*km* floe of ice consisting of thick first year ice and multiyear ice crushed against its north and northeast walls. The accelerometer data on the north face of the structure showed the presence of cyclic and

asymmetrical vibration similar to beat frequency with peak values of 4% of *g*. The extensometer on the same face also showed a clear cyclic behaviour with a frequency of 1.4*Hz* and peak amplitudes ranged up to 10*mm* (Figure 2.5). The load calculation based on the MEDOF panels and the strain gauges showed amplified loading events during that period (Timco and Wright, 2005). Based on the analysis of the data for the entire year of 1985-86, a Joint Industry Project (JIP) report identified five similar events (Jefferies et al., 2008). The amplified ice loading was found to occur when intermittent crushing became synchronized across the entire caisson, resulting in 'phase-locked' behaviour. During non-simultaneous loading, the structure vibrated slowly in a truly randomly excited vibration but when the ice crushing synchronized, the structure responded with five-fold increase in acceleration.

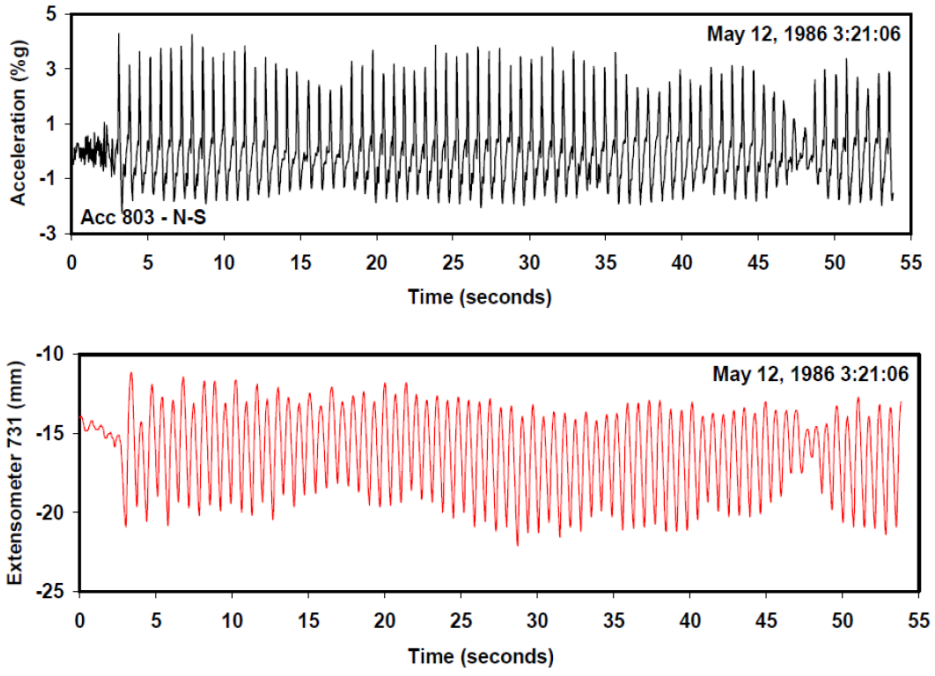

Figure 2.5 Accelerometer and extensometer data of north face of the Molikpaq on May 12, 1986 (Timco and Wright, 2005)

It should be noted here that the amplified ice loading due to 'phase-locked' intermittent crushing was only present for a few hours out of many thousands of hours of structure interaction with ice, and the process is highly dependent on structural displacement. In the case of the Norströmsgrund lighthouse, 'phase-locked' behaviour only occurred during steady-state vibration of the structure, with no amplification of global loads (Bjerkås and Skiple, 2005). No phase-locked intermittent crushing that is associated with transient vibration was recorded for the Norströmsgrund lighthouse. As mentioned by Jefferies et al (2008), the difference in behaviour shown by these two structures can be attributed to the difference in waterline stiffness.

The observed behaviours suggest that dynamic ice-structure interaction leading to ice-induced vibrations can occur in both first-year and multi-year ice. The multi-year ice has very little salinity compared to first-year ice, due to brine drainage (Notz and Worster, 2009; Timco and Weeks, 2010); however, in the context of dynamic ice-structure interaction, both ice types show similar behaviour suggesting little influence of brine volume on the underpinning failure mechanism. Experimental investigations for different ice types and grain orientation also suggest that the failure mode is usually independent of ice type and grain orientation (Tuhkuri, 1995). Hence, when studying the failure mechanism under controlled conditions, researchers often perform tests using a freshwater polycrystalline ice sample, which is adopted in the presented tests in Chapters 4 and 5. The effect of brine volume on dynamic ice-structure interaction is reserved for future work.

2.2 Review of Dynamic Ice-Structure Interaction Models

To model the observed phenomenon during ice-structure interaction, a number of approaches have been proposed so far. The most commonly employed engineering approaches to modelling dynamic ice-structure interactions can be broadly classified into two major categories. The first

approach considered ice to have a characteristic crushing frequency (or crushing length) as suggested by Matlock et al. (1969). Ice was assumed to be an ideal elastic-brittle material and the model was represented by a carriage transporting a series of uniformly spaced elastic-brittle teeth (Figure 2.6). When a tooth was in contact with the structure, the force was assumed to be linearly dependent on the deformation of the tooth. At the maximum deformation of the tooth, fracture occurred instantaneously causing the force to drop to zero which remains zero until the next tooth comes into contact. The methodology resulted in a 'sawtooth' forcing function with periods where the force remained zero because of no contact. The model considered uniform spacing between the teeth which caused the failure frequency to be proportional to ice velocity. The model has been studied widely and is currently included in the design code of ISO 19906 (2010). However, one of the major limitations of the model is the consideration of the 'passive' role of the structure during an interaction, whereas in reality, the response of the structure can significantly affect the ice force. Also, based on the nonlinear dynamics of the model, it was found that the nonlinear response of the model can be highly influenced by the existence of multiple periodic solutions, dependent on the initial condition (Karr et al., 1993).

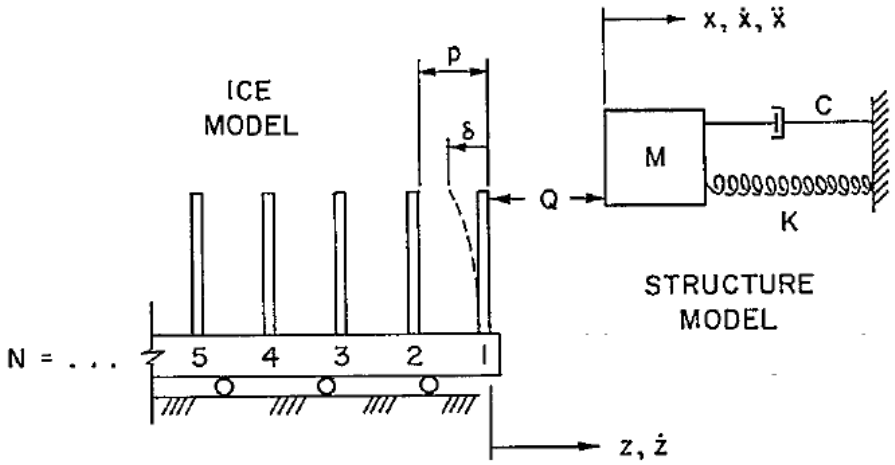

Figure 2.6 Mechanical representation of ice-structure interaction model by Matlock (Matlock et al., 1969)

Based on Peyton's measurement and the Cook Inlet data, Blenkarn (1970) was the first to propose that the dynamics of ice structure interaction is governed by ice sheet velocity, structural flexibility and ice strength, which itself is a function of loading rate. The compressive strength vs. stress-rate curve proposed by Peyton (Figure 2.7) suggests that the proportional relationship between ice force and the relative velocity is not always positive, coining the idea of 'negative damping' in ice-structure interaction. Based on this idea, the structure vibrates under self-excitation as a result of dynamic instability, due to the negative velocity dependence of the ice crushing strength that appears in the ice velocity region of the ductile-brittle transition. This resulted in a different line of thinking, where the ice-structure interaction and associated vibrations are considered self-excited in nature. Blenkarn (1970) assumed the ice force to be a function of the relative velocity between the structure and the ice and considered that the effective mass of the ice floe and the stiffness of the structure govern the vibration. By simplifying Peyton's strength vs. stress-rate curve into three linear relationships (one with a positive slope, one with a negative slope and one with zero slope), (Määttänen, 1978) later presented a rigorous model for self-excited ice-induced vibration. The source of the negative damping in the self-excited system was due to the negative

slope in the strength vs. stress-rate curve, although the existence of such dependency in all ice-structure interaction has been questioned by other authors (Sodhi, 1988). An uncertainty analysis of the self-excited ice-structure interaction model found that the response of the structure and the conditions for IIV can be highly sensitive to ice and structural parameters (Hossain et al., 2018).

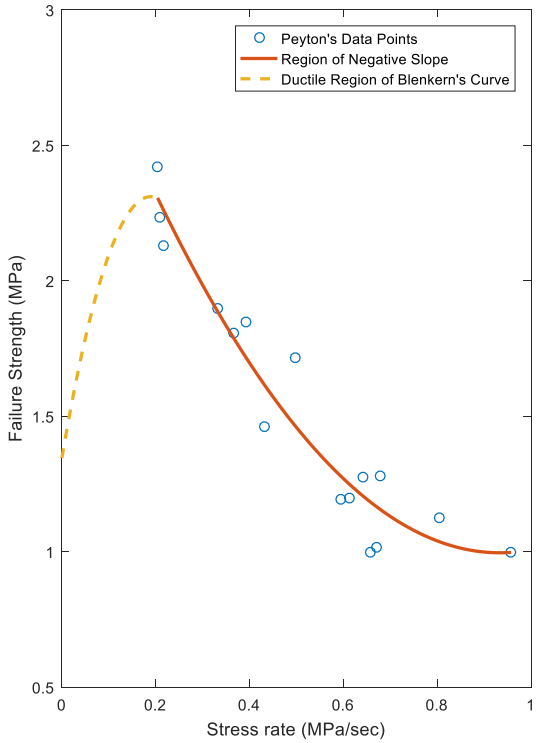

Figure 2.7 Original Blenkarn's curve based on Peyton's compressive data (drawn after Blenkarn, 1970)

Over the last 50 years, a number of authors have proposed different ice-structure interaction modelling approaches based on these two ideas. In his model, Sodhi (1994) presented the ice sheet as a single elastic element where each failure event has been divided into three separate phases: loading, extrusion and separation. The model is similar to pushing a spring-mass system sliding on a frictional surface, where the difference in kinetic and coefficient of friction result in a stick-slip motion observed in intermittent crushing. However, at higher relative velocity during the

extrusion phase, a steady-state, constant-velocity motion takes place. (Huang and Liu, 2009) extended the Matlock model by incorporating the crushing strength vs strain-rate relationship for calculating ice force. A closed form solution for SDOF structures was obtained by expressing the nonlinear relationship into two separate power law equations. The Matlock model was also extended for 2D ice-induced vibration, including the transverse vibration of the structure (McQueen and Srinil, 2015). The authors proposed 3 nonlinear equations to describe the compressive strength vs. strain-rate relationship for different strain-rate ranges. Ice strength was also considered to be a function of ice temperature, brine content, grain size, air volume and ice wedge angle.

As an ice sheet continuously crushes against wide structures, the influence of local contact effects (irregular contact) produces the opportunity for non-simultaneous ice failure across the structure (Kry, 1978). The idea of non-simultaneous failure implies that at any one point in time, different local areas of the failure region can be in different stages of failure. The concept was implemented in ice-structure interaction models by Eranti (1992) who considered the failure process to be divided into a number of zones. The fracture length of each zone was calculated based on the maximum ice force, which was obtained from the strength vs. strain-rate relationship. Each time the zonal ice force reached a critical value, ice was assumed to break a finite length in front of the zonal contact face. The interaction process was divided into six different stages and ice force was calculated using separate equations for each stage. The model was extended by integrating it with the Matlock model to simulate full-scale interaction for round structures (Withalm and Hoffmann, 2010). The idea of dividing the ice structure interaction process into a number of independent zones was also adopted by Hendrikse and Metrikine (2015). In their model, each individual zone was represented as a mechanical representation of an elastic-viscoplastic material model known as

the Bingham element which captures the velocity dependency of ice for the force-displacement relationship. Ice was assumed to behave elastically up to a certain load limit and the plastic deformation starts at 30% of the failure load. The elastic stiffness was considered to be proportional to the expected mean load level of brittle crushing based on ice thickness, structure width and a constant crushing strength of ice.

Kärnä et al. (1999) used a substructure technique to model the ice, soil and the structure where the ice volume was separated into near-field and far-field areas. All the nonlinearities due to the ice crushing process and relative displacements were described in the near-field layer. Both the near-field and far-field area were further divided into zones, where the interactive forces as well as relative displacements between the ice and structure were defined at specific contact points. The failure force was considered to be a function of characteristic ice failure pressure, which was based on the nominal contact area and a lognormal distribution. The crushing pressure was assumed to decrease by a factor of 2 when the relative velocity between the ice and the structure exceeded a transitional range. Ice force was considered to be dependent on the relative displacement between the structure and each contact zone.

Another approach to modelling ice-structure interaction utilizes the Van der Pol equation as an ice force oscillator and the dynamic ice structure interaction was referred to as the coupling vibration between two dynamic systems (Wang and Xu, 1991). The dynamic ice force was regarded as an independent dynamic system and was modelled using a second order differential equation which includes separate terms for the sawtooth periodic nature of the ice force and a term for relative velocity between the ice and the structure. The model was further extended by incorporating the stress vs. strain-rate relationship using two non-linear equations (Ji and Oterkus, 2016). A

characteristic failure frequency for ice proportional to ice velocity and inversely proportional to ice diameter and ice failure length was also included.

2.3 Compressive Ice Failure and High-Pressure Zones (*hpz*s)

2.3.1 Initiation and propagation of cracks

During tensile fracture in ice, cracks primarily develop due to the accumulation of dislocations at the grain boundaries (Schulson and Duval, 2009). However, under compressive loading, cracks can nucleate across ice crystals and the mechanism of failure is associated with the linkage of a large number of cracks and the formation of wing and comb cracks, making the failure process highly complex (Schulson, 2001). Crack nucleation occurs when local stress concentration exceeds the cohesive or theoretical cleavage strength of the material, resulting in the appearance of cracks where none were present before. In the absence of pre-existing flaws, crack nucleation is considered the first step in the mechanical failure of ice, as a means to relieve stress at grain boundaries. A comprehensive review of the mechanisms for crack nucleation can be found in the works of Frost (2001).

Although the onset of crack nucleation results in a wide variety of cracks of different sizes and locations in the specimen, experimental investigations suggest some observable properties, as discussed below (Sanderson, 1988):

- The average length of nucleated cracks, $2a$, is roughly proportional to the grain diameter d, with an approximate relation of $2a \sim 0.65d$.

- The orientations of the cracks are clustered around the axis of compression, such that 90% of the cracks are aligned within the angle of 45^{o} to the direction of the principal compressive stress axis.
- For coarsely grained ice ($d \geq 5mm$) a mean crack density is about one crack per grain.

As compressive stresses increase, the nucleated cracks start to coalesce, and once the local stress level exceeds some critical value, 'wing cracks' begin to form, initiating the crack propagation (Kachanov, 1982). As shown in Figure 2.8, the applied compressive stress causes both sides of the crack to slide relative to each other due to shear stresses and, as a result, tensile stress regions develop around the tips of the cracks. As the 'wing cracks' grow, they begin to align themselves with the direction of principal compressive stress. The problem has been analysed in two dimensions by Ashby and Hallam (Née Cooksley) (1986), who found the length of the wing crack, which usually develops in a stable manner, is a function of the current stress conditions and the mechanical properties of ice. The authors also suggest that cracks in approximate ranges of orientation between 30° and 60° relative to principal compression will nucleate, since these angles are most favorable for sliding. Flaws oriented at angles outside this range require significantly higher stresses to form cracks. This type of fracture model was incorporated into a probabilistic fracture mechanics model of scale effects during compressive ice failure by Taylor (2010).

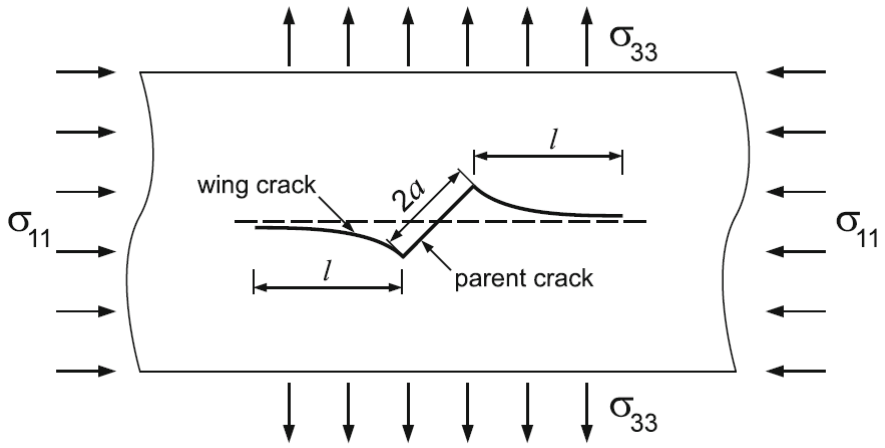

Figure 2.8 Wing cracks of length $\boldsymbol{l}$ forming at the tips of an existing crack of length $\boldsymbol{2a}$ (Staroszczyk, 2019)

2.3.2 Modes of fracture

Sanderson (1988) identified six principal failure mechanisms based on indentation experiments: creep, radial cracking, circumferential cracking, buckling, spalling and crushing. Creep refers to a time-dependent continuum mode of failure with no formation of cracks, and unstable elastic buckling occurs in a thin ice sheet but rapidly leads to circumferential cracks. These two modes of failure are not associated with dynamic ice-structure interaction and are not discussed further.

Among the other four modes of failures (Figure 2.9), Sanderson (1988) classified radial cracking and circumferential cracking as 'global' failures and spalling and crushing as 'local' failures. In reality, however, none of these failure modes occur exclusively and almost all of the failure events are a combination of these failure modes. Palmer et al. (1983) described radial cracking as fracture involving the growth of vertical cracks directed radially from the contact region and running through the whole thickness. These primarily occur when the aspect ratio D/h (D = diameter of the structure; h = thickness of the ice sheet) is high and their initial propagation is stable.

Circumferential cracks can either result from an out-of-plane bending moment due to eccentric loading or as a result of elastic buckling (Sanderson, 1988). The combined radial and circumferential cracking can produce triangular and trapezoidal fragments in large ice sheets. During a full-scale ice-induced vibration lock-in event of the Norströmsgrund lighthouse, the formation of a circumferential crack resulted in a synchronization of the local ice failure by limiting the amount of competing ice (Bjerkås et al., 2013a).

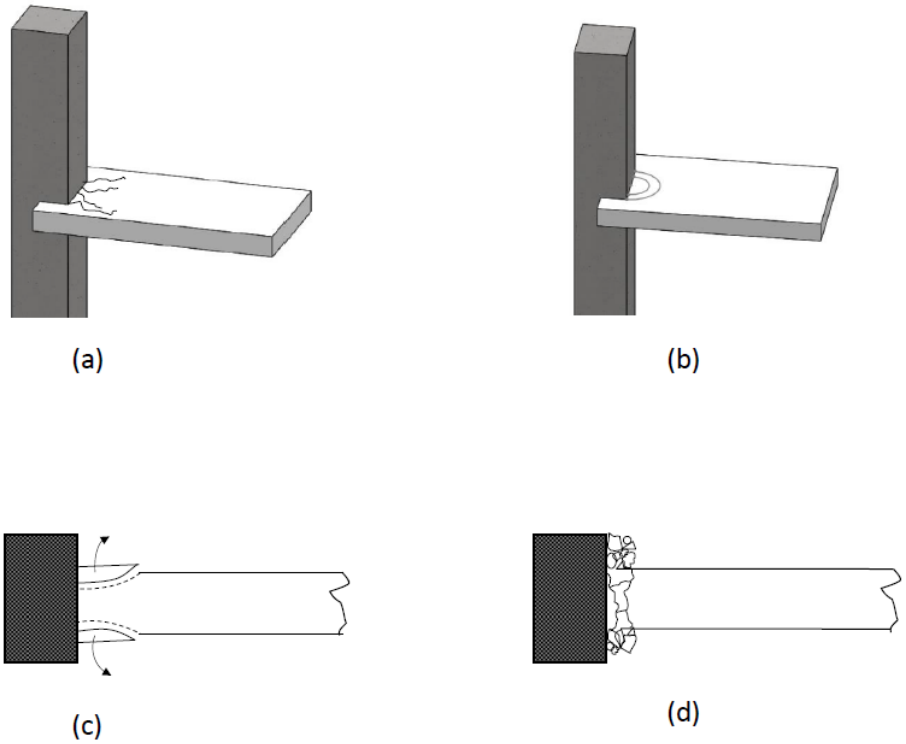

Figure 2.9 Modes of failure during dynamic ice-structure interaction; (a) radial cracking; (b) circumferential cracking; (c) spalling; (d) crushing (modified after Sanderson, 1988)

Local spalling or flaking is characterized by the formation of relatively large fragments of ice, which initiate near the center and run to a free surface. This type of fracture plays an important role in the localization of loads in high pressure zones and scale effects in ice pressure behaviour

(Jordaan, 2001). Croasdale et al. (1977) highlighted the tendency of fractures to run to free edges during spalling failures. In an approach to model the behaviour based on a plasticity theory, the authors used a Tresca yield criterion and assumed failure to occur on slip planes as a result of plastic yielding. The process model developed by Daley (1991) for ice sheet failure assumes that brittle failure results from a sequence of through-body shear cracks which are triggered once the failure stress on a failure plane reaches a critical limit.

Crushing processes result in the pulverization and removal of material from the contact zone, producing a flatter ice edge, which results in a redistribution of stress. Local crushing often occurs after a spall and continues until the total load increases sufficiently to trigger another fracture (Taylor, 2010). The crushing process involves a number of microstructural changes resulting in 'damage', and at higher interaction rates, the damage becomes localized into a layer adjacent to the interaction plane (Jordaan et al., 2008). This layer is associated with the formation of "high-pressure zones (*hpz*s)". The damage process occurs from the continuous evolution of the system of microcracks, due to the irreversible movements associated with dislocation, grain boundary sliding and voids in ice, which generally increases in a relatively orderly manner (Jordaan and Mckenna, 1988). Crushing also involves extrusion of the ice particles from the damage layer in a continuous manner. A schematic of the crushing process and the formation of *hpz*s is shown in Figure 2.10.

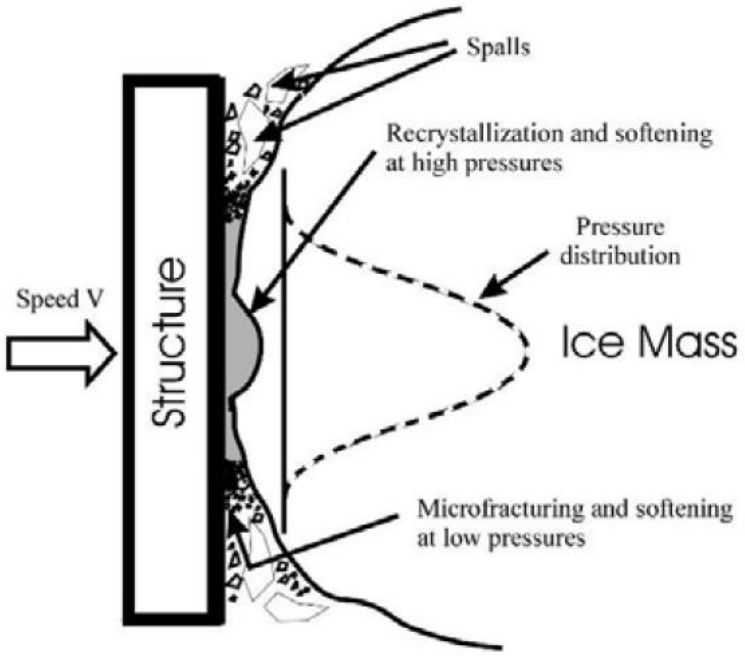

Figure 2.10 Illustration of crushing of ice between solid ice and structure (drawn after Jordaan and Taylor, 2011)

Through a series of 66 edge indentation tests with varying interaction speeds, indenter widths, ice thicknesses, strain rates and aspect ratios, Timco (1987) proposed a failure mode map for the brittle range as a function of strain-rate and aspect ratio (Figure 2.11). Radial cracks were observed to occur most commonly for high aspect ratios and typically radiated from the corners of the indenter, which tended to be initially stable. For high aspect ratio and low strain rates, Timco (1987) reported that radial and circumferential cracking occurred without any crushing. As strain rates increased, particularly for thick ice, the failure behaviour was dominated by spalling and crushing. Although deformation mode maps are useful in visualizing the interplay of different failure modes, making quantitative generalization based on them is not recommended (Sanderson, 1988). Other factors, such as absolute thickness, which are not captured in the failure mode maps can significantly affect the failure behaviour.

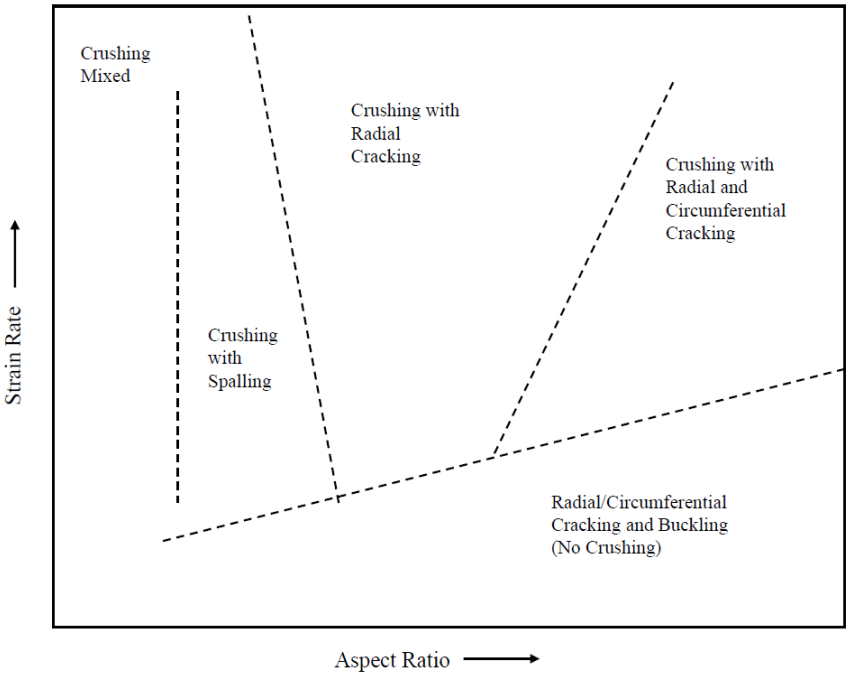

Figure 2.11 Deformation mode map of ice failure showing the regions of strain rate and aspect ratio (based on Timco, 1987)

2.3.3 Mechanics of hpzs and cyclic failure in compression

For ice sheets, during interaction with a structure, the state of stress is multiaxial and cleavage cracks that form near the contact interface tend to propagate to the top and bottom free surfaces of the ice sheets, creating spalls. Such processes create wedge-shaped fronts of ice, creating regions of intense pressure, termed as 'high pressure zones (*hpz*s)' shown in Figure 2.12. A majority of the ice load gets transmitted to the structure through these localized regions (Johnston et al., 1998); however, continuous spalling causes the *hpz*s only to possess a small fraction of the nominal interaction area (Frederking, 2004; Taylor et al., 2008). Spalling causes redistribution of the applied load into smaller contact areas and thus plays an important role in the development of *hpz*s, both spatially and temporarily. The behaviour of the *hpz*s is influenced by damage processes, which typically include microcracking in zones of high shear and low confinement, as well as

dynamic recrystallization and localized pressure melting in regions of high shear and high confinement (Meglis et al., 1999; Melanson et al., 1999; Barrette et al., 2002). During medium-scale indentation tests at Hobson's Choice Ice Island (Frederking et al., 1990), an extensive white layer of crushed material with occasional 'blue' recrystallized zones was observed (Jordaan, 2001). A distinct boundary between damaged ice and parent ice was visible at some depth from the contact interface, where lateral grain motion along the boundary was evident. Consequently, a layer of highly microstructurally modified ice forms adjacent to the ice-structure contact surface, where localized pressure melting and pressure softening causes a reduction in the load bearing capacity, leading to an extrusion of ice particles from beneath the contact zone. The release of such pressure contributes to reversing the thermodynamic process, leading to partial recovery of the strength within the layer, i.e., hardening. The next cycle of loading and extrusion can result from this hardening and the process can be repeated. This repeating pattern of softening and hardening has been linked to the cyclical nature of loading (Jordaan, 2001; Jordaan et al., 2009; O'Rourke et al., 2016a). The other aspect of the ice-crushing process, i.e., spalling, has also been reported to be dynamic in nature, and some other have linked spalling frequency to observed loading dynamics (Gagnon, 1999, 2011) while others point out that fracture processes and associated loads are highly random due to randomly distributed flaws and therefore it is unexpected that ice would exhibit any characteristic spalling or fracture frequency (Jordaan, 2001; Taylor and Jordaan, 2015), and the coupled interplay between fracture, crushing and structural response must be examined in further detail to understand dynamic ice-structure interactions.

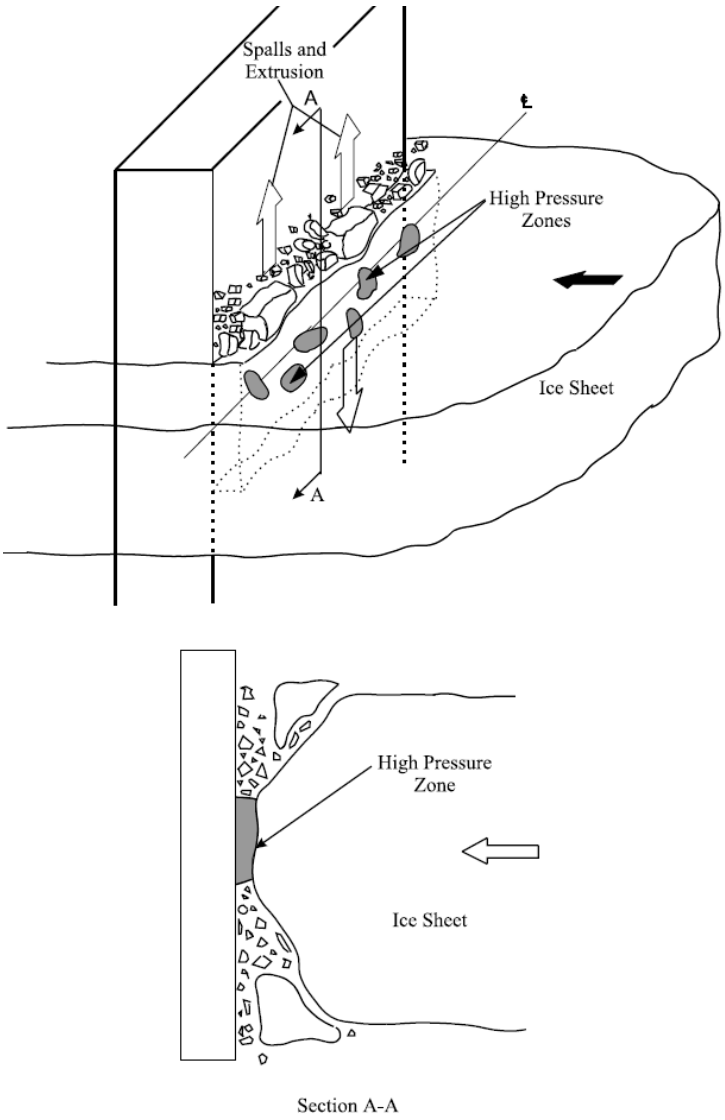

Figure 2.12 Schematic illustration of the main process of spalling, extrusion and high-pressure zone formation (Jordaan, 2001)

The crushing process, when accompanied by vibration, can be often distinguished by the extrusion of the crushed ice in the form of a very fine-grained material produced by extensive recrystallization. In an intermittent or sawtooth failure cycle, extrusion occurs slowly and steadily during loading, whereas very fast extrusion occurs during unloading. Similar behaviour was also observed during extrusion of crushed ice confined under two parallel plates (Spencer et al., 1992; Singh et al., 1995). A series of small-scale indentation experiments was able to reproduce this behaviour confirming its scale independence (Barrette et al., 2002; Mackey et al., 2007; Wells et

al., 2011; Browne et al., 2013; O'Rourke et al., 2016a). In their two papers, O'Rourke et al postulate that the elusive root cause of the regular cyclic loading is the microstructural change of ice (layer formation) and the dynamic way in which it develops and extrudes (O'Rourke et al., 2016a, 2016b). The regular failure of an *hpz* in such cases constitutes a self-sustained oscillation, characterized by a cyclical process of supply and dissipation of energy (Pikovsky et al., 2003). The dissipating energy can be linked to the viscoelastic deformation enhanced by the distributed damage and spalling fracture, while the driving force of the ice floe (or actuator) supplies energy to the system. Small scale experiments suggest that degree of structural compliance has an important effect on the frequency, amplitude of the loading patterns and crushing strength of ice (Browne et al., 2013). Hence, a structural feedback mechanism regarding synchronization of *hpz*s is considered to be very important. Jordaan and Singh (1994) proposed the idea of in-phase and anti-phase synchronization, where the failure in one *hpz* causes increase in load in the other *hpz*s for the first case and decrease in load in the later. (O'Rourke et al., 2016a) observed this behavior in their small-scale experiments. Although much work is needed for a complete understanding of such mechanisms, this sheds light on the coupled ice-structure interaction behavior of ice-induced vibrations. Moreover, this information may help to highlight gaps that exist between the complex reality of ice compressive failure and the simplifications made to make models more tractable.

2.3.4 Non-simultaneous failure and probabilistic averaging

Kry (1978) presented the first statistical treatment of non-simultaneous ice failure and introduced the concept of independent failure zones. The mechanism is primarily governed by the birth, evolution and death of an individual *hpz*s, which changes both spatially and temporally. To illustrate this idea, Ashby et al. (1986) performed indentation tests of brittle wax sheets by a

cylindrical structure. As shown in Figure 2.13, at any given time the load can be transmitted through several distinct points, the position of which change in time as a result of fractures and spalls. As suggested by the authors, the treatment of such behaviour requires a probabilistic approach which is considered in several works (Taylor and Jordaan, 2011; Taylor and Richard, 2014; Taylor et al., 2019).

Jordaan et al. (1993) proposed a probabilistic treatment of *hpz*s for estimating the local ice loads; the load on a design area is applied through a random number of *hpz*s, each with a random force. The number of *hpz*s was modelled as a spatial Poisson process and the zonal force was modelled using a gamma distribution. A Monte Carlo simulation based on this model was compared with the ship trial data from the Louis St. Laurent and was found to be in good agreement (Johnston et al., 1998). Ralph and Jordaan (2017) extended the model to account for the exposure based on *hpz* rate, which is determined by interaction speed. Takeuchi and Saeki (1994) used a shot-noise model to statistically produce intermittent peaks of local ice pressures of independent ice failure zones at the ice-structure interaction interface. A shot noise process consists of a series of events at random times and of random magnitude, each of which produces a fixed shaped rise and recession (Weiss, 1977). Kujala (1996) developed a statistical model for non-simultaneous ice crushing as a compound Poisson process and the properties for the statistical variables were determined based on full-scale onboard measurement from the icebreaker Sampo in the northern Baltic Sea. Kamesaki et al. (1997) studied non-simultaneous failure behaviour using vertical rectangular indenters and cylindrical indenters in laboratory conditions. Over the range of structure widths considered (100 mm to 1500 mm) the mean load remained approximately constant, while the variance decreased slightly for increasing width. The authors also indicated that the failure zones were approximately on the order of ice thickness, which was first proposed by Kry (1978).

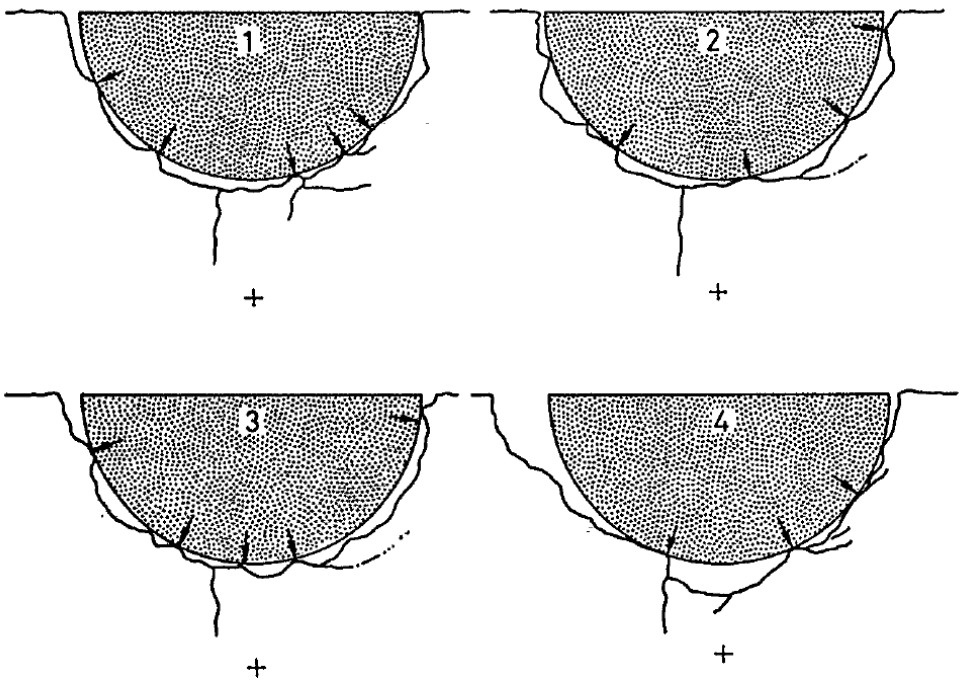

Figure 2.13 Non-simultaneous failure illustrated by tests on brittle wax sheets (Ashby et al., 1986)

2.4 Review of Ice Indentation Tests

The global failure pressure of ice decreases with the increase in interaction area, a phenomenon commonly known as a pressure-area relationship in ice (Sanderson, 1988). Indentation tests are an effective way to study the pressure behaviour in the contact interface and the associated failure mechanism. The nominal pressure is usually measured by measuring the deformation caused by ice pressure on a selected area and calculating the force based on the deformation. However, to study the pressure distribution across the interface, electric gauges are required, and two types of electric gauges have been used so far: polyvinylidene fluoride (PDVF) film, which is piezo-electric (Joensuu, 1990), and the tactile pressure sensor (Sodhi et al., 1998). Although these gauges have their disadvantages, especially in calibration, the high resolution data provide valuable information about the mechanics of formation and evolution of high-pressure zones (*hpz*s).

In this section, some of the full-scale and laboratory-scale indentation tests and their results are discussed in chronological order. Since the focus of the thesis is primarily on fixed structures, results from ship ramming tests are not included. Interested readers can find them in the work of Riska (2018).

2.4.1 Laboratory indentation tests at WARC

This test series was carried out in 1988 at the Wärtsilä Arctic Research Center (WARC) with the cooperation of the Helsinki University of Technology and the results can be found in the work of Riska (1991) . The primary goal was to measure the ice pressure distribution across the contact area with PVDF film and observe the nature of the contact through a transparent Lexan plate. The tests were carried out with brackish ice from the northern Baltic, and the average height of the sample was 40*cm* with a cross section of 25*cm*×25*cm*. Some specimens were cut to form a wedge and the wedge angle varied between 60° and 120°. Two test geometries were used; one with an inclined plate (angle with vertical 45°) and the other with a horizontal plate (shown in Figure 2.14).

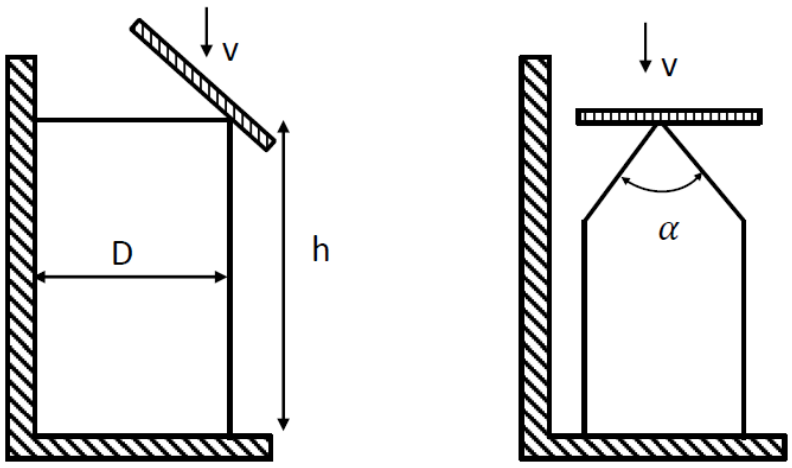

Figure 2.14 Geometry of the test types (based on Riska, 1991)

The specimen was crushed in a test rig and the indenter was pushed using a hydraulic actuator. The temperature of the cold room was kept constant at -6°*C* and the indentation speed ranged from 5-15*cm/s*. The force-time history showed regular ice failure behavior with triangular peaks as shown in Figure 2.15, and the maximum pressure recorded was 36*MPa*. However, the visual observation and the data from the PVDF film suggested an interesting feature of the contact area. Most of the transmitted pressures were observed to be concentrated towards the center in line-like form, suggesting the existence of 'high-pressure zones (*hpz*s)'. The correlation between pressure sensors was almost zero in any direction from any chosen element except with the adjacent element; there the correlation was slightly below 0.5. A later full-scale test on an icebreaker (IB Sampo) equipped with PVDF film attached to the hull also showed the existence of a narrow high-pressure band towards the center.

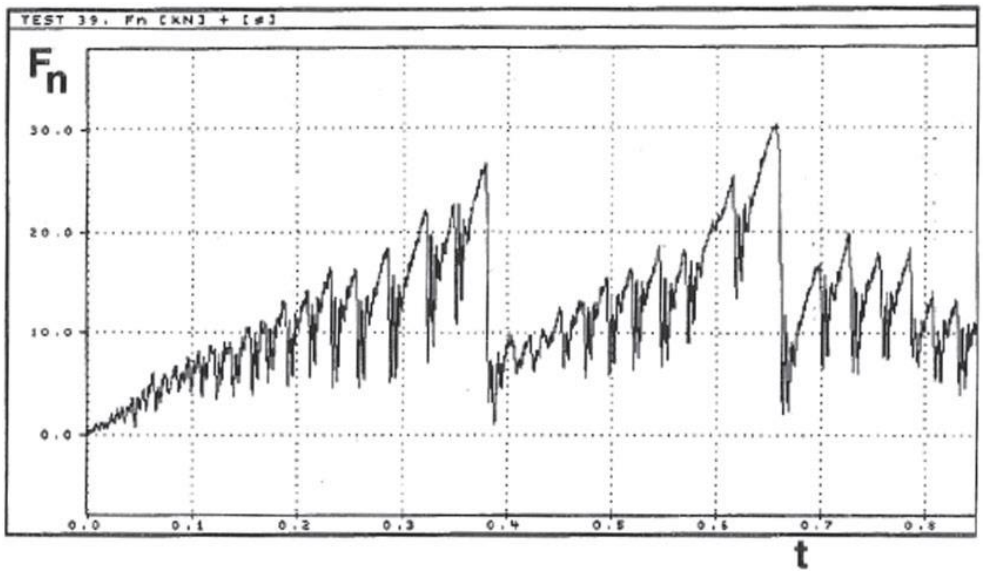

Figure 2.15 Force-time history of a wedge-shaped specimen (Riska, 2018)

2.4.2 Medium-scale indentation tests at Hobson's Choice Island

A total of 11 medium-scale indentation tests were carried out in 1989 on Hobson's Choice Ice Island, which was a 2.5*km* wide, 8*km* long and 45*km* thick floating ice block that broke away from Ward Hunt Ice Shelf, Ellesmere Island in 1982. The primary results were reported by Frederking et al. (1990) and Kennedy et al. (1994) but some of the results were also discussed in later papers (Gagnon, 1994; Jordaan, 2001).

The tests were carried out using a single actuator indentation system with a force capacity of 4.5*MN*. The maximum stroke of the actuator was 300*mm,* with a maximum velocity of 100*mm/s*. Three types of indenters were used for the tests:

- A 'rigid' spherical indenter of $0.8m^2$ area with a 1.28*m* radius of curvature and 1m overall diameter. Seven 100*mm* diameter pressure cells were located in the indenter.
- A circular, flat, 'compliant' indenter of $0.8m^2$ area, comprising a 1*m* diameter 17*mm* thick plate welded to stiffeners at 300*mm* spacing. Eight pressure sensors were used to measure the pressure, each of which comprises a rigid 13*mm* diameter cylinder supported by a miniature load cell, yielding the average pressure.
- A 'rigid' flat rectangular indenter of $0.375m^2$ area (0.5*m* high and 0.75*m* wide) with a thickness of 40*mm*. Nine 13*mm* diameter pressure sensors were built into its face.

The tests were carried out in a 65*m* long trench with a 3*m*×3*m* cross-section with varying indentation rates. For slow indentation tests, the load increased monotonically, which resulted in a permanent depression with substantial damage in the vicinity of the indenter. Neither ejection of the crushed ice nor localized spalling was observed, but the thin section of the damaged zone

showed significant evidence of recrystallization. For faster indentation rates, reported results showed a similar force-time history plot as shown in Figure 2.15, suggesting dynamic activity during ice crushing. However, the pressure across the contact area was not uniform with the local pressures in the center of the contact area being 3 times higher reaching a value of up to 75*MPa*. Extrusion of crushed ice particles was observed from the interaction interface and the thin-section showed the existence of the damaged layer with occasional 'blue zones'/*hpz*s (Figure 2.16). The ice in the 'blue zones' was not necessarily undamaged although the appearance was similar to the 'virgin' ice. Thin sections suggested that severe grain modification, primarily recrystallization was the major feature of these zones, which allowed them to sustain such high pressures. The formation of the layer and the extrusion of ice particles were linked to the dynamic activity observed in the force time-history (Jordaan, 2001).

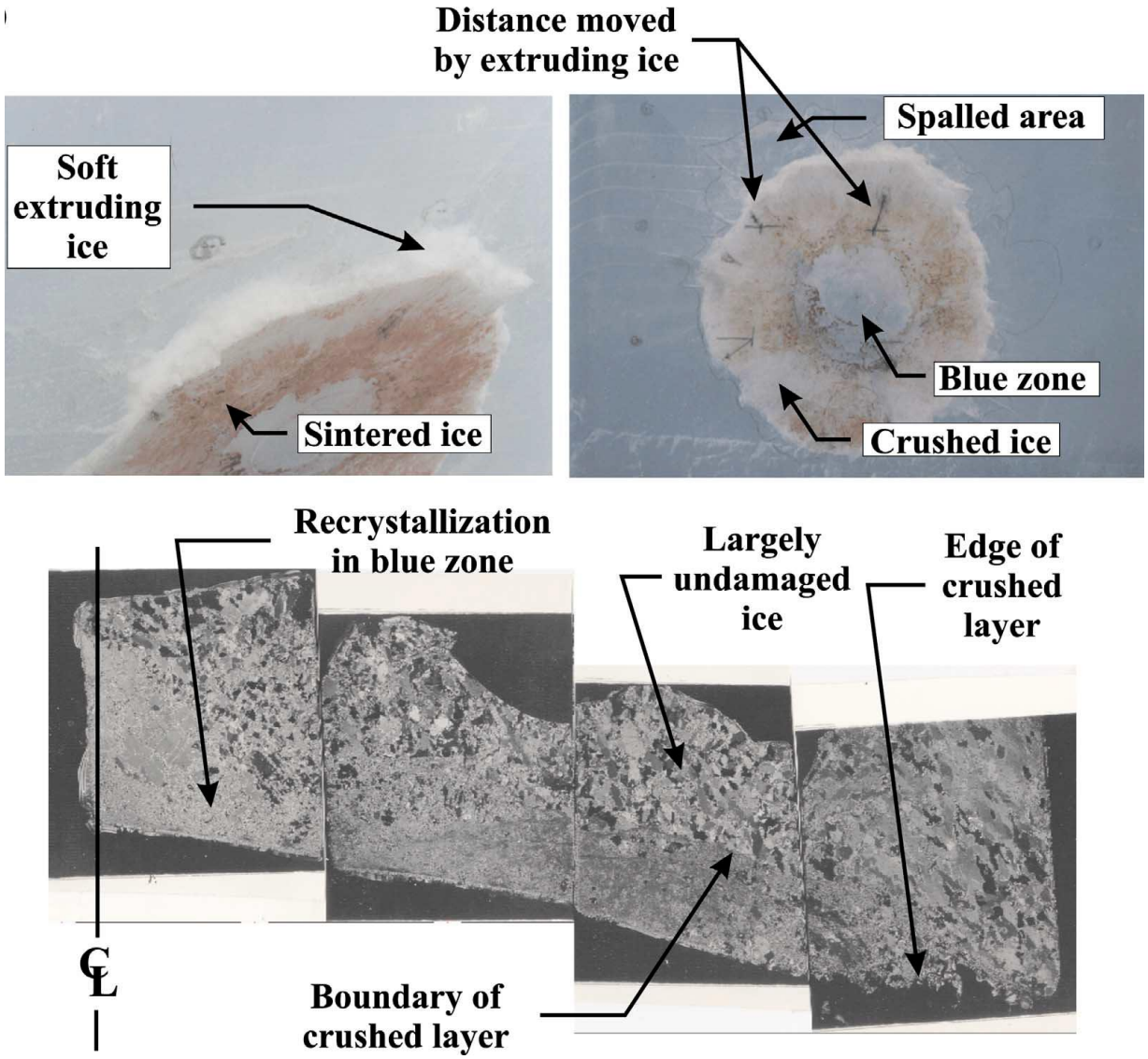

Figure 2.16 Photographs (top) and thin-sections (bottom) of the indented surface (Jordaan, 2001)

2.4.3 Ice crushing tests at NRC, Ottawa

This test series was carried out at the National Research Council of Canada, Ottawa in 1992. The aim of the test series was to investigate the details of the ice crushing process during ice edge indentation and the influence of several factors such as the clearance between the test structure and

the ice, grain orientation of S2 ice and indentation speed. The results of the test series are reported by Tuhkuri (Tuhkuri, 1995, 1996).

The experimental setup consisted of a load frame, a hydraulic actuator, three steel support systems, a test plate and an ice specimen surrounded by acrylic plates for confinement (Figure 2.17). The clearance between the test plate and the edge of the acrylic plate was termed gap height (shown as h in Figure 2.17). The following variations in the ice loading configuration were tested:

1. Width of ice block [*mm*]: 60, 120
2. Actuator velocity [*mm/s*]: 1, 10, 20, 50
3. Gap height [*mm*]: 20, 30, 40 50
4. Wedge angle of ice block [°]: 90, 120, 180
5. Orientation of the columnar grains
6. Ice type (S1 or S2)

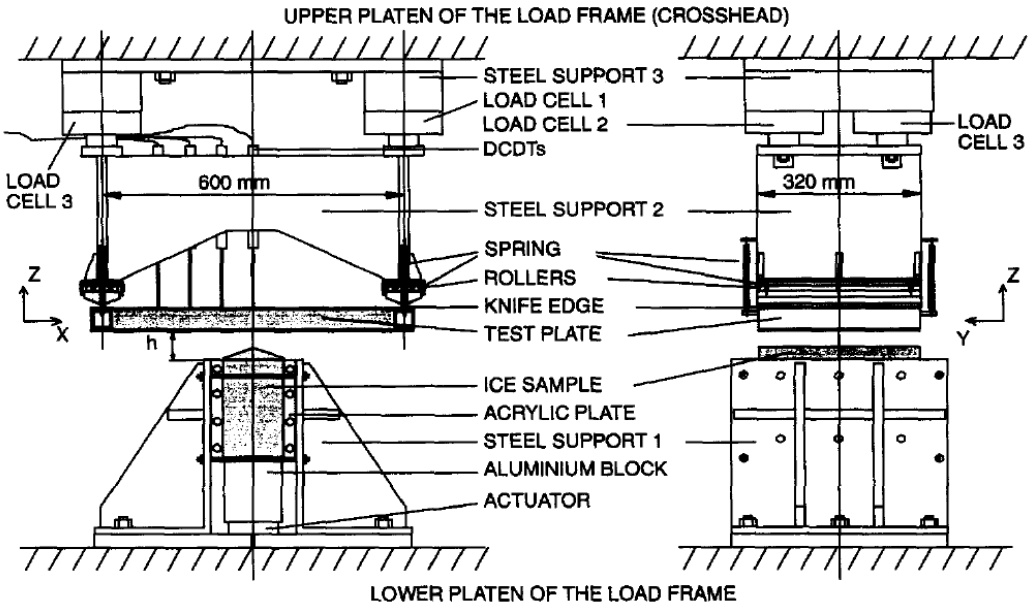

Figure 2.17 Experimental setup of the tests series at NRC in 1992 (Tuhkuri, 1995)

Based on the results, the author identified three of the variables to be most important: gap height, grain orientation and initial wedge angle. The gap height in this case affected the degrees of confinement. The initial wedge angle affected only the onset of the failure process, but the gap height and the grain orientation affected the overall failure process. For both smaller and larger gap heights, a contact line was observed in the thin sections, suggesting the presence of *hpz*s, although the gap height significantly affected the size of the contact area. When the gap height was large, the ice surface in the process zone was clear and smooth, indicating that the surface was formed by macro cracks or spalling. However, when the gap height was small, a layer of the crushed ice was formed and the parent ice below the layer was damaged by microcracking. The ice load was found to be dependent on ice type, grain orientation and loading velocity, although the failure and contact type were independent of these parameters.

2.4.4 Medium-scale indentation tests by JOIA

A Medium Scale Field Indentation Test (MSFIT) was carried out by the Japan Ocean Industries Association (JOIA) over a period of five years (1996-2001), consisting of over thirty tests to measure ice loads on offshore structures in the harbour of Notoro Lagoon in Hokkaido, Japan, connected to the sea of Okhotsk. The test setup, ice conditions and the results were discussed in a combination of papers (Takeuchi et al., 1997; Saeki et al., 1998; Sodhi et al., 1998; Kamio et al., 2000; Akagawa et al., 2001).

The schematic of the test structure is shown in Figure 2.18. A 1.5*m* wide segmented indenter (which could be widened up to 3*m*) was used as the model's structure. A 100*tonf* load cell was mounted between the hydraulic ram and test beam, which was capable of measuring forces in three directions and moments parallel to the indenter face. Four thin pressure sensing panels were

installed on the face of the segmented indenter (Figure 2.19). The primary advantage of the tactile sensors is the high resolution spatial and temporal information provided about the relative pressure distribution in both horizontal and vertical directions, as measured across the face of the structure, providing detailed information regarding the formation and evolution of the high pressure zones (*hpz*s). Each of the panels was about 0.3*mm* thick, 238*mm* wide and 238*mm* high. Within the plastic sheets encasing a transducer panel, there were conducting surfaces along horizontal and vertical directions in a grid pattern with a spacing of 5.4*mm*. There were 44 rows and 44 columns of grid points in each panel. With the help of software developed by the manufacturer of the pressure sensing panel, the pressure at each grid point was monitored, which had an area of 5.4*mm*×5.4*mm*. With four panels taped adjacent to each other, there were 44 rows and 176 columns of grid points. The panels were capable of measuring pressure at each grid point up to a maximum pressure of 6.86*MPa*. Displacement rates were held constant for a given test and ranged between 0.03*cm/s* and 3*cm/s*.

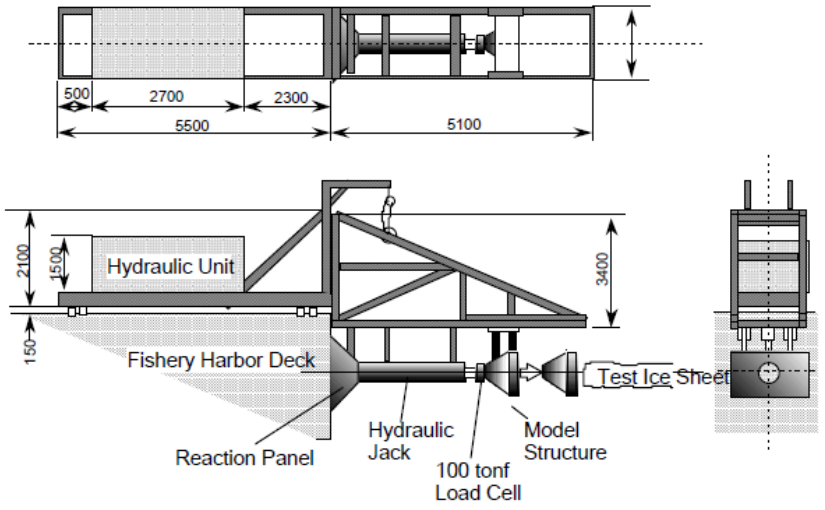

Figure 2.18 Schematic of MSFIT test setup (Akagawa et al., 2001)

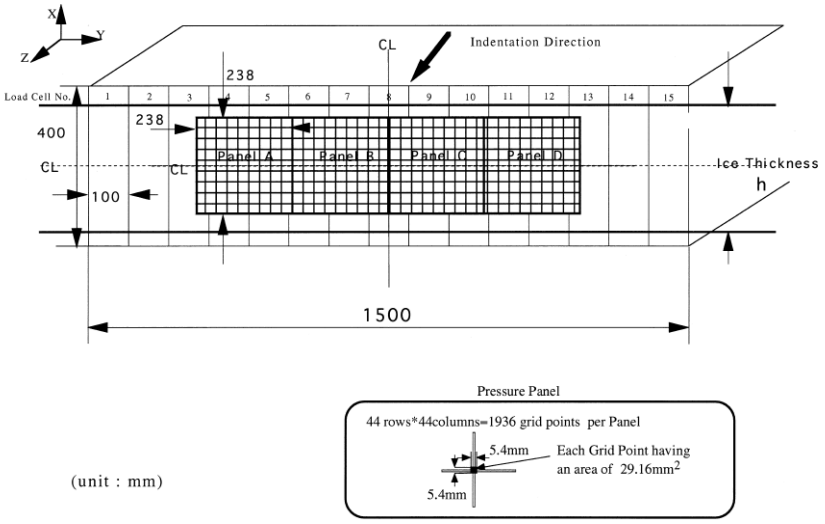

Figure 2.19 Pressure sensing panels installed in the segmented indenter (Sodhi et al., 1998)

The mean pressure measured at a local panel at a fixed position on a structure is simply the total force acting over the nominal area of the panel. Based on the size of the panel, the measured pressure can result from a single *hpz*, multiple *hpz*s or partial *hpz*s acting over the loaded area. Therefore, extracting characteristics of a single *hpz* is not possible when using panels. Tactile sensors overcome some of these limitations by providing pressure data at a much higher resolution. The nature of the data provides valuable information regarding the formation and evolution of individual *hpz*s during an interaction. The higher resolution of the data, allows extracting characteristics for individual *hpz*s more effectively than was possible in the past.

Based on the available data from JOIA measurement series, Richard and Taylor (2014) developed an analysis algorithm for automatic *hpz* detection and tracking. The *hpz*s have been defined mathematically having two attributes: an area defined by a pressure contour in which the pressure within each cell of the tactile sensor is higher than a chosen threshold pressure, and an area that does not move about its centroid for more than 150*mm* within the subsequent time step. For each time frame of tactile sensor recording, *hpz*s were identified by locating the positions of the contours

(isolines) where the *hpz* candidate exceeded the pressure threshold. The isoline detection was made using the MATLAB contouring algorithm. An *hpz* contour that did not cover at least the area of a single element of the tactile sensor (i.e., approximately $5mm^2$) was rejected. *Hpz*s were tracked using a slightly modified version (Blair and Dufresne, http://physics.georgetown.edu/matlab/) of the IDL tracking algorithm (Crocker and Grier, 1996). To track *hpz*s, the locations of the centroid of individual *hpz*s were resolved in time into "trajectories" on the vertical plane. A centroid was not allowed to move farther than 150*mm* from its previous location. For cases where there would be more than one centroid found within the 150*mm* radius from the previous centroid location, the search radius was reduced to 75*mm* and the new position of the centroid was recalculated using the tracking algorithm. Cases for which the tracking could not be resolved in this way were rejected. The method was able to quantify a number of *hpz* characteristics for a given pressure threshold such as duration, force time-trace, area time-trace, minimum and maximum pressure time-trace etc. (Richard and Taylor, 2014). Based on the individual characteristics of the *hpz*s, probabilistic frameworks for modelling loads on local areas and global areas were also developed (Rocky S. Taylor and Richard, 2014; Taylor et al., 2019).

2.4.5 Forced vibration tests at HSVA

In the field of fluid-structure interaction, the forced vibration system has been used to predict frequency lock-in vortex induced vibration of structures (Sarpkaya, 1978; Gopalkrishnan, 1993). A similar idea was used by Hendrikse and Metrikine (2016) for an edge indentation test program at Hamburg Ship Model Basin (HSVA) as a part of the 'Deciphering Ice Induced Vibration' program (Hendrikse et al., 2012; Määttänen et al., 2012). The goal of the tests was to observe the

local pressure, contact between ice and structure and the global load, while maintaining a controlled harmonic motion of the structure resembling frequency lock-in.

The test setup consisted of a rigid beam with a cylindrical indenter with a diameter of 220mm at the ice level (Figure 2.20). The beam was equipped with a Tekscan tactile sensor at the ice level with a resolution of 3.5 Sensels/cm^2, a pressure range of 0-175MPa and a sampling frequency of 100Hz. To protect the sensor from ice abrasion, 0.5mm thick aluminium foil was used to cover the sensor. About one third from the top of the structure, the beam was rigidly connected to an EXLAR GSX50 electric linear actuator, which controlled the displacement of the structure. The ice sample was produced using NaCl-doped water with a salinity of 6.8% and embedded air bubbles with 200-500μm. During the tests the temperature of the ice was approximately -2℃ with an average density of 830kg/m^3, average salinity of 3.3% and uniaxial compressive strength of 270kPa at a strain-rate of $10^{-3}s^{-1}$(Hendrikse and Metrikine, 2016).

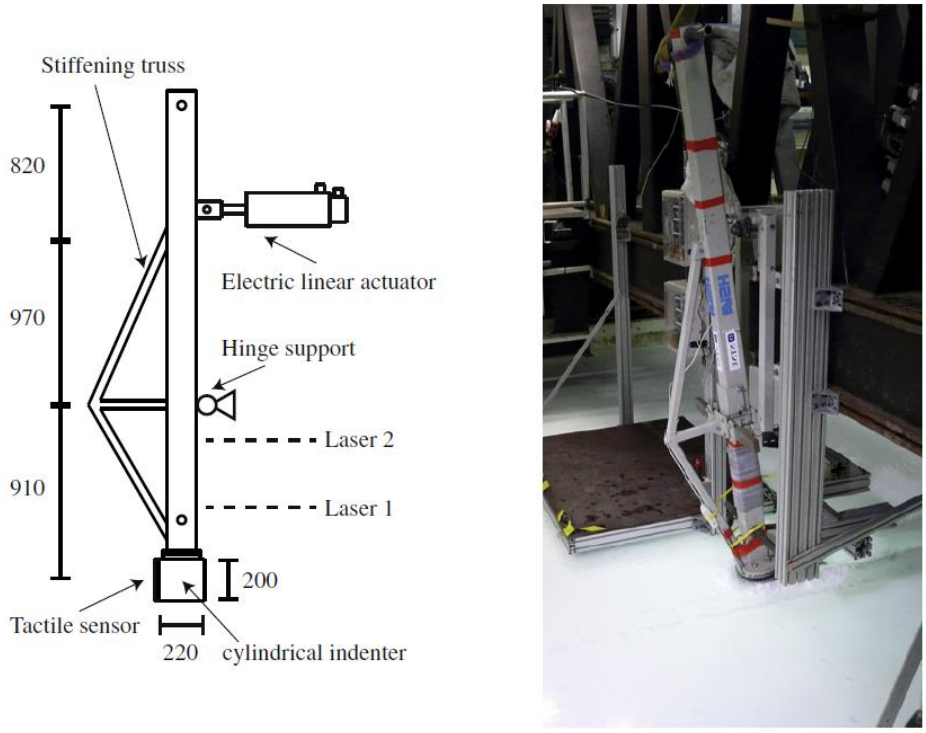

Figure 2.20 Test arrangement for forced vibration experiment (Hendrikse and Metrikine, 2016)

Based on the observed results, the authors concluded that the change in the ice behaviour is primarily dominated by the relative velocity between ice and structure. As soon as the relative velocity becomes small enough, a change from brittle to transitional or ductile behaviour is observed which results in an increase in global load. The authors also suggest that, for a particular ice-structure interaction, a maximum natural frequency exists, above which frequency lock-in cannot occur. However, such a frequency would be dependent on the type and condition of the ice.

2.4.6 Small-scale indentation tests

Small-scale indentation tests of confined ice samples, usually with a spherical indenter, are an effective way to simulate and study *hpz*s under controlled conditions. Such tests can be performed in the Material Testing System (MTS) and the range of the parameters for study can be varied

widely. Figure 2.21 shows the general arrangement of such a test setup. Results from these tests show that the characteristics of the crushed ice beneath the indenter are similar to the medium scale indentation tests at Hobson's Choice Island. The different properties of the *hpz*, such as the depth of the layer, the microstructure of the crushed ice, and the effect of fracture/spalling on *hpz* development can be studied through these studies, which can be translated to full-scale ice-structure interaction. A selection of such tests is discussed in this section. For more details on individual tests, the reader is referred to the original articles.

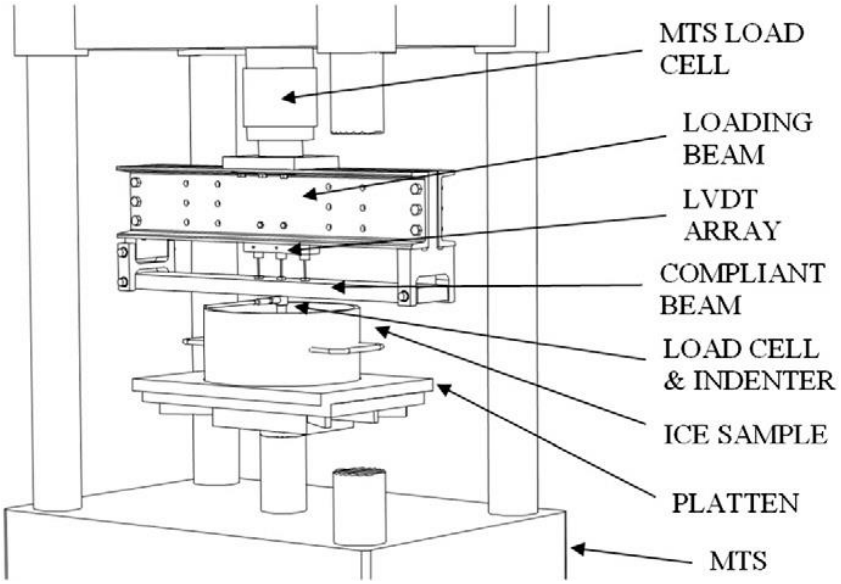

Figure 2.21 General arrangement of small-scale indentation setup (Browne et al., 2013)

Barrette et al. (2002) carried out small-scale confined ice indentation tests using a spherical indenter (20*mm* diameter, 25.6*mm* radius of curvature) and freshwater polycrystalline ice samples (150*mm* diameter, 60-130*mm* height). The tests were scaled down by a reduction factor of 50 from the medium scale tests carried out at Hobson's Choice Island. Tests were carried out for different indentation rates (ranging from 0.1*mm/s* to 10*mm/s*) and test temperatures (-2°*C*, -10°*C*, -20°*C*). For the range of the parameters, cyclic loading was present in all tests and the damage layer was

found up to 5*mm* below the indented surface. For the same indentation speed, the test carried out at -2°*C* showed uniform grain refinement with almost no signs of microcracking along the indented surface, whereas the test carried out at -20°*C* were heavily dominated by microcracking. For -10°*C*, the indented surface consisted of a dense network of microcracks with heavy recrystallization at the center. Thin sections of the indented surface from all tests show the presence of recrystallization, and the thin section at -10°*C* was nearly identical to the thin section of the medium-scale tests, which was performed at -14°*C*, suggesting the similarity in the crushing process.

Mackey et al. (2007) carried out a series of tests on 200×200×100*mm* ice samples to study the effects of indenter size, indentation rates and the location of indentation on ice failure behaviour. On analyzing the results for the indentation tests, it was observed that the large-scale fractures occurred regularly, especially in the cases of edge tests and some intermediate distance tests. The authors also observed some noteworthy similarities and differences due to the change in indentation location. The initial slope for loads at the same speeds and different locations were almost similar, but these slopes change drastically when the distances to the edge become significant, leading to large-scale fracture and massive load drops. The authors suggested a link between some failure behaviours and its implications on the reduction of load. According to the visual records and the data obtained from the tests, the authors inferred that a significant load drop was noticed every time a large-scale fracture or significant spalls were observed. These fractures led to load drops of almost 60% to 80%.

Wells et al. (2011) performed similar tests for different indentation rates and indentation depths. Tactile pressure sensors were used to record the pressure distribution at the indented surface. The

localized pressure was found to be 2 to 8 times higher than the average pressures and was highly localized and non-stationary. Based on the data from the load cell and tactile pressure sensors, the authors made an important distinction between the spalling and crushing events. Both spalling and crushing resulted in a load drop; however, spalling caused a significant reduction in the contact area, whereas during crushing, the change in contact area was negligible.

Another series of tests carried out by Browne at al. (2013) studied the effect of ice temperature, sample size, indenter size and structural compliance on *hpz* failure behaviour. The effects of temperature on microcracking and recrystallization were similar to the results of Barrette et al (2002). Analysis of the loading patterns showed that ice failed in a ductile manner with rare spalling events, which resulted in a damage layer dominated by a recrystallized layer at warm temperatures, while the ice failure at cold temperatures was a combination of crushing and localized spalling that often led to cyclic loading. The cyclic loading pattern was significantly higher for the more compliant system, which also resulted in higher average load drops, due to structural feedback.

The continuous development and extrusion of the damaged layer in a single *hpz* can induce vibration to the structure (Jordaan, 2001); however, most actual interactions involve multiple independent *hpz*s, as highlighted in the JOIA data. It was previously hypothesized that the local structural feedback after the failure of an *hpz* can increase the load in an adjacent *hpz,* and this load sharing mechanism can result in a global structural vibration through a cascading effect (Jordaan and Singh, 1994). O'Rourke et al. (2016a, 2016b) used small-scale indentation tests to identify the criteria for such structural vibrations, using single indenter and double indenter tests. Two compliant beams of different stiffness, length and natural frequency were used to perform tests on

a Materials Testing System in a cold room set at -10°*C*. A 20*mm* spherical indenter was used at indentation speeds that ranged from 4 to 19*mm/s*.

For single indenter tests, the test data and analysis showed that sawtooth failure was observed in many tests, with evidence of a locked-in phenomenon in some tests. Regular sawtooth loading was more predominant in the tests that were performed on more flexible beams, whereas the tests with stiffer beams comprised different types of failure modes, such as continuous crushing with abrupt spalls and irregular sawtooth failure. It was also observed that this sawtooth activity increased with an increase in indentation speed. Locked-in conditions were observed on a stiffer beam at higher indentation speeds when the frequency of the sawtooth failure matched the natural frequency of the structure. These conditions were observed only during the initial phase of the testing, when the contact areas were too small. The thin sections of the indented ice suggest that the sawtooth failure comprised of increase in layer thickness, whereas the locked-in loading involved vibrations within the damaged layer. For double indenter tests, the load sharing mechanism was observed if the *hpz*s were in-phase, resulting in a structural vibration in its first natural mode. However, a condition of anti-phase was also found to exist, which resulted in the beam to vibrate in its higher mode, where the load sharing caused a reduction in the vibration.

2.5 Summary

The key points of the chapter are highlighted below:

- Dynamic ice-structure interaction can lead to severe ice-induced vibrations. Although in most cases the vibration is observed for narrow structures such as lighthouse or channel markers, wide offshore platforms can also experience such vibrations.

- The modelling approaches for dynamic ice-structure interaction can be broadly classified into two categories: forced vibration and self-excited vibration. Both approaches offer some success when compared with particular events or test cases, but show limitations due to insufficiently accurate treatment of ice behavior in existing models.
- The compressive ice failure process is highly complex, due to the interplay of various mechanisms such as fracture, damage, recrystallization, and poses the primary challenge in modelling dynamic ice-structure interaction. However, one of the key features of the compressive ice failure process is the development of high-pressure zones (*hpz*s), through which most of the loads are transmitted between the structure and ice. These regions cover a very small portion of the global interaction area and have been observed to exist at different scales of interaction.
- Indentation tests provide an excellent opportunity to study the formation and evolution of *hpz*s under controlled conditions. The results suggest that the characteristics of the *hpz*s can be highly dependent on interaction parameters such as *hpz* size, structural compliance, indentation speed etc. A dynamic ice-structure interaction model based on *hpz*s should account for such dependence.

Reference

Akagawa, S., Saeki, H., Takeuchi, T., Sakai, M., Matsushita, H., Kamio, Z., Terashima, T., Nakazawa, N., 2001. Medium-Scale Field Ice Indentation Test-Winter 1996-2000 Test Program, in: Proceedings of the 16th International Conference on Port and Ocean Engineering Under Arctic Conditions (POAC'01). Ottawa, Canada, vol. 2 pp. 567–576.

Ashby, M.F., Hallam (Née Cooksley), S.D., 1986. The failure of brittle solids containing small cracks under compressive stress states. Acta Metall. 34, 497–510. https://doi.org/10.1016/0001-6160(86)90086-6

Ashby, M.F., Palmer, A., Thouless, M., Goodman, D.J., Howard, M., Hallam, S.D., Murrell, S.A.F., Jones, N., Sanderson, T.J.O., Ponter, A.R.S., 1986. Nonsimultaneous Failure And Ice Loads On Arctic Structures, in: Offshore Technology Conference. Houston, Texas. https://doi.org/10.4043/5127-MS

Barrette, P., Pond, J., Jordaan, I., 2002. Ice damage and layer formation in small-scale indentation experiments, in: Proceedings of the 16th IAHR International Symposium on Ice. International Association for Hydraulic Research, Dunedin, New Zealand, vol. 3 pp. 246–253.

Bjerkås, M., Alsos, H.S., Meese, A., 2013a. Ice induced vibrations-observations of a full scale lock-in event, in: The Twenty-Third International Offshore and Polar Engineering Conference. International Society of Offshore and Polar Engineers, Alaska, USA, pp. 1272–1279.

Bjerkås, M., Lonoy, C., Gurtner, A., 2013b. Ice- Induced Vibrations and Effects of Ice Temperature. Int. J. Offshore Polar Eng. 23, 9–14.

Bjerkås, M., Skiple, A., 2005. Occurrence of continuous and intermittent crushing during ice-structure interaction, in: Proceedings of the 18th International Conference on Port and Ocean Engineering under Arctic Conditions (POAC'05). PostDam,NY, vol. 3 pp. 1131–1140.

Blenkarn, K.A., 1970. Measurement and analysis of ice forces on cook inlet structures, in: Proceedings of the Annual Offshore Technology Conference. Dallas, TX, United States, vol. 1970-April pp. 365–375. https://doi.org/10.4043/1261-MS

Browne, T., Taylor, R., Jordaan, I., Gürtner, A., 2013. Small-scale ice indentation tests with variable structural compliance. Cold Reg. Sci. Technol. 88, 2–9. https://doi.org/10.1016/j.coldregions.2012.12.006

Croasdale, K.R., Morgenstern, N.R., Nuttall, J.B., 1977. Indentation Tests to Investigate Ice Pressures on Vertical Piers. J. Glaciol. 19, 301–312. https://doi.org/10.3189/S0022143000029361

Crocker, J.C., Grier, D.G., 1996. Methods of Digital Video Microscopy for Colloidal Studies. J. Colloid Interface Sci. https://doi.org/10.1006/jcis.1996.0217

Daley, C., 1991. Ice edge contact a brittle failure process model, Acta Polytechnica Scandinavica, Mechanical Engineering Series. D.Tech, Helsinki University of Technology.

Engelbrektson, A., 1977. Dynamic ice loads on a lighthouse structure, in: Proceedings of the 4th International Conference on Port and Ocean Engineering under Arctic Conditions (POAC'77). St.John's, Newfoundland, vol. 2 pp. 654–663.

Eranti, E., 1992. Dynamic ice structure interaction: theory and applications, PhD Dissertation. VTT Technical Research Center of Finland, Helsinki University of Technology.

Frederking, R., 2004. Ice pressure variations during indentation, in: Proceeding of the 17th IAHR International Symposium on Ice. International Association for Hydraulic Research, Saint Petersburg, Russia, vol. 2 pp. 307–314.

Frederking, R., Jordaan, I.J., McCallum, J.S., 1990. Field tests of ice indentation at medium scale: Hobson's Choice ice island 1989, in: Proceedings of the 10th IAHR International Symposium on Ice. International Association for Hydraulic Research, Espoo, Finland, vol. 2 pp. 931–944.

Frederking, R., Sudom, D., 2006. Maximum ice force on the Molikpaq during the April 12, 1986 event. Cold Reg. Sci. Technol. 46, 147–166. https://doi.org/10.1016/j.coldregions.2006.08.019

Frost, H.J., 2001. Mechanisms of crack nucleation in ice. Eng. Fract. Mech. https://doi.org/10.1016/S0013-7944(01)00036-4

Gagnon, R., 2011. An inside look at ice-crushing induced vibration and lock-in, in: Proceedings of the 21st International Conference on Port and Ocean Engineering under Arctic Conditions (POAC'11). Montreal, Canada.

Gagnon, R., 1999. Consistent observations of ice crushing in laboratory tests and field experiments covering three orders of magnitude in scale, in: Proceedings of The15th International Conference on Port and Ocean Engineering under Arctic Conditions (POAC'99). Helsinki, Finland, vol. 1 p. 12.

Gagnon, R.E., 1994. Generation of melt during crushing experiments on freshwater ice. Cold Reg. Sci. Technol. 22, 385–398. https://doi.org/10.1016/0165-232X(94)90022-1

Gopalkrishnan, R., 1993. Vortex-Induced Forces on Oscillating Bluff Cylinders, PhD Thesis. Woods Hole Oceanographic Institution, Massachusetts Institute of Technology.

Hendrikse, H., Metrikine, A., 2016. Edge indentation of ice with a displacement-controlled oscillating cylindrical structure. Cold Reg. Sci. Technol. https://doi.org/10.1016/j.coldregions.2015.10.013

Hendrikse, H., Metrikine, A., 2015. Interpretation and prediction of ice induced vibrations based on contact area variation. Int. J. Solids Struct. 75–76, 336–348. https://doi.org/10.1016/j.ijsolstr.2015.08.023

Hendrikse, H., Metrikine, A., Evers, K.U., 2012. A method to measure the added mass and added damping in dynamic ice-structure interation: Deciphering ice induced vibrations, part 3, in: Proceeding of the 21st IAHR International Symposium on Ice. International Association for Hydraulic Research, Dalian, China, pp. 972–984.

Hossain, R., Taylor, R., Moro, L., 2018. An assessment of sensitivity of the self-excited modelling approach for simulating dynamic ice-structure interactions to changes in temperature and scale effects. Ocean Eng. 165, 410–425. https://doi.org/10.1016/j.oceaneng.2018.07.029

Huang, G., Liu, P., 2009. A dynamic model for ice-induced vibration of structures. J. Offshore Mech. Arct. Eng. 131, 1–6. https://doi.org/10.1115/1.2979795

ISO 19906, 2010. Petroleum and natural gas industries — Arctic offshore structures. Int. Organ. Stand.

Jefferies, M., Kärnä, T., Løset, S., 2008. Field data on the magnification of ice loads on vertical structures, in: Proceedings of the 19th IAHR International Symposium on Ice. International Association for Hydraulic Research, Vancouver, BC, Canada., vol. 2 pp. 1325–1344.

Jefferies, M., Wright, W., 1988. Dynamic response of “Molikpaq” to ice structure interaction, in: Proceedings of the International Offshore Mechanics and Arctic Engineering Symposium. Houston, Texas, USA, vol. 4 pp. 201–220.

Ji, X., Oterkus, E., 2016. A dynamic ice-structure interaction model for ice-induced vibrations by using van der pol equation. Ocean Eng. 128, 147–152. https://doi.org/10.1016/j.oceaneng.2016.10.028

Joensuu, A., 1990. Ice pressure measurements using PVDF film. J. Offshore Mech. Arct. Eng. 112, 91–95. https://doi.org/10.1115/1.2919841

Johnston, M.E., Croasdale, K.R., Jordaan, I.J., 1998. Localized pressures during ice-structure interaction: relevance to design criteria. Cold Reg. Sci. Technol. 27, 105–117. https://doi.org/10.1016/S0165-232X(97)00026-8

Jordaan, I., Bruce, J., Hewitt, K., Frederking, R., 2011. Re-evaluation of ice loads and pressures measured in 1986 on the Molikpaq structure, in: Proceedings of the 21st International Conference on Port and Ocean Engineering under Arctic Conditions (POAC'11). Montréal, Canada.

Jordaan, I., Mckenna, R., 1988. Modelling of progressive damage in ice, in: Proceeding of 9th International Symposium on Ice. International Association for Hydraulic Research, Sapporo, Japan, vol. 2 pp. 585–624.

Jordaan, I., Singh, S., 1994. Compressive Ice failure: Critical Zones of High Pressure, in: Proceeding of the 12th IAHR International Symposium on Ice. International Association for Hydraulic Research, Trondheim, Norway, vol. 1 pp. 505–514.

Jordaan, I., Taylor, R., 2011. Viscoelasticity, damage and ice behaviour in compression, in: Proceedings of the 21st International Conference on Port and Ocean Engineering under Arctic Conditions (POAC'11). Montréal, Canada.

Jordaan, I., Xiao, J., Wells, J., Derradji-Aouat, A., 2008. Ice crushing and cyclic loading in compression, in: Proceeding of the 19th IAHR International Symposium on Ice. International Association for Hydraulic Research, Vancouver, British Columbia, pp. 1011–1023.

Jordaan, I.J., 2001. Mechanics of ice-structure interaction. Fract. Ice 68, 1923–1960. https://doi.org/10.1016/S0013-7944(01)00032-7

Jordaan, I.J., Taylor, R.S., Wells, J., (2009). Ice Crushing, Damaged Layers and Pressure-Area Relationships. Proceedings of the 20th International Conference on Port and Ocean Engineering under Arctic Conditions. Lulea, Sweden.

Jordaan, I.J., Maes, M.A., Brown, P.W., Hermans, I.P., 1993. Probabilistic Analysis of Local Ice Pressures. J. Offshore Mech. Arct. Eng. 115, 83–89. https://doi.org/doi:10.1115/1.2920096

Kachanov, M.L., 1982. A microcrack model of rock inelasticity part II: Propagation of microcracks. Mech. Mater. https://doi.org/10.1016/0167-6636(82)90022-9

Kamesaki, K., Tsukuda, H., Yamauchi, Y., 1997. Experimental Studies On Nonsimultaneous Failure Characteristics of Vertical Sided Indentors, in: Proceedings of 7th International Offshore and Polar Engineering Conference (ISOPE'97). International Society of Offshore and Polar Engineers, Honolulu, Hawaii, USA, vol. 2 pp. 387–393.

Kamio, Z., Takawaki, T., Matsushita, H., Takeuchi, T., Sakai, M., Terashima, T., Akagawa, S., Nakazawa, N., Saeki, H., 2000. Medium Scale Field Indentation Tests: Physical Characteristics of First-Year Sea Ice At Notoro Lagoon, Hokkaido, in: The Tenth International Offshore and Polar Engineering Conference. International Society of Offshore and Polar Engineers.

Kärnä, T., Kamesaki, K., Tsukuda, H., 1999. A numerical model for dynamic ice– structure interaction. Comput. Struct. 72, 645–658. https://doi.org/10.1016/S0045-7949(98)00337-X

Kärnä, T., Qu, Y., Yue, Q., 2006. Baltic model of global ice forces on vertical structures, in: Proceeding of the 18th IAHR International Symposium on Ice. International Association for Hydraulic Research, Sapporo, Japan, vol. 2 pp. 253–260.

Karr, D.G., Troesch, A.W., Wingate, W.C., 1993. Nonlinear dynamic response of a simple ice-structure interaction model. J. Offshore Mech. Arct. Eng. 115, 246–252. https://doi.org/10.1115/1.2920119

Kennedy, K.P., Jordaan, I.J., Maes, M.A., Prodanovic, A., 1994. Dynamic activity in medium-scale ice indentation tests. Cold Reg. Sci. Technol. https://doi.org/10.1016/0165-232X(94)90004-3

Kry, P.R., 1978. A Statistical Prediction of Effective Ice Crushing Stresses on Wide Structure, in: Proceedings of the 5th IAHR International Symposium on Ice. International Association for Hydraulic Research, Lulea, Sweden, vol. 1 pp. 33–47.

Kujala, P., 1996. Modelling of nonsimultaneous ice crushing as a poisson random process. Int. J. Offshore Polar Eng. 6, 138–143.

Løset, S., Shkhinek, K.N., Gudmestad, O., Høyland, K., 2006. Actions from ice on arctic offshore and coastal structures. LAN, St. Petersburg, Russia.

Määttänen, M., 1978. On conditions for the rise of self-excited ice-induced autonomous oscillations in slender marine pile structures. Winter Navigation Research Board.

Määttänen, M., Løset, S., Metrikine, A., Evers, K.-U., Hendrikse, H., Lønøy, C., Metrikin, I., Nord, T., Sukhorukov, S., 2012. Novel ice induced vibration testing in large-scale facility: Deciphering

ice induced vibrations, Part 1, in: Proceedings of the 21st IAHR International Symposium on Ice. International Association for Hydraulic Research, Dalian, China, pp. 946–958.

Mackey, T., Wells, J., Jordaan, I., Derradji-Aouat, A., 2007. Experiments on the fracture of polycrystalline ice, in: Proceedings of the 19th International Conference on Port and Ocean Engineering under Arctic Conditions (POAC'07). Dalian, China, vol. 1 pp. 339–349.

Matlock, H., Dawkins, W.P., Panak, J.J., 1969. A model for the prediction of ice-structure interaction, in: Proceedings of the Annual Offshore Technology Conference. Dallas, Texas, vol. 1969-May pp. 687–693.

McQueen, H., Srinil, N., 2015. Modelling two-dimensional ice-induced vibrations of offshore structures with geometric nonlinearities, in: Proceedings of the ASME 2015 34th International Conference on Ocean, Offshore and Arctic Engineering (OMAE2015). American Society of Mechanical Engineers (ASME), vol. 8 . https://doi.org/10.1115/OMAE201541075

Meglis, I.L., Melanson, P.M., Jordaan, I.J., 1999. Microstructural change in ice: II. Creep behavior under triaxial stress conditions. J. Glaciol. 45, 438–448. https://doi.org/10.3189/S0022143000001295

Melanson, P.M., Meglis, I.L., Jordaan, I.J., Stone, B.M., 1999. Microstructural change in ice: I. Constant-deformation-rate tests under triaxial stress conditions. J. Glaciol. 45, 417–437. https://doi.org/10.3189/S0022143000001271

Notz, D., Worster, M.G., 2009. Desalination processes of sea ice revisited. J. Geophys. Res. Ocean. 114. https://doi.org/10.1029/2008JC004885

O’Rourke, B.J., Jordaan, I.J., Taylor, R., Gürtner, A., 2016a. Experimental investigation of oscillation of loads in ice high-pressure zones, part 2: Double indentor system — Coupling and synchronization of high-pressure zones. Cold Reg. Sci. Technol. 124, 11–24. https://doi.org/10.1016/j.coldregions.2015.12.002

O’Rourke, B.J., Jordaan, I.J., Taylor, R.S., Gürtner, A., 2016b. Experimental investigation of oscillation of loads in ice high-pressure zones, part 1: Single indentor system. Cold Reg. Sci. Technol. 124, 25–39. https://doi.org/10.1016/j.coldregions.2015.12.005

Palmer, A., Goodman, D.J., Ashby, M.F., Evans, A.G., Hutchinson, J.W., Ponter, A.R.S., 1983. Fracture and its Role in Determining Ice Forces on Offshore Structures. Ann. Glaciol. 4, 216–221. https://doi.org/DOI: 10.3189/S0260305500005504

Peyton, H., 1968. Sea ice forces. Ice pressure against structures., Technical Memorandum. National Research Council of Canada, Ottawa, Canada.

Pikovsky, A., Rosenblum, M., Kurths, J., 2003. Synchronization: a universal concept in nonlinear sciences. Cambridge university press.

Ralph, F., Jordaan, I., 2017. Local Design Pressures During Ship Ram Events Modeling the Occurrence and Intensity of High Pressure Zones, in: Proceedings of the ASME 2017 36th International Conference on Offshore Mechanics and Arctic Engineering (OMAE 2017). American Society of Mechanical Engineers (ASME), Trondheim, Norway, vol. 8 . https://doi.org/10.1115/OMAE2017-62545

Richard, M., Taylor, R.S., 2014. Analysis of high pressure zone attributes from tactile pressure sensor field data, in: ASME 2014 33rd International Conference on Ocean, Offshore and Arctic

Engineering (OMAE 2014). American Society of Mechanical Engineers (ASME), San Francisco, CA, United states. https://doi.org/10.1115/OMAE2014-24342

Riska, K., 2018. Ice edge failure process and modelling ice pressure. Philos. Trans. R. Soc. A Math. Phys. Eng. Sci. 376, 20170340. https://doi.org/10.1098/rsta.2017.0340

Riska, K., 1991. Observations of the line-like nature of ship-ice contact, in: Proceedings of the 11th International Conference on Port and Ocean Engineering under Arctic Conditions (POAC'91). St. John's, NL, Canada, vol. 2 pp. 785–811.

Saeki, H., Hirayama, K., Takeuchi, T., Akagawa, S., Kawamura, M., Nakazawa, N., Terashima, T., Matsushita, H., Sakai, M., Honda, H., 1998. Medium-Scale Field Indentation Test (MSFIT): Results of 1997 Winter Tests, The Eighth International Offshore and Polar Engineering Conference. International Society of Offshore and Polar Engineers.

Sanderson, T.J.O., 1988. Ice mechanics : risks to offshore structures. London, UK ; Boston : Graham & Trotman, London, UK ; Boston.

Sarpkaya, T., 1978. Fluid Forces on Oscillating Cylinders. J Waterw Port Coast. Ocean Div Proc ASCE 104, 275–290.

Schulson, E.M., 2001. Brittle failure of ice. Eng. Fract. Mech. 68, 1839–1887. https://doi.org/https://doi.org/10.1016/S0013-7944(01)00037-6

Schulson, E.M., Duval, P., 2009. Creep and fracture of ice. Cambridge University Press Cambridge.

Schwarz, J., Jochmann, P., 2001. Ice force measurements within the LOLEIF-project, in: Proceedings of the 16th International Conference on Port and Ocean Engineering under Arctic Conditions (POAC'01). Ottawa, Canada, vol. 2 pp. 669–682.

Singh, S.K., Jordaan, I.J., Xiao, J., Spencer, P.A., 1995. The flow properties of crushed ice. J. Offshore Mech. Arct. Eng. 117, 276–282. https://doi.org/10.1115/1.2827234

Sodhi, D., 1994. A Theoretical Model for Ice-structure Interaction, in: Proceedings of the ASME 1994 13th International Conference on Ocean, Offshore and Arctic Engineering (OMAE1994). American Society of Mechanical Engineers (ASME), New York, vol. IV pp. 29–34.

Sodhi, D., 1988. Ice-induced vibration of structures, in: Proceeding of the 9th IAHR International Symposium on Ice. International Association for Hydraulic Research, Sapporo, Japan, vol. 2 pp. 625–657.

Sodhi, D.S., Takeuchi, T., Nakazawa, N., Akagawa, S., Saeki, H., 1998. Medium-scale indentation tests on sea ice at various speeds. Cold Reg. Sci. Technol. 28, 161–182. https://doi.org/10.1016/S0165-232X(98)00017-2

Spencer, P., Masterson, D.M., Lucas, J., Jordaan, I.J., 1992. The Flow Properties of Crushed Ice I: Experimental Observation and Apparatus, in: Proceedings of the 11th IAHR International Symposium on Ice. International Association for Hydraulic Research, vol. 1 pp. 158–168.

Staroszczyk, R., 2019. Ice Mechanics for Geophysical and Civil Engineering Applications. Springer International Publishing, Cham. https://doi.org/10.1007/978-3-030-03038-4

Takeuchi, T., Masaki, T., Akagawa, S., Kawamura, M., Nakazawa, N., Terashima, T., Honda, H., Saeki, H., Hirayama, K., 1997. Medium-Scale Field Indentation Tests (MSFIT) - Ice Failure

Characteristics In Ice/Structure Interactions, in: The Seventh International Offshore and Polar Engineering Conference. International Society of Offshore and Polar Engineers, Hawaii, USA.

Takeuchi, T., Saeki, H., 1994. Ice load on wide structure in non-simultaneous failure of ice sheet by shot noise model, in: Proceedings of the 12th IAHR International Symposium on Ice. International Association for Hydraulic Research, Trondheim, Norway, vol. 1 pp. 219–228.

Taylor, R., Frederking, R., Jordaan, I., 2008. The nature of high pressure zones in compressive ice failure, in: Proceeding the 19th IAHR International Symposium on Ice. International Association for Hydraulic Research, Vancouver, BC, Canada., vol. 2 pp. 1001–1010.

Taylor, R.S., 2010. Analysis of scale effect in compressive ice failure and implications for design. PhD Thesis, Memorial University of Newfoundland.

Taylor, R.S., Jordaan, I.J., 2011. The Effects of Non-simultaneous Failure, Pressure Correlation, And Probabilistic Averaging On Global Ice Load Estimates, in: The Twenty-First International Offshore and Polar Engineering Conference. International Society of Offshore and Polar Engineers, Hawaii, USA.

Taylor, R.S., Richard, M., 2014. Development of a probabilistic ice load model based on empirical descriptions of high pressure zone attributes, in: Proceedings of the ASME 2014 33rd International Conference on Ocean, Offshore and Arctic Engineering (OMAE2014). American Society of Mechanical Engineers (ASME), vol. 10 . https://doi.org/10.1115/OMAE2014-24353

Taylor, R.S., Richard, M., Hossain, R., 2019. A Probabilistic High-Pressure Zone Model for Local and Global Loads During Ice-Structure Interactions. J. Offshore Mech. Arct. Eng. 141. https://doi.org/10.1115/1.4042386

Timco, G., 1987. Indentation and Penetration of Edge-Loaded Freshwater Ice Sheets in the Brittle Range. J. Offshore Mech. Arct. Eng. 109, 287–294.

Timco, G., Wright, B., 2005. Multi-Year Ice Loads on the Molikpaq: May 12, 1986 Event;, in: Proceedings 18th International Conference on Port and Ocean Engineering under Arctic Conditions (POAC '05). Postdam, NY, vol. 1 pp. 453–462.

Timco, G.W., Weeks, W.F., 2010. A review of the engineering properties of sea ice. Cold Reg. Sci. Technol. 60, 107–129. https://doi.org/10.1016/j.coldregions.2009.10.003

Tuhkuri, J., 1996. Experimental investigations and computational fracture mechanics modelling of brittle ice fragmentation, Acta Polytechnica Scandinavica, Mechanical Engineering Series.

Tuhkuri, J., 1995. Experimental observations of the brittle failure process of ice and ice-structure contact. Cold Reg. Sci. Technol. 23, 265–278. https://doi.org/10.1016/0165-232X(94)00018-S

Wang, L., Xu, J., 1991. Description of dynamic ice-structure interaction and the ice force oscillator model, in: Proceedings of the 11th International Conference on Port and Ocean Engineering under Arctic Conditions (POAC'91). St. John's, NL, Canada, vol. 1 pp. 141–154.

Weiss, G., 1977. Shot noise models for the generation of synthetic streamflow data. Water Resour. Res. 13, 101–108. https://doi.org/10.1029/WR013i001p00101

Wells, J., Jordaan, I., Derradji-Aouat, A., Taylor, R., 2011. Small-scale laboratory experiments on the indentation failure of polycrystalline ice in compression: Main results and pressure distribution. Cold Reg. Sci. Technol. 65, 314–325. https://doi.org/10.1016/j.coldregions.2010.11.002

Withalm, M., Hoffmann, N.P., 2010. Simulation of full-scale ice-structure-interaction by an extended Matlock-model. Cold Reg. Sci. Technol. 60, 130–136. https://doi.org/10.1016/j.coldregions.2009.09.006

Wright, B., Timco, G., 1994. A Review of Ice Forces and Failure Modes on the Molikpaq, in: Proceedings of the 12th IAHR International Symposium on Ice. International Association for Hydraulic Research, Trondheim, Norway, vol. 2 pp. 816–825.

Xu, J., Bernt, J.L., 1981. Dynamic response of a jacket platform subjected to ice loads, in: Proceedings of the 6th International Conference on Port and Ocean Engineering under Arctic Conditions (POAC'81). Quebec, Canada, vol. 1 pp. 502–516.

Yang, G., 2000. Bohai Sea ice conditions. J. Cold Reg. Eng. 14, 54–67. https://doi.org/10.1061/(ASCE)0887-381X(2000)14:2(54)

Yue, Q., Li, L., 2003. Ice problems in Bohai Sea oil exploitation, in: Proceedings of the 17th International Conference on Port and Ocean Engineering under Arctic Conditions (POAC'03). Trondheim, Norway, vol. 1 pp. 151–164.

Yue, Q., Zhang, X., Bi, X., Shi, Z., 2001. Measurements and analysis of ice induced steady state vibration, in: Proceedings of the 16th International Conference on Port and Ocean Engineering under Arctic Conditions (POAC'01). Ottawa, Canada, pp. 413–420.

Chapter: 3 An Assessment of Sensitivity of the Self-excited Modelling Approach for Simulating Dynamic Ice-Structure Interactions to Changes in Temperature and Scale Effects

Preface

The chapter has been published as an original research article in the journal of Ocean Engineering[1]. As the primary author, I was responsible for conducting the literature review, developing the model, performing the analysis and writing the article. My co-authors Dr. Rocky Taylor and Dr. Lorenzo Moro provided valuable feedback at different stages of the analysis and preparation of the article.

[1] Hossain, R., Taylor, R., Moro, L., 2018. An assessment of sensitivity of the self-excited modelling approach for simulating dynamic ice-structure interactions to changes in temperature and scale effects. Ocean Eng. 165, 410–425. https://doi.org/10.1016/j.oceaneng.2018.07.029

Based on the experimental results available in the literature, the effect of temperature and scale has been considered in the compressive strength vs. stress-rate relationship. The self-excited ice-induced vibration model was then evaluated to identify how these effects can propagate through the model and affect the predicted ice-induced vibration response. The results suggest that the uncertainty associated with these effects can be significant and a more robust approach is required for modelling ice-induced vibrations.

Abstract

Empirical relationships of compressive ice strength as a function of stress rate have been utilized in models of vibrations that arise during coupled ice-structure interactions. Central to current self-excited models (SEM) is a deterministic relationship of compressive ice strength as a function of stress rate based on uniaxial compressive strength data obtained from thin, first-year sea ice. However, full-scale observations, laboratory test data and fundamental knowledge of ice material behaviour suggest that any such relationship would be influenced by factors such as temperature and the scale of the interaction. In this chapter, the influence of temperature and scale effects is examined and first-order estimates of their effect on modifying the assumed strength vs. stress rate relationship are presented. This approach is used to assess the sensitivity of the SEM method to changes in environmental and interaction conditions. Results suggest that accounting for changes in ice temperature and the scale of interaction considerably affect ice-induced vibration responses predicted by the model. Additional large-scale experiments, full-scale data and the development of physics-based models of ice compressive failure are needed to better account for different ice conditions and different sized structures that may be considered in design.

3.1 Introduction

3.1.1 Background

When designing structures for ice environments, ice-induced vibrations (IIV), especially steady state vibrations, are an important engineering consideration. The international standard for petroleum and natural gas industries – Arctic offshore structures (ISO 19906, 2010) provides design guidelines for dynamic ice actions (section A.8.2.6 of ISO 19906, 2010) and explicitly discusses the susceptibility of IIV through frequency lock-in (section A.8.2.14 of ISO 19906, 2010). Frequency lock-in refers to the condition when ice fails at a frequency close to the natural frequency of the structure (primarily due to crushing) and causes a dynamic amplification in structural response. Such behavior has been observed in the field especially when the natural frequency of the structure is within the range of 1-2*Hz* (Peyton, 1968; Jefferies and Wright, 1988; Bjerkås et al., 2013a). The guideline provided in the ISO code recommends identifying the lowest structural mode susceptible to IIV and checking the stability criterion through modal damping. To calculate the modal amplitude at the ice action point, the method referred in the ISO code (Määttänen, 1978) uses the compressive strength - stress rate relationship proposed by Blenkarn (1970). This relationship (shown in Figure 3.1) uses uniaxial compressive data collected by Peyton on thin, first-year ice on Cook inlet, Alaska (Peyton, 1968). The data shows ice strength increases as a function of loading rate up to a certain point and then start decreasing as loading rate is increased further until reaching to a point after which it is almost constant. Such behavior has also been observed and reported by other authors (Schwarz, 1970; Wu et al., 1976; Michel and Toussaint, 1977). It has been postulated that the negative slope in that relationship serves as a source of negative damping and if this is greater than the structural damping then the structural

response will grow over time. Blenkarn termed this as self-excited vibration to explain IIV and a rigorous model was later proposed by Määttänen. Although the Peyton relationship was based on uniaxial compression test data, this relationship has been treated as universal and has been applied to full-scale lighthouse structures. However, fundamental material behavior of ice suggests that such relationship would be significantly influenced by ice properties and interaction conditions. In this chapter, the variation in ice strength-stress rate relationship subjected to a variation in ice temperature and interaction scale is inferred based on the fundamental ice material behavior. The inference is then used to evaluate how such variation can propagate through the dynamic ice-structure interaction and affect IIV response.

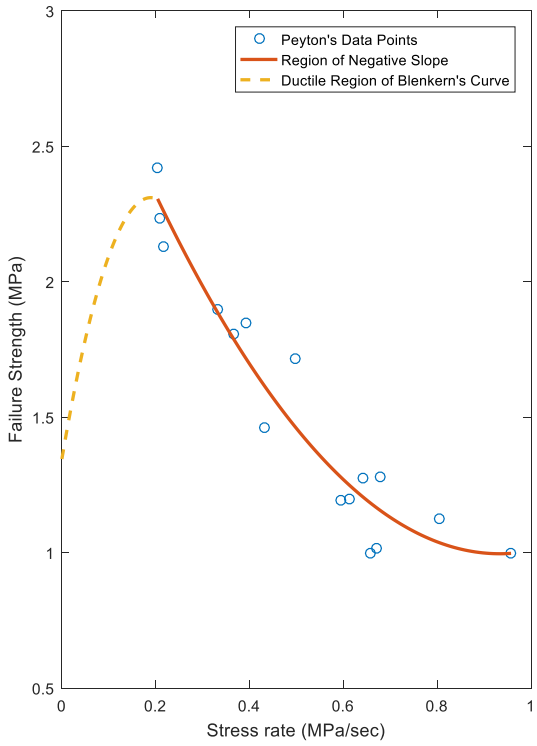

Figure 3.1 Original Blenkarn's curve based on Peyton's compressive data (drawn after Blenkarn (1970))

3.1.2 Literature review

The first scientific interest in understanding the dynamic nature of ice-structure interactions associated with IIV arose in the late 1960s when this phenomenon was first observed on fixed vertical-pile offshore platforms in Cook Inlet, Alaska (Peyton, 1968; Blenkarn, 1970). Through the use of full-scale measurements, both authors concluded that a moving ice field can induce severe vibrations to slender offshore structures; however, the explanation offered by each author regarding the cause of these IIV differed significantly. In these earliest analyses, the ice failure process was described as a stick-slip type phenomenon that followed a sawtooth loading pattern. Comparing his observations to his laboratory test series, Peyton (1968) concluded that ice has a "characteristic failure frequency". The notion that these vibrations were of a self-excited nature was first proposed by Blenkarn (1970), who correctly identified that both the properties of the ice and the structure play an important role in governing the interaction dynamics. Blenkarn also highlighted the need to consider the natural vibration modes of the structure to assess its susceptibility to damped or steady-state resonant vibrations, a condition commonly referred to as "lock-in". The physical ice conditions observed to be of most significance by Blenkarn were ice speed and thickness.

Less than a decade later, similar problems were encountered with navigational aids and lighthouse structures built in the Gulf of Bothnia, Finland, ultimately resulting in damage and in some instances failure of these structures (Engelbrektson, 1977; Määttänen, 1978). Research undertaken by Määttänen further explored the self-excited nature of ice–structure interactions associated with IIV on full-scale lighthouses (Määttänen, 1977, 1978). Similarly, channel markers in Gulf of Bothnia were also found to be prone to ice-induced vibrations. One of these markers was

instrumented in Winter 1987-1988 and severe stresses were recorded due to steady-state vibrations or “lock-in” phenomenon (Nordlund et al., 1988). Very few cycles were required for the structure to reach peak amplitude from rest which led the authors to believe that the excitation mechanism has a significant force component that is dependent on the displacement and/or velocity of the structure. Due to the observed shift between high-level and low-level amplitude, the excitation mechanism was thought to be comprised of a random force superimposed by an interaction force that is dependent on the structural displacement or velocity.

Similar dynamic effects, which ultimately led to cases of structural failure, were later reported on jacket platforms in the Bohai Sea, China (Xu and Bernt, 1981). Two jacket platforms (one of which was a small flare jacket) were reported to collapse within a period of 10 years. Based on field measurements on a full-scale six-legged jacket platform in combination with numerical analysis, it was concluded that an amplified resonant response can be expected under a certain combination of ice floe velocity, spatial ice load distribution and damping properties of the structure. To help mitigate these vibrations ice breaking cones were installed at the water level. While this did reduce the extent of ice crushing, a different cyclic failure process leading to vibrations was observed due to repeated flexural cusp failures. Also, during high tidal currents, the failure frequency of the thin ice could potentially reach of the natural frequencies of the structure (Yue and Bi, 2000; Yue et al., 2007).

In Canada, observations of dynamic ice forces acting on bridge piers (Neill, 1976; Montgomery et al., 1980) highlighted that in some structures the dynamic response of the pier may exceed the static response during a peak ice force event. As offshore technology continued improve and evolve in the 1980s, operations moved further north into increasingly challenging ice conditions.

During this time it was believed that IIV issues were most relevant for narrow structures and this issue was less of a concern for wide structures. This belief was challenged during the winter of 1986, when thick multi-year ice caused severe ice-induced vibrations leading to partial liquefaction of the foundation of the 90*m* wide Molikpaq Mobile Arctic Caisson structure, which was operating in the Beaufort Sea (Jefferies and Wright, 1988; Frederking and Sudom, 2006). Cyclic behavior with a frequency of approximately 1.4*Hz* was recorded with peak vibration amplitudes up to 10*mm* which lasted for four minutes (Timco and Wright, 2005). These IIV and associated foundation issues created significant concerns about the stability of the structure, which ultimately resulted in an evacuation of the platform. A comprehensive review of these early observations was provided by Sodhi (1988), and these incidents, along with uncertainties associated with full-scale measurements from the Molikpaq have been broadly discussed in the ice mechanics community (Jordaan et al., 2011; Taylor and Jordaan, 2011b).

To help further understand this issue, many laboratory research programs using small-scale compliant structures have been carried out (Määttänen, 1981, 1983, 2008; Toyama et al., 1983; Jordaan and Timco, 1988; Sodhi, 1989; Kärnä and Muhonen, 1990; Finn et al., 1993; Kärnä et al., 2003; Huang et al., 2007; Määttänen et al., 2011; Browne et al., 2013; Taylor et al., 2013; O'Rourke et al., 2016a, 2016b). From these studies it is observed that, in general, for speeds up to some lower limit velocity the ice loads exhibit a sawtooth pattern with a failure frequency that is proportional to the ice speed. Once the ice speed exceeds this lower limit, the IIV frequency tends to lock-in to a natural frequency of the system (typically less than the natural frequency of the structure) and the loading pattern exhibits a more sinusoidal character. As the ice speed is further increased beyond a certain upper limit velocity, the ice failure behaviour transitions to a random brittle mode with reduced amplitude. Emerging from this collective body of work is a general

consensus regarding classification of modes of dynamic ice-structure interaction as a function of loading rate into the four types put forward by (Kärnä and Trunen, 1990) described below and depicted in Figure 3.2:

(a) Creep or damage enhanced creep at a very slow loading rate where ice fails in ductile manner. The structure experiences very high global load however, no structural vibration occurs.

(b) Sawtooth or intermittent ice crushing at a faster loading rate where the loading pattern can be periodic in nature comprising of a loading and unloading phase. The structure and ice move quasi-statically in the loading phase followed by an unloading event primarily due to spalling. The sudden load drop results in a transient vibration with a relatively high acceleration. The associated acceleration may be important in designing non-structural components and devices supported by the main structure. Depending on the damping of the structure, the transient vibration eventually dies out before entering in the next loading phase.

(c) Frequency lock-in or steady-state vibration at higher loading rate where the response of the structure may become more sinusoidal in nature. The frequency of the ice force gets locked into the natural frequency of the structure even though ice speed changes slightly. If the ice speed remains within the range, the steady-state vibration can sustain for a long period having nearly constant amplitude (Yue et al., 2009). Evidence of such vibrations in full-scale have been reported by Bjerkås et al. (2013a), Nordlund et al. (1988) and others.

(d) Random or continuous ice crushing which occurs at very high interaction speed. The failure is brittle and random in nature causing a lower global load and structural displacement.

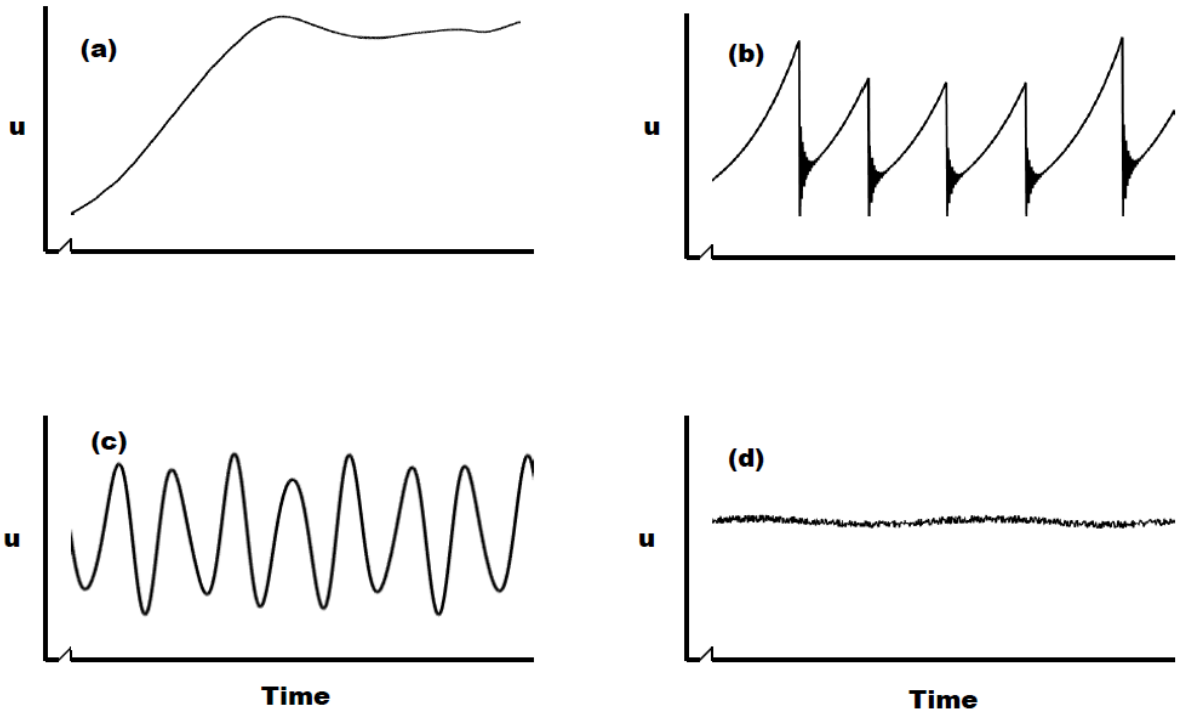

Figure 3.2 Structural Displacement vs. time for different modes of ice-structure interaction; (a) creep or damage enhanced creep, (b) sawtooth, (c) frequency lock-in and (d) random stationary. Loading rate is ascending from (a) to (d)

3.1.3 IIV modelling approaches

The most commonly employed engineering approaches to modelling ice-induced vibration can be broadly classified into two major categories. The first group considered the ice to have a characteristic crushing failure frequency (or crushing length). Matlock et al. (1969) was the first to introduce an ice-structure interaction model based on this idea and such approaches have been used to explain full-scale ice-induced vibration occurrences (Gagnon, 2012). In his classical model, Matlock assumed ice to be an ideal elastic-brittle material and the model was represented by a carriage transporting a series of uniformly spaced elastic-brittle teeth. When a tooth is in contact with the structure, the force is assumed to be linearly dependent on the deformation of the

tooth. Sodhi (1994) later modified the model using results from a number of test series (Sodhi and Nakazawa, 1988; Sodhi, 1989, 1992; Sodhi and Chin, 1992). In his model, one force cycle is divided into three phases (loading, extrusion and separation) each having its own mathematical formulation and was able to replicate the essential features of intermittent crushing. Huang and Liu (2009) also extended the Matlock model by including the discrete failure behavior, dependence of ice strength on ice velocity and randomness of failure.

The other commonly employed approach considers ice-induced vibration to be self-excited in nature. Blenkarn (1970) was the first to introduce this idea, which was later incorporated into a coupled dynamic ice-structure interaction model by Määttänen (1978). The Määttänen self-excited model (SEM) utilizes the crushing strength vs stress-rate curve first proposed by Blenkarn shown in Figure 3.1. Based on Peyton's measurements, Blenkarn proposed that the crushing strength vs stress-rate curve has a negative slope beyond a certain loading rate. Sustained ice-induced vibrations are explained in the context of this negative damping effect. The effect of relative velocity in dynamic ice-structure interactions has been considered by other researchers as well. Based on their test results, Tsuchiya et al. (1985) proposed that maximum resistance of ice should be recalculated in each time step taking into account the effect of relative velocity. Daoud and Lee (1986) considered the ice force function to follow a predefined sawtooth function and defined the velocity dependence with a Heaviside step function having the value 1 for positive relative velocity and 0 otherwise.

Kry (1978) proposed the idea of independent zones of crushing in front of a wide structure and considered that effective stresses for each zone are developed independently of the adjacent zones. Daley (1991) developed an ice failure model based on a progressive sequence of through-body

shear cracks triggered once a critical stress limit is reached, resulting in a sudden drop in force due to flaking events. Eranti (1992) used this zonal ice force concept to develop his ice-structure interaction model. The indenter is assumed to penetrate into each zone until a critical ice pressure is reached which is both loading rate dependent and has a certain degree of randomness. The ice zone fails a finite distance ahead and the indenter is able to move within this zone with only minor resistance of the failed ice. Kärnä extended the idea of zonal force to simulate response of full three dimensional structures using the finite element method (Kärnä, 1992; Kärnä et al., 1999). The model also includes the soil-structure interaction to account for the foundation behavior. Ice action is considered in two phases: elastic far field and non-linear near field which are further divide into zones where the interactive forces as well as the relative displacement between the ice and structure are defined at specific contact points. The far-field response is described using rigid-body motion of ice mass and elastic displacement of ice edge. Failure in the near-field area is assumed to be horizontal splits where each layer fails independently due to the compressive force applied on it. Failure force is a function of characteristic ice failure pressure which is sampled from a log normal distribution using a base value and nominal contact area. Also, it is assumed that crushing pressure decreases by a factor of 2 when the relative velocity exceeds a certain range. Withalm and Hoffmann (2010) used the zonal ice force concept to extend the Matlock model for full-scale round structures. Ice-induced vibration has also been linked to contact area (Hendrikse and Metrikine, 2015) and the reduced velocity concept used in vortex-induced vibration (Palmer et al., 2010).

Despite the above progress, significant gaps remain in explaining IIV and developing engineering models that are linked to fundamental mechanics of ice failure. In this chapter, the effects of temperature and scale on the strength vs. loading-rate curve (shown in Figure 3.1) are investigated

to identifying how accounting for such effects influences design assessments of susceptibility of structures to ice-induced vibration and assess if accounting for such factors increases agreement with full-scale observations. While it is clear that the assumption of the universality of this relationship is convenient for analysis purposes, it is less clear if such a relationship holds for different ice conditions and scales, since insufficient full-scale data exists on which to validate such an assumption. For this reason, in the analysis presented herein, inferences have been made regarding the anticipated effects of these factors on the strength vs stress rate relationship to explore its effect on steady state ice-induced vibrations.

3.2 Model Description

3.2.1 Self-excited model (SEM)

Models identified in the current ISO 19906 guidelines include negative damping of ice as a contributing factor in frequency lock-in. To identify the lock-in frequency, ISO suggests identifying the natural modes which are sensitive to ice-induced vibration. The conditions for dynamic stability developed by Määttänen (1978) and Kärnä et al. (1999) can be used in such cases. For a natural mode n, the dynamic stability can be achieved if the relative damping coefficient of the structure ζ_n is larger than the opposite contribution of ice action. Mathematically, dynamic stability will be achieved if the following equation is satisfied:

$$\boldsymbol{\zeta_n \geq \frac{\emptyset_{nC}{}^2}{4\pi f_n M_n} . h . \theta} \qquad (3.1)$$

where

ζ_n is the damping ratio of the eigenmode;

$\emptyset_{nC}$ is the non-normalized modal amplitude at the ice action point;

M_n is the true modal mass, expressed in kilograms; $[kg]$

f_n is the natural frequency of the eigenmode, expressed in hertz; $[Hz]$

h is the ice thickness, expressed in meters; $[m]$

θ is a coefficient, the suggested value of which is 40×10^6 kilograms per metre-second; $[kg/ms]$

Once the lowest natural mode susceptible to frequency-lock in is identified, a sawtooth forcing function with a frequency equal to the natural frequency of the mode is generated. In this approach, the forcing function accounts for ice-structure coupling by using the strength vs. stress rate relationship to calculate the instantaneous ice force as a function of the relative velocity between the ice and the structure, as is described further below.

In the present study, the Määttänen SEM has been used since this model is based solely on the strength-stress rate relationship whereas the Kärnä model accounts for rate dependence by decreasing ice strength by a factor of 2 when the relative velocity between the ice and structure exceeds a transitional range (100-250*mm/s*) (Kärnä et al., 1999). In Määttänen's SEM the following assumptions have been made:

- Ice is always in a continuous crushing state hence the strength vs. stress-rate curve can be used, except for cases where the structure's velocity is greater than ice velocity. In such cases, the interaction force goes to zero.
- The crushing strength is averaged out over the interaction area.
- The elastic deformation of ice and the viscoelastic behavior are ignored.

At the beginning of a loading cycle, the deflection of the structure increases as the ice sheet advances, leading to an increase in resistance from the structure. As the structural resistance continues to build with increasing deflection, the rate of deflection relative to the ice velocity begins to decrease, leading to an increase in the loading rate. This phase of the interaction cycle continues until the structure comes to rest for an instant (at its peak deflection), at which point the resistance from the structure has increased to the point that it exceeds the maximum ice strength, causing the structural movement to change direction triggering the onset of rebounding. As the structure begins to rebound it starts to move towards the ice sheet, causing the loading rate to further increase, which in turn cause the ice crushing strength to decrease. As the structure accelerates during the rebounding process, the loading rate further increases; resulting in continued decreases in ice strength. Since the structural deflection decreases during rebounding, the associated resistance force also decreases. As rebounding continues further the structure eventually begins to decelerate, and the loading rate begins to decrease (since the structure is advancing more slowly towards the ice) causing the ice strength to begin to increase again. The structure continues to decelerate until it eventually comes to rest for an instant before the structural movement again reverses direction and begins deflecting at the onset of the next loading cycle.

The equation for dynamic ice-structure interaction is as follows:

$$[\boldsymbol{M}]\{\ddot{\boldsymbol{x}}\} + [\boldsymbol{C}]\{\dot{\boldsymbol{x}}\} + [\boldsymbol{K}]\{\boldsymbol{x}\} = \{\boldsymbol{F}\} \qquad (3.2)$$

According to the self-excitation vibration model, ice force is only a function of relative velocity. Considering only one mode of vibration, the equation can be simplified as:

$$\boldsymbol{m\ddot{x} + c\dot{x} + kx = F(v - \dot{x})} \qquad (3.3)$$

where $\boldsymbol{v}$ is the ice drift velocity.

For small motion, the forcing function can be expanded as:

$$\boldsymbol{F(v - \dot{x}) = F(v) - \dot{x}\frac{\partial F(v)}{\partial v}} \tag{3.4}$$

So equation (3.3) becomes:

$$\boldsymbol{m\ddot{x} + \left(c + \frac{\partial F}{\partial v}\right)\dot{x} + kx = F(v)} \tag{3.5}$$

If the term $\frac{\partial F}{\partial v}$ is negative and numerically greater than the structural damping coefficient *c*, then there will be net negative damping in equation (3.5), which would lead to the growth of a structural response with time (self-excited vibration).

The roots of the equation (3.5) are complex conjugate pairs and the appearance of the self-excited vibration depends on the sign of the real part (vibration will arise for positive real part and no vibration will arise if the sign is negative). The stability condition is valid only for one ice velocity at a time. However, when assessing the potential onset of oscillations, it is sufficient to check for stability at the ice velocity corresponding to the steepest negative slope in the non-linear crushing strength vs. loading rate curve. For a root with a positive real part, vibration amplitudes are supposed to increase exponentially, however, in practice such growth will tend to limit cycles. This occurs even for constant ice velocities since the oscillation of the relative velocity will occur due to the deflection-rebound cycle of the structure. Correspondingly, as the relative velocity changes, the instantaneous strength moves along the curve, and once it returns to the positive slope region, this will suppress further amplitude growth. Thus, all self-excited ice-induced vibration will have a stable limit cycle which is also termed as stability as-large (e.g. the condition is satisfied). For a root with a negative real part, vibration amplitudes decay exponentially. However, if the roots of the equilibrium equations are not calculated at the point with steepest negative slope

of the strength vs loading rate curve, obtaining negative real parts still does not guarantee absolute stability. A change in relative velocity in the deflection-rebound cycle described above can result in vibration of the structure due to oscillation of the relative velocity, which can very soon yield to such a velocity that the corresponding point in the strength vs stress-rate curve no longer lies on the area of negative slope suppressing further amplitude growth.

The loading rate (stress-rate) of the ice sheet is calculated with the equation originally deduced by (Blenkarn, 1970)

$$\dot{\boldsymbol{\sigma}} = (\boldsymbol{v_0} - \dot{\boldsymbol{x}}_{\boldsymbol{i}}) \frac{\boldsymbol{4\sigma_c}}{\boldsymbol{\pi a}} \boldsymbol{\cos(\theta)} \qquad (3.6)$$

where v_0 is the ice drift velocity, $\dot{x}_i$ is the velocity of the structure at the point of action, σ_c is ice crushing stress and a is the radius of the structure. The cosine term takes into account the circular form of the load distribution assumed in this model, as shown in Figure 3.3.

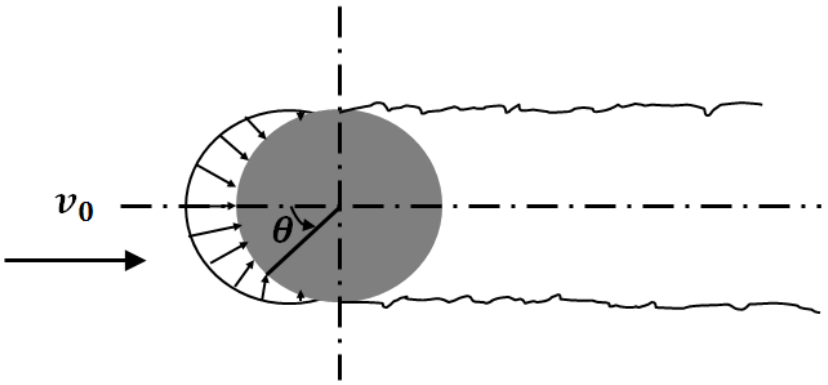

Figure 3.3 Ice pressure on a circular structure (reproduced after (Määttänen, 1978))

The ice crushing strength can be obtained from the simplified version of the piecewise linear Peyton curve shown in Figure 3.4 for j^{th} time step as

$$\boldsymbol{\sigma_c = \alpha_j + \beta_j \dot{\sigma}} \quad (3.7)$$

The linearized version of the curve requires the following parameters to define the strength-stress rate relationship:

α = Intercept in the y-axis (equal to σ_0 when loading rate is zero)

β = Slope of the crushing strength-stress rate curve

$\dot{\sigma}_1$ = Limit stress-rate of ductile region; was considered to be 0.2*MPa/s* in the original SEM

$\dot{\sigma}_2$ = Limit stress-rate of transition region; was considered to be 0.8*MPa/s* in the original SEM

By solving the two sets of equations, explicit expressions for stress rate ($\dot{\sigma}$) and crushing strength σ_c can be obtained as follows:

$$\boldsymbol{\dot{\sigma} = \frac{\alpha_j}{\frac{\pi a}{4(v_0 - \dot{x}_i)\cos(\theta)} - \beta_j}} \quad (3.8)$$

$$\boldsymbol{\sigma_c = \frac{\pi a \alpha_j}{\pi a - 4\beta_j(v_0 - \dot{x}_i)\cos(\theta)}} \quad (3.9)$$

The crushing strength of ice would be equal to the global pressure applied by ice on the structure at the waterline. Thus, integrating the ice crushing strength along the waterline circumference of the structure will give the ice-induced force, *F*, applied on the structure at the waterline given as

$$\boldsymbol{F = 2\int_0^{\pi/2} \sigma_c \, a\cos(\theta)\, h d\theta = 2ah\int_0^{\pi/2} \frac{\pi a \alpha_j \cos(\theta)}{\pi a - 4\beta_j(v_0 - \dot{x}_i)\cos(\theta)} d\theta} \quad (3.10)$$

where h is the ice thickness.

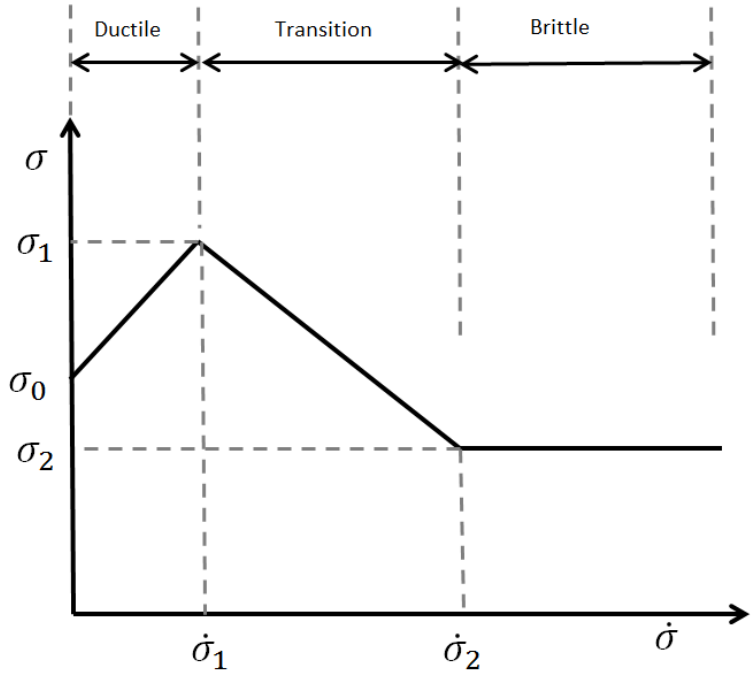

Figure 3.4 Linearized version of Blenkarn's curve (drawn after Määttänen (1978))

Using the forcing function from equation (3.10), we can now solve the system equation mentioned in equation (3.3) numerically.

3.2.2 Modification of Peyton curve parameters

The simplified assumption of linear relationship enables identification of the stability criterion in a straight forward way. As outlined above, the roots should be calculated at the steepest point of the negatively sloped portion of the strength vs. stress rate curve to ensure stability of the system (this also applies for numerical integration, as is employed here). From fundamental understanding of ice material behaviour (Michel and Toussaint, 1977; Sanderson, 1988; Schulson and Duval, 2009) it is known that changing ice conditions such as temperature and scale will influence ice

strength. On this basis, it is proposed here that changes in such conditions would be expected to affect the strength vs. stress rate curves, yielding a "family" of curves rather than a single universal curve. To ensure stability of the system for the range of conditions expected in a given design scenario, the roots should be obtained for conditions that yield the curve with highest negative slope. To perform such an analysis, it is first necessary to assess how changes in these conditions would influence the Peyton curve parameters, so that the effects of such variations on ice-induced vibration response can be assessed. In the present analysis, only the effects of temperature and pressure scale on crushing strength have been considered. Other deterministic (e.g. grain size, ice density, salinity, etc.) and probabilistic factors (randomness due to fracture) could be considered as well, but are beyond the scope of the present work.

3.2.3 Effect of temperature on Peyton curve parameters

While the effect of temperature on the Peyton strength vs. stress-rate relationship have not been reported in the literature, such effects have been studied from small-scale experiments for both freshwater ice (Wu et al., 1976) and saline ice (Schwarz, 1970). In the present work, only saline ice is considered and the work of Schwartz (1970) provides useful insights here. For the Peyton uniaxial compressive strength dataset, the average temperature for that season was reported to be $\approx$ -10°*C* (Blenkarn, 1970) and this value is assumed to be representative of the mean ice temperature for the reference strength-stress rate curve.

Schwarz (1970) found that uniaxial compressive strength of sea ice is a function of ice temperature, and that as the temperature increases, the ice becomes weaker due to growth of brine pockets, similar to the effect observed for flexural strength (e.g. Timco and Weeks, 2010) Based on these results, it is reasonable to infer that a similar trend would be expected for the Peyton relationship

as well. To provide a first-order estimate of this effect, a temperature correction factor is calculated as the ratio of maximum strength at the temperature of interest to the maximum strength at $-10℃$ from Schwarz (1970) at three stress rates: ~10^{-2}, 0.2, 0.8. These factors were applied to the Peyton relationship to account for the effect of temperature (-2°*C*, -5°*C*, -10°*C*, -20°*C*) as shown in Figure 3.5. Linear interpolation was used to obtain maximum strength at -5°*C* and -2°*C* from the data of Schwarz (1970).

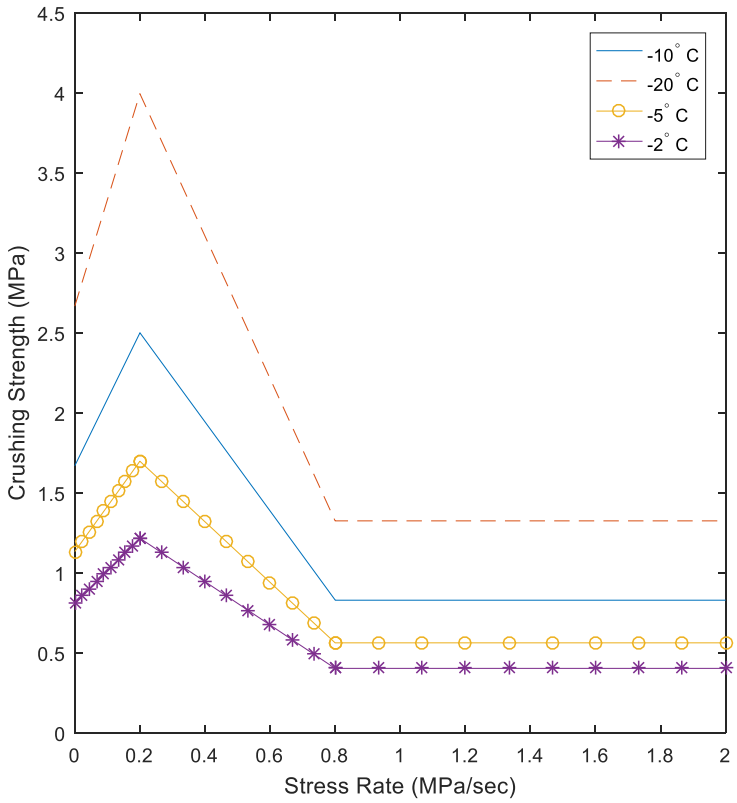

Figure 3.5 Modified Peyton`s curves based on the effect of temperature

The corresponding intercept and slope values for the modified Peyton curves considering temperature effects are listed in Table 3.1 below.

Table 3.1. α and β values for different regions in modified Peyton curves taking temperature effect into account

Parameters / Temperature	$0 < \dot{\sigma} \leq 0.2$		$0.2 < \dot{\sigma} \leq 0.8$		$\dot{\sigma} > 0.8$	
	α	β	α	β	α	β
-20$°C$	2.668	6.640	4.885	-4.449	1.326	0
-10$°C$	1.667	4.150	3.058	-2.783	0.830	0
-5$°C$	1.134	2.822	2.077	-1.891	0.564	0
-2$°C$	0.813	2.023	1.488	-1.356	0.404	0

3.2.4 Effect of ice thickness and structure width on Peyton curve parameters

The pressure-area data compiled by Sanderson (1988) corresponds to a number of datasets covering a range of scales, which clearly show a trend of decreasing average pressure with increasing interaction area. Given the importance of these scale effects for ice load estimation, as is reflected in the design methodology in ISO 19906 (2010), the strength vs. stress-rate relationships used in SEM should also account for such effects. As shown in Figure 3.6 below, there is good general agreement between the data from Sanderson, Schwarz (1970) and Peyton (1968), as well as the value obtained using the global average pressure model from ISO 19906 (evaluated at the same area as in Peyton`s data).

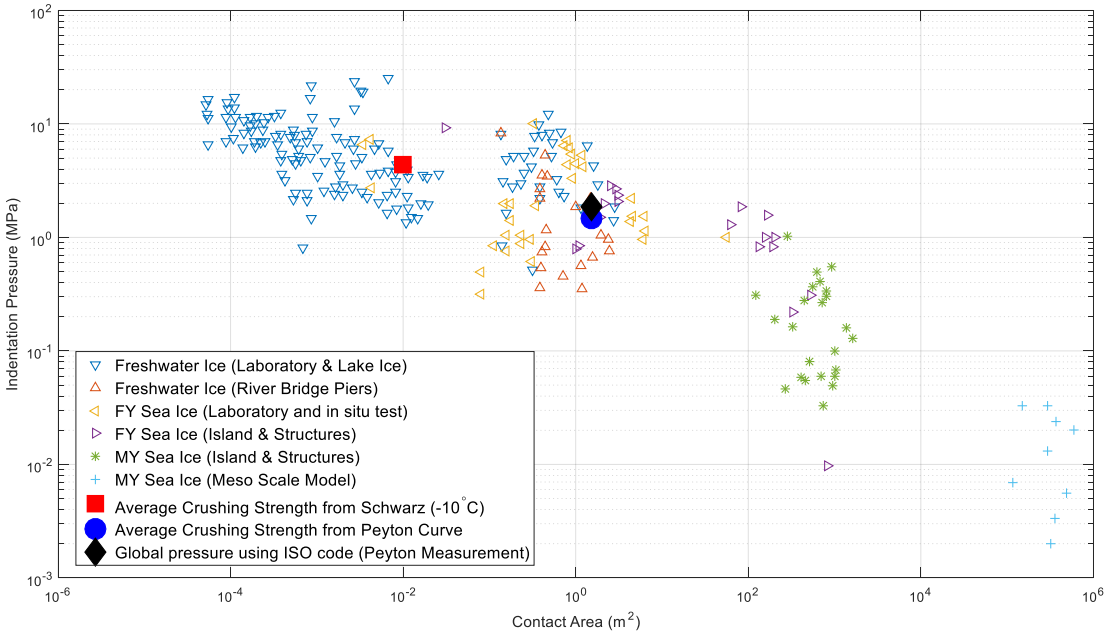

Figure 3.6 Reproduction of Sanderson`s Pressure-Area curve showing results from Peyton and Schwarz for comparison

As discussed in detail in Taylor (2010), decreases in pressure due to increasing ice thickness tend to be associated more with probabilistic aspects of localized spalling fracture, while width effects tend to be more associated with averaging of local ice pressures across the width of the structure. Since the mechanisms associated with pressure-thickness scale effects and pressure-width scale effect are different, it is logical here to treat these effects separately. The approach of treating scale effects for sea ice as a combination of a thickness and a width scaling effect has also been discussed by other authors (e.g. Løset et al., 2006; ISO 19906, 2010). The global ice pressure model provided in ISO 19906 (2010) accounts for the effects of ice thickness and structure width on average global pressures. The scaling relationships embodied in the ISO 19906 model to account for the effect of width and thickness have been applied here to scale the Peyton curves for the range of ice thickness and structure widths of interest, as is shown in Figure 3.7. As one would expect, the magnitude of the peak and the slopes of the curve becomes less steep for increasing width, as well as increasing

ice thickness. It is noted here that the values of width and thickness for the base case in this analysis (e.g. Peyton`s uniaxial compression tests) was not reported by Peyton in his original paper. However, since SEM considers the relationship to be universal these values can be inferred from values observed in Peyton's field test measurements. The structural pile used in Cook Inlet tests had a diameter of 4.3m (Sanderson, 1988) and an average thickness of ice for that season was 0.36*m* (Blenkarn, 1970). It should be mentioned here that while the scale of the interaction can influence the dominant ice failure mode, as is discussed in section 3.2.1, application of the SEM is assumed to correspond only to events where continuous crushing occurs. During full-scale interactions, continuous crushing only occurs during a relatively small proportion of all interactions and other ice failure modes result in more random loading patterns that are not associated with observations of IIV (Jefferies and Wright, 1988; Jefferies et al., 2008). This allows for simplification of the methodology by limiting the analysis to scenarios where the ice fails in continuous crushing.

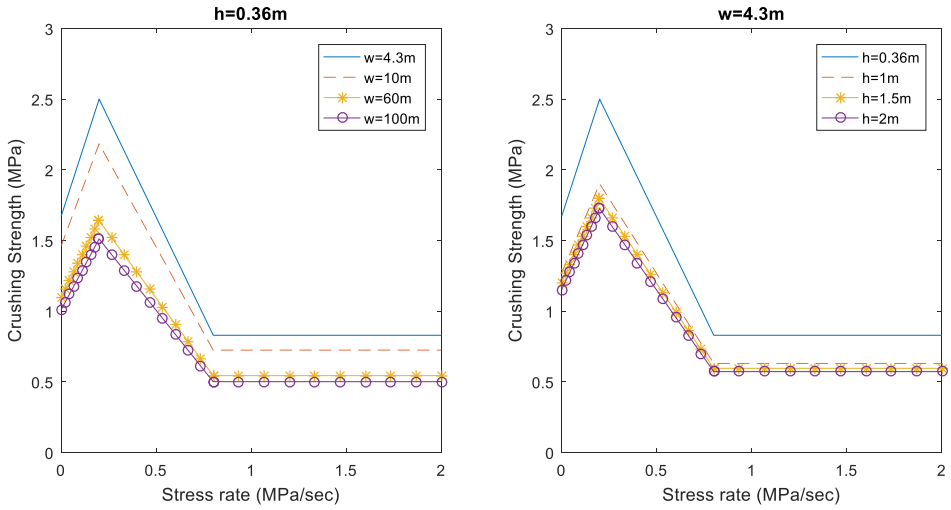

Figure 3.7 Variation in strength-stress relationship due to: (left) width scale effect for constant ice thickness (h=0.36m); and (right) thickness scale effect for structure of constant width (w = 4.3m).

The intercept and slope values for modified Peyton's curve considering the scale effect are listed in Table 3.2 & Table 3.3.

Table 3.2. α and β values for different regions in modified Peyton's curve taking the effect of structure's width into account

Parameters / Width (m)	$0 < \dot{\sigma} \leq 0.2$		$0.2 < \dot{\sigma} \leq 0.8$		$\dot{\sigma} > 0.8$	
	α	β	α	β	α	β
4.3	1.670	4.150	3.058	-2.783	0.830	0
10	1.459	3.632	2.672	-2.434	0.725	0
60	1.095	2.727	2.006	-1.827	0.544	0
100	1.009	2.513	1.849	-1.684	0.502	0

Table 3.3. α and β values for different regions in modified Peyton's curve taking the effect of ice thickness into account

Parameters / Thickness (m)	$0 < \dot{\sigma} \leq 0.2$		$0.2 < \dot{\sigma} \leq 0.8$		$\dot{\sigma} > 0.8$	
	α	β	α	β	α	β
0.36	1.670	4.150	3.058	-2.783	0.830	0
1	1.270	3.161	2.326	-2.119	0.631	0
1.5	1.200	2.987	2.198	-2.001	0.596	0
2	1.153	2.869	2.111	-1.923	0.573	0

3.3 Results and Analysis

To implement the model described in section 3.2.1, the SEM analysis routine was programmed in MATLAB. The structure chosen as a basis for the analysis was the Norströmsgrund lighthouse, since the structure has experienced a number of ice-induced vibration events that have been

reported in the literature. Also, the structure has been analyzed previously using the SEM (Nandan et al., 2011) which allows for direct comparison of results to verify proper functioning of the analysis routines. In their analysis, Nandan et al. (2011) used a 15 node lumped mass model with translational and rotational degrees of freedom and the ice force was considered to be acting only on the waterline node. However, a Single Degree of Freedom (SDOF) representation of the model was found to be very efficient computationally without a loss of accuracy. The SDOF parameters for the structure were obtained from a Joint Industry Project (JIP), which was arranged to validate different ice-induced vibration models (Kärnä et al., 2013) thus making the parameters independent of the analysis. The numerical integration was done by forward time integration scheme using the RK4 algorithm. A summary of the structural parameters for the SDOF models are given in Table 3.4.

Table 3.4. Structural parameters used in the analysis

Structural parameters	Value
Mass (kg)	11.7×10^6
Stiffness (N/m)	3.22×10^9
Damping Ratio	0.02
Waterline Diameter (m)/Width (m)	7.5

The model was first validated using the same ice parameters (thickness, velocity) used by Nandan et al. (2011) with the original strength-stress rate relationship. Once the model was found to be in agreement for the original strength-stress rate relationship, individual analysis was performed using the modified Peyton's curve discussed in sections 3.2.3 & 3.2.4. From these analyses the acceleration of the structure was used to characterize the ice-induced vibration response. In the foregoing, a sinusoidal response with constant amplitude has been termed as steady-state ice-

induced vibration (SS-IIV), whereas a decaying response has been termed as damped ice-induced vibration (D-IIV). Since SS-IIV is more significant from a structural perspective, particular attention has been placed on this type of response.

3.3.1 Structural response: base case for analysis (validation)

The base case used in this analysis is based on the results of Nandan et al. (2011), who conducted a simulation for an interaction event having a duration of one hundred seconds, which included a stepwise variation in ice thickness and drift speed. Ice thickness was assumed to be $0.5m$ for the first 5 seconds, after which an instantaneous change of the ice thickness to a value of $1.5m$ occurred and continued until t = 58 seconds. Another step change then occurred just after 58 seconds and the ice thickness returned to $0.5m$ again which continued until the end of the simulation. Ice drift speed starts at $0.2m/s$ and increased to $0.25m/s$ at 10 seconds and to $0.35m/s$ at 30 seconds. Results obtained for this case are shown in Figure 3.8 and exhibit SS-IIV that initiate at t = 30 seconds due to the change in ice drift speed and continue until t = 58 seconds. These SS-IIV are characterized by a significant amplitude and a frequency close to the natural frequency of the structure. After t = 58 seconds, when the ice thickness decreases, the response returns to a damped vibration mode. The results show that ice-induced vibration is strongly correlated with both ice thickness and drift speed and are in excellent agreement with the result of Nandan et al. (2011).

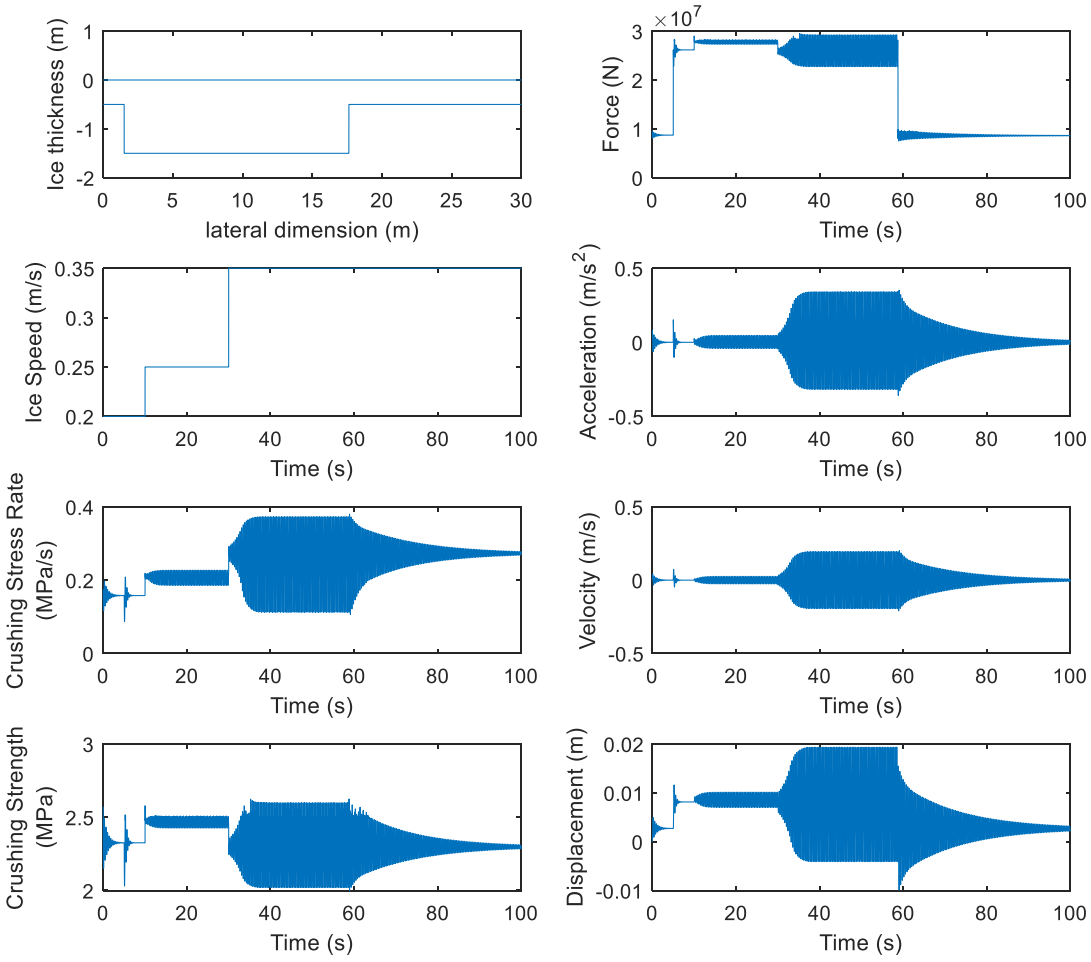

Figure 3.8 Results showing variation of structural response based on ice thickness and drift speed profile. Similar results were obtained by Nandan et al. (2011)

3.3.2 Analysis cases considered

Using the approach described in section 3.2, a series of modified Peyton relationships were generated, yielding the corresponding curve coefficients for each of the analysis cases summarized below:

Table 3.5. Summary of analysis cases and associated parameters

Case	Ice Thickness (m)	Ice temperature (℃)	Ice speed (m/s)	Modified Peyton Curve Parameters					
				$0 < \dot{\sigma} \leq 0.2$		$0.2 < \dot{\sigma} \leq 0.8$		$\dot{\sigma} > 0.8$	
				α	β	α	β	α	β
A	0.4	-20	0.8	2.668	6.640	4.885	-4.449	1.326	0
B	0.4	-10	0.8	1.67	4.15	3.058	-2.783	0.83	0
C	0.4	-5	0.8	1.134	2.822	2.077	-1.891	0.564	0
D	0.4	-2	0.8	0.813	2.023	1.488	-1.356	0.404	0
E	1.5	-20	0.8	2.668	6.640	4.885	-4.449	1.326	0
F	1.5	-10	0.8	1.67	4.15	3.058	-2.783	0.83	0
G	1.5	-5	0.8	1.134	2.822	2.077	-1.891	0.564	0
H	1.5	-2	0.8	0.813	2.023	1.488	-1.356	0.404	0
I	0.36	-10	0.8	1.67	4.15	3.058	-2.783	0.83	0
J	1	-10	0.8	1.67	4.15	3.058	-2.783	0.83	0
K	1.5	-10	0.8	1.67	4.15	3.058	-2.783	0.83	0
L	2	-10	0.8	1.67	4.15	3.058	-2.783	0.83	0
M	0.36	-10	0.8	1.67	4.15	3.058	-2.783	0.83	0
N	1	-10	0.8	1.27	3.161	2.326	-2.119	0.631	0
O	1.5	-10	0.8	1.2	2.987	2.198	-2.001	0.596	0
P	2	-10	0.8	1.153	2.869	2.111	-1.923	0.573	0
Q	1	-10	0.6	1.67	4.15	3.058	-2.783	0.83	0
R	1	-10	0.6	1.551	3.859	2.841	-2.587	0.771	0

Using the inputs and parameter values associated with each of the analysis cases outlined in Table 3.5 above, a series of Matlab simulations was conducted and results were plotted to allow for comparison with the base case described in section 3.3.1. An assessment of the influence of

temperature and scale effects on the strength vs. stress-rate curve and the corresponding predictions of structural response during dynamic ice-structure interactions are provided in the sections that follow.

3.3.3 Effect of temperature on SEM results

As depicted in Figure 3.5, as the ice becomes warmer the strength vs. stress-rate relationship is expected to have a lower peak strength value and a reduced slope. Moreover, the ice failure tends to fail in a more ductile manner at higher temperatures, which is anticipated to excite less dynamic response in the structure. This rationale is consistent with analysis results obtained here, as well as recent medium-scale experimental results obtained by (Birajdar et al., 2016, 2017) As shown in Figure 3.9, the amplitude of damped and steady-state vibration was found to decrease with increasing ice temperature (Cases A-H). The mode of the vibration was also found to be highly dependent on ice temperature and for a given ice velocity and thickness combination, a threshold temperature may exist above which SS-IIV does not occur at all. While this result is consistent with expectations based on fundamental mechanics and also with recent observations from small-scale test (Browne et al., 2013; O'Rourke et al., 2015) and medium-scale indentation experiments with compliant structures (Birajdar et al., 2016), this is contrary to the assessment provided by Bjerkås et al. (2013b). He hypothesized that observations of more frequent ice-induced vibration during the spring season was attributable to the ice cover being warmer due to higher solar heat flux and the thermal erosion of ice. Since ice during spring is warmer, thicker and faster moving, it is unclear which of these factors dominates the correlation of increased SS-IIV with spring ice conditions. As examined in Section 3.3.1, since increasing the thickness and velocity are both expected to increase the likelihood of SS-IIV, and results here suggest lower likelihood of SS-IIV

for warmer ice, it would be valuable to revisit available full-scale data to further clarify the role of temperature in full-scale IIV.

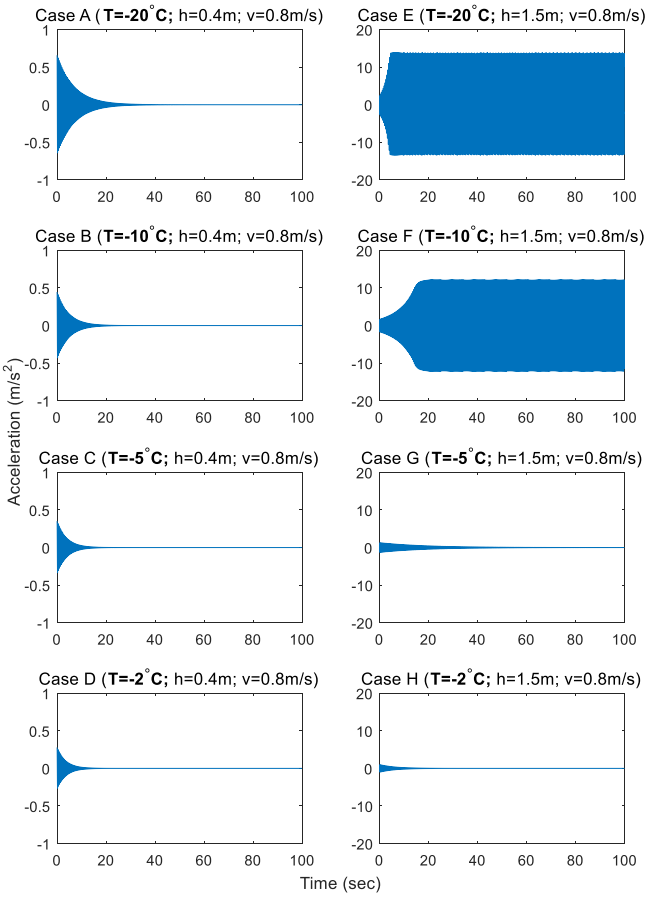

Figure 3.9 Effect of temperature on SEM results for two different ice thickness values showing over a range of temperatures; (Left) damped IIV occurring for **h = 0.4 m, v = 0.8 m/s**; (Right) SS-IIV occurring for **h = 1.5 m, v = 0.8 m/s**

3.3.4 Effect of pressure-thickness scale effect on SEM results

From full-scale data it is observed that a distinct pressure-thickness effect, wherein average pressures were found to decrease with increasing thickness for a structure of given width, has been observed from a variety of datasets (e.g. Kärnä et al., 2006; Taylor, 2010; Taylor and Jordaan, 2015). It is reasonable to assume that this effect also would result in a decrease in the peak strength

and in the slope of the strength vs. stress-rate curve (Figure 3.7). Since the ice force equation (3.10) is a linear function of ice thickness, increasing ice thickness will proportionally increase the global load on the structure, albeit accounting for the pressure-thickness effect has a 'mitigating' effect on the rate at which this ice load increases. This in turn influences the susceptibility of the structure to ice-induced vibration and accounting for this pressure-thickness scale effect is expected to reduce the likelihood of IIV occurring. This result is illustrated in Figure 3.10, which includes a comparison of SEM results for different ice thicknesses, when pressure-thickness effects are not accounted for (Cases I-L) and when pressure-thickness effects are included (Cases M-P).

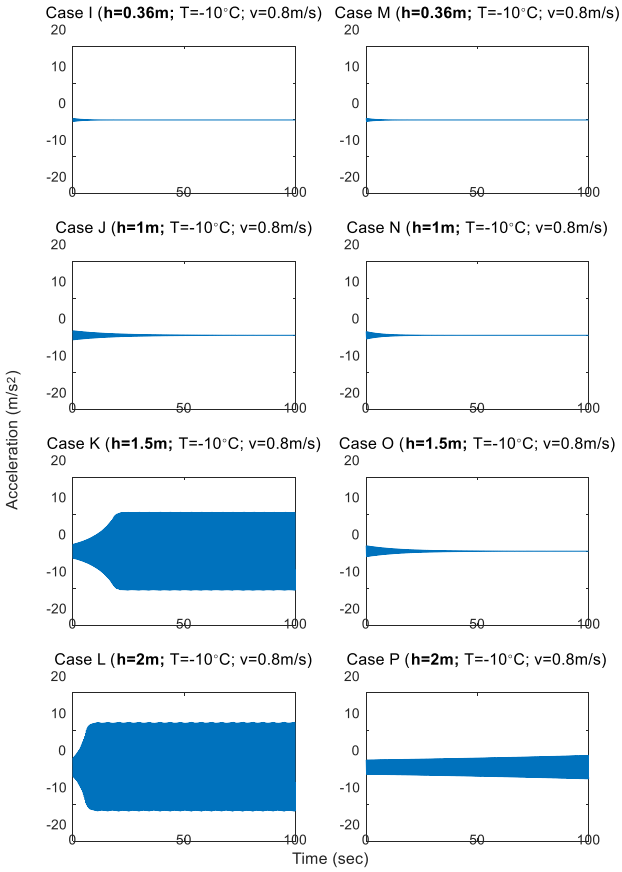

Figure 3.10 Structural acceleration predicted by SEM for a range of ice thickness values: (Left) without pressure-thickness effect; (Right) including pressure-thickness effect; (**v=0.8*m/s*, w = 4.3*m*, T =$-10°C$**)

As may be observed from Figure 3.10 above, while the direct relationship between ice thickness and ice force dominates the overall response, accounting for the pressure-thickness effect in the strength vs. stress-rate curve does have a significant effect on the predicted amplitude of ice-induced vibration. For the cases considered here, the estimated peak amplitude of the vibration when thickness effects were not included (Cases I–L) were found to be about twice as high as predicted values obtained when thickness effects are included in the strength vs. stress-rate curve (Cases M–P).

3.3.5 Effect of pressure-width scale effect on SEM results

Similar to ice thickness, increasing structure width is also associated with decreasing average global pressures. Width effects are generally attributed to the effects of statistical averaging of non-simultaneous loads that act across the face of the structure (e.g. Kry, 1978). Assuming the pressure-width scale effect would have similar influence on the average strength embodied in the Peyton relationship, it may be inferred that the peak strength and slopes of the strength vs. stress-rate curve would decrease (Figure 3.7). For the base case used in this analysis, the original Peyton curve used to represent the ice behaviour corresponds to a pile diameter of $4.3m$. For the Norströmsgrund lighthouse, which is used as the representative structural system for this analysis, the reported width at the waterline is $7.5m$ (Kärnä et al., 2013). Figure 3.7 shows a family of inferred strength vs. stress-rate relationships that have been obtained for different structure widths by scaling the original Peyton relationship using the width effect relationship embodied in the ISO 19906 global ice pressure equation. Using the same approach, a modified strength vs. stress-rate relationship is obtained for a width of $7.5m$ (Norströmsgrund lighthouse). To assess the significance of width effect on IIV response, results have been obtained by simulating the response of the Norströmsgrund lighthouse using the original Peyton curve with no width effect accounted

for (left side of Figure 3.11), as well as using a modified strength vs. stress-rate relationship which accounts for the width effect corresponding to a width of 7.5m (right side of Figure 3.11).

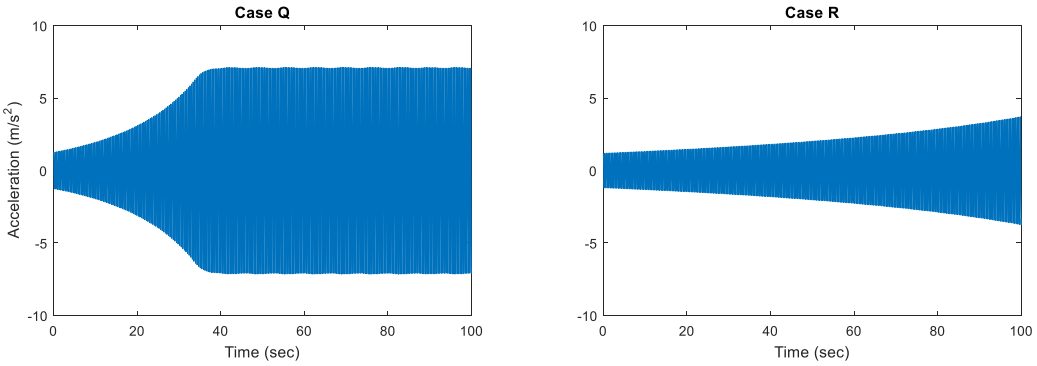

Figure 3.11 SEM model results showing structural accelerations. (Left) without the pressure-width effect; (Right) with the pressure-width effect ($\boldsymbol{h = 1.0m, v = 0.6\,m/s, T = -10}$℃)

As may be observed from Figure 3.11 above, when width effects are accounted for, SS-IIV does not occur within the simulation period and the vibration amplitude is also significantly smaller. In the above case, the width of the structure is identical (7.5m) in both simulation cases, only the ice strength relationship is changed. For design applications where the actual width of the structure may be changed, it is important to note since that ice force is also a function of structure radius in the SEM model, increasing the structure width has both 'aggravating' (due to increase of loaded area) and 'mitigating' effects (due to decreasing average pressure) on ice-induced vibration when pressure-width effect is considered.

To obtain further insight on pressure-width effect, the acceleration response has been calculated with and without this effect for three different structural configurations (Diameter, D = 2m, 5m, 10m) under similar ice conditions; see Figure 3.12. In practice, changes in structural dimensions would be expected to result in corresponding changes to the mass, stiffness and damping of the structure. For the present investigation, to more clearly illustrate the pressure-width effect and

simplify the analysis, it has been assumed that in each of the cases considered the structural configurations are such that they yield the same SDOF structural parameters at the waterline (e.g. mass, stiffness, damping). Since it has been assumed for this section of the analysis that only the waterline diameter is changed, as expected, smaller waterline widths correspond to lower total ice loads resulting in insufficient force to excite steady-state vibration, regardless of whether or not the width effects are accounted for. However, it is important to note that since the base case (Peyton's curve) corresponds to a width of $4.3m$, for widths less than this value, accounting for the pressure-width effect results in higher pressures, which in turn results in a larger amplitude response. For widths close to the base case diameter of $4.3m$ (e.g. $5m$), accounting for the width effect is not expected to have a pronounced effect, as is reflected in the result in Figure 3.12. As width is further increased (e.g. $D = 10m$) the pressure-width effect results in decreased global pressures resulting in a potentially more significant reduction in predicted vibration amplitude for wider structures.

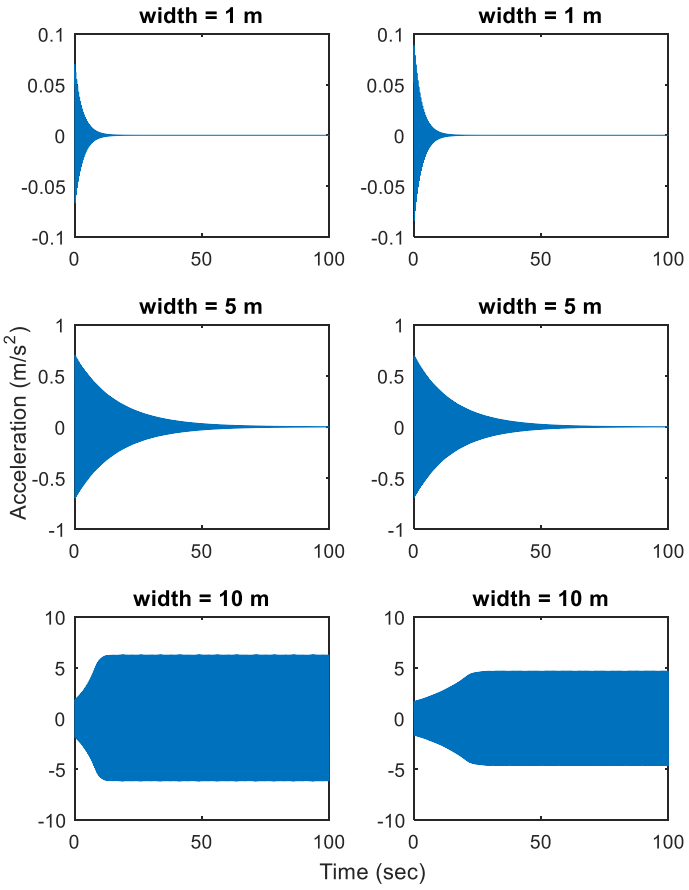

Figure 3.12 SEM model results showing structural accelerations for three different structure width (2m; 5m; 10m): (left) without pressure-width effect; (right) including pressure-width effect; ($\boldsymbol{h = 1.0m, v = 0.6\,m/s, T = -10}$℃)

3.4 Discussion of implications for design

To assess the potential implications of the above analysis for design, steady state acceleration contours as a function of ice thickness and velocity (after Nandan et al., 2011) have been examined for the Norströmsgrund lighthouse structure. Since the width of the structure will be fixed for a given design, in this section emphasis is placed on the influence of temperature and thickness. To this end, the modified strength vs. stress-rate relationships that have been updated to account for the effects of temperature (Figure 3.5) and pressure-thickness scale effect (Figure 3.7) have been used. To ensure consistency throughout this analysis, steady-state acceleration values have been

used in these plots, which are assumed to correspond to the maximum acceleration values in the last several seconds of the results obtained for each analysis case. As may be observed from Figure 3.13, temperature appears to have a significant influence on the extent of predicted SS-IIV acceleration response over the range thickness and velocities considered. Consistent with results discussed in section 3.3.3, accounting for temperature effects in the SEM suggests that colder ice is more likely to induce vibrations in the structure.

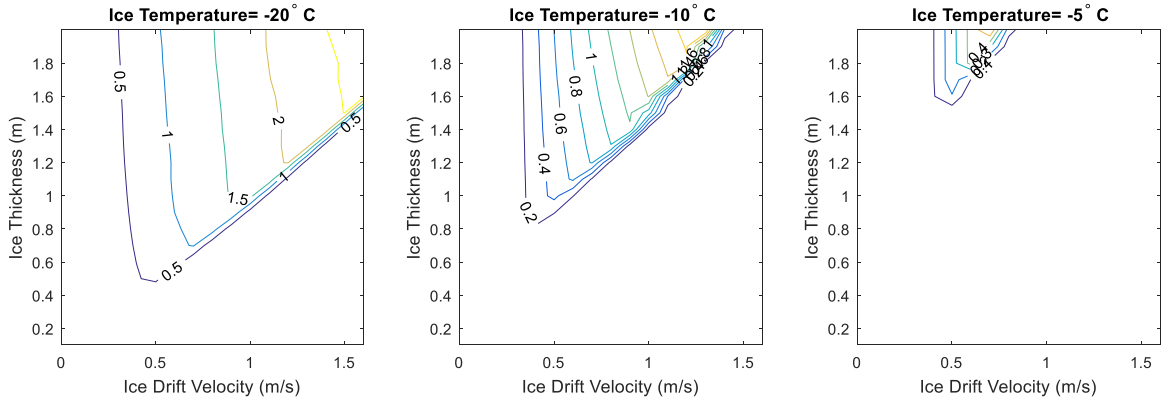

Figure 3.13 Steady-state acceleration contour in 'g' (gravitational acceleration) for ice thickness and velocity profile for different temperatures

To examine the implications of the pressure-thickness scale effect, a comparison of results from steady-state acceleration contour plots for SEM analysis excluding and including this effect have been plotted in Figure 3.14. As may be observed from this plot, the expected range of conditions resulting in IIV and the severity of the dynamic response when IIV does occur, are both expected to decrease when pressure-thickness scale effects are accounted for in the model.

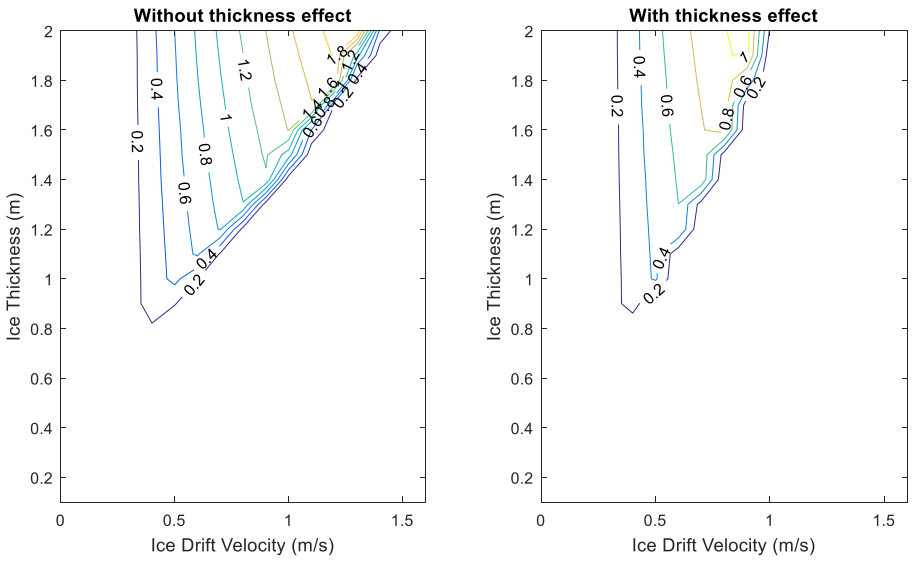

Figure 3.14 Steady-state acceleration contour in 'g' for ice thickness and velocity profile (Left) without considering thickness effect; (Right) considering thickness effect

Similarly, using a 10m wide structure for comparison purposes, the influence of width-effect on steady-state acceleration has also been analyzed as a function of ice thickness and velocity. Results in Figure 3.15 show that, accounting the pressure-width scale effect also tends to decrease the expected range of conditions resulting in IIV and the severity of the dynamic response for widths greater than 4.3m (the width corresponding to Peyton's measurements).

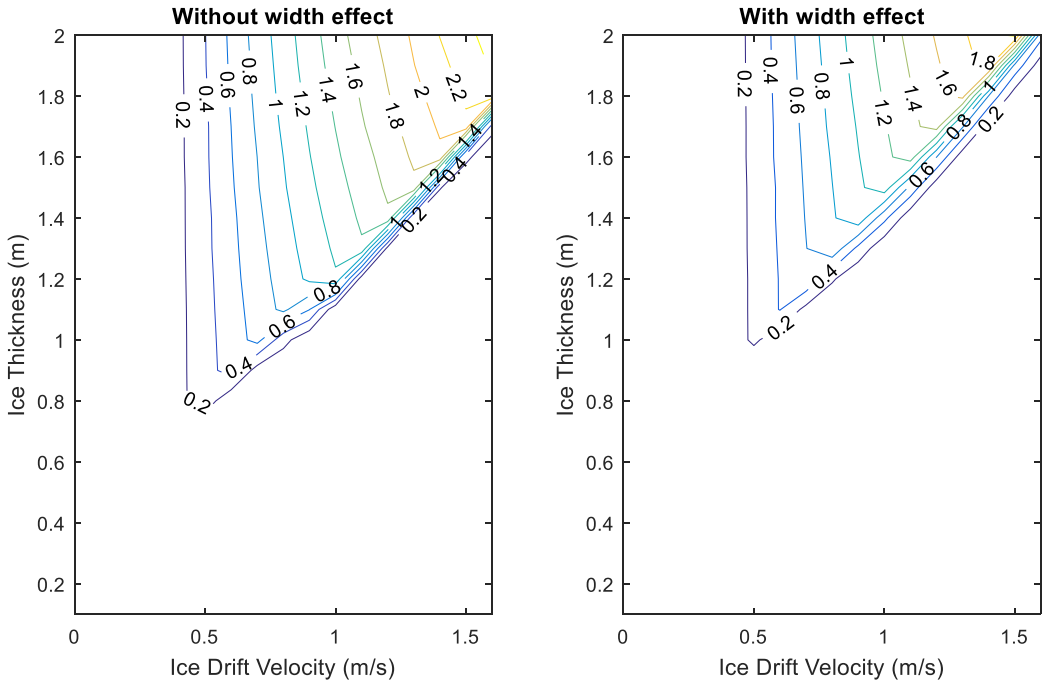

Figure 3.15 Steady-state acceleration contour in 'g' for ice thickness and velocity profile (Left) without considering width effect; (Right) considering width effect (structure width=10m)

3.5 Concluding Remarks

Despite considerable advances in ice mechanics and modelling of dynamic ice-structure interactions in recent decades, significant uncertainties still exist. Changes in ice properties and behaviour are expected throughout the season as ice conditions evolve (especially due to changes in temperature and ice thickness). Moreover, the strength of ice is known to vary widely throughout a given interaction, as well as from interaction to interaction. The triaxial state of stress and the prevalence of fracture during ice compressive failure highly complicates the modelling of ice-structure interactions. The fundamental question posed by this research is to assess how sensitive results obtained using the SEM approach are to variations in temperature and scale. The analysis presented in this chapter represents an approximate, first order estimate of these effects based on information from full-scale data, laboratory tests, as well as fundamental knowledge of ice material

behaviour. This information was used to assess how changes in temperature, ice thickness and structure width may impact the modelled strength vs. stress-rate relationship and associated IIV.

From this work it has been observed that changes in ice temperature, thickness and structure width are expected to have significant effects on predicted dynamic response of the structure as compared with those predicted using baseline conditions. These results suggest that as ice temperature increases higher ice drift velocity is necessary to induce SS-IIV and the expected intensity of these vibrations may be lower for warm ice than would be expected for colder ice. When pressure-thickness and pressure-width scale effects were accounted for, as the ice thickness and structure width increase beyond the baseline values, the predicted threshold speed to trigger SS-IIV increases and the intensity of the dynamic response may be lower than predicted using Peyton`s original curve.

It is important to reiterate here that this analysis is a first-order sensitivity assessment to provide guidance for ongoing research in this area and the modified relationships developed here are not intended for use in design practice. Further work is needed to address uncertainties in coupled ice-structure interactions, especially those associated with the effects of temperature and scale. The incorporation of ice load models based on statistical distributions of high pressure zones and linked to the physics of ice compressive failure are seen as a promising direction (Taylor and Richard, 2014). Recent experimental *hpz* studies on dynamic coupling during ice-structure interactions at small-scale (Browne et al., 2013; Taylor et al., 2013; Habib et al., 2015; O'Rourke et al., 2016a, 2016b) and medium-scale (Birajdar et al., 2016, 2017) provide important insights.

References

Birajdar, P., Taylor, R., Habib, K., Hossain, R., 2016. Analysis of Medium-Scale Laboratory Tests on Ice Crushing Dynamics, in: Arctic Technology Conference. Offshore Technology Conference, St. John's, NL, Canada. https://doi.org/10.4043/27482-MS

Birajdar, P., Taylor, R., Hossain, R., 2017. Analysis of the effect of structural compliance during medium-scale laboratory tests on ice crushing dynamics, in: Proceedings of the 27th International Ocean and Polar Engineering Conference. International Society of Offshore and Polar Engineers, San Francisco, California, USA.

Bjerkås, M., Alsos, H.S., Meese, A., 2013a. Ice induced vibrations-observations of a full scale lock-in event, in: The Twenty-Third International Offshore and Polar Engineering Conference. International Society of Offshore and Polar Engineers, Alaska, USA, pp. 1272–1279.

Bjerkås, M., Lonoy, C., Gurtner, A., 2013b. Ice- Induced Vibrations and Effects of Ice Temperature. Int. J. Offshore Polar Eng. 23, 9–14.

Bjerkås, M., Skiple, A., 2005. Occurrence of continuous and intermittent crushing during ice-structure interaction, in: Proceedings of the 18th International Conference on Port and Ocean Engineering under Arctic Conditions (POAC'05). PostDam,NY, vol. 3 pp. 1131–1140.

Blenkarn, K.A., 1970. Measurement and analysis of ice forces on cook inlet structures, in: Proceedings of the Annual Offshore Technology Conference. Dallas, TX, United States, vol. 1970-April pp. 365–375. https://doi.org/10.4043/1261-MS

Browne, T., Taylor, R., Jordaan, I., Gürtner, A., 2013. Small-scale ice indentation tests with variable structural compliance. Cold Reg. Sci. Technol. 88, 2–9. https://doi.org/10.1016/j.coldregions.2012.12.006

Daley, C., 1991. Ice edge contact a brittle failure process model, Acta Polytechnica Scandinavica, Mechanical Engineering Series. D.Tech, Helsinki University of Technology.

Daoud, N., Lee, F.C., 1986. Ice-induced dynamic loads on offshore structures, in: Proceedings of the ASME 1986 5th International Conference on Ocean, Offshore and Arctic Engineering (OMAE1986). American Society of Mechanical Engineers (ASME), vol. IV pp. 212–218.

Engelbrektson, A., 1977. Dynamic ice loads on a lighthouse structure, in: Proceedings of the 4th International Conference on Port and Ocean Engineering under Arctic Conditions (POAC'77). St.John's, Newfoundland, vol. 2 pp. 654–663.

Eranti, E., 1992. Dynamic ice structure interaction: theory and applications, PhD Dissertation. VTT Technical Research Center of Finland, Helsinki University of Technology.

Finn, D.W., Jones, S.J., Jordaan, I.J., 1993. Vertical and inclined edge-indentation of freshwater ice sheets. Cold Reg. Sci. Technol. https://doi.org/10.1016/0165-232X(93)90042-7

Frederking, R., Sudom, D., 2006. Maximum ice force on the Molikpaq during the April 12, 1986 event. Cold Reg. Sci. Technol. 46, 147–166. https://doi.org/10.1016/j.coldregions.2006.08.019

Gagnon, R., 2012. An explanation for the Molikpaq May 12, 1986 event. Cold Reg. Sci. Technol. 82, 75–93. https://doi.org/10.1016/j.coldregions.2012.05.009

Habib, K.B., Bruneau, S., Taylor, R.S., Jordaan, I.J., 2015. Experimental study of dynamics during crushing of freshwater truncated conical ice specimens, in: Roceedings of the ASME 2015 34th International Conference on Ocean, Offshore and Arctic Engineering (OMAE2015). St. John's, NL, Canada, vol. 8 . https://doi.org/10.1115/OMAE201541904

Huang, G., Liu, P., 2009. A dynamic model for ice-induced vibration of structures. J. Offshore Mech. Arct. Eng. 131, 1–6. https://doi.org/10.1115/1.2979795

Huang, Y., Shi, Q., Song, A., 2007. Model test study of the interaction between ice and a compliant vertical narrow structure. Cold Reg. Sci. Technol. 49, 151–160. https://doi.org/10.1016/j.coldregions.2007.01.004

ISO 19906, 2010. Petroleum and natural gas industries — Arctic offshore structures. Int. Organ. Stand.

Jefferies, M., Kärnä, T., Løset, S., 2008. Field data on the magnification of ice loads on vertical structures, in: Proceedings of the 19th IAHR International Symposium on Ice. International Association for Hydraulic Research, Vancouver, BC, Canada., vol. 2 pp. 1325–1344.

Jefferies, M., Wright, W., 1988. Dynamic response of "Molikpaq" to ice structure interaction, in: Proceedings of the International Offshore Mechanics and Arctic Engineering Symposium. Houston, Texas, USA, vol. 4 pp. 201–220.

Jordaan, I., Bruce, J., Hewitt, K., Frederking, R., 2011. Re-evaluation of ice loads and pressures measured in 1986 on the Molikpaq structure, in: Proceedings of the 21st International Conference on Port and Ocean Engineering under Arctic Conditions (POAC'11). Montréal, Canada.

Jordaan, I., Timco, G., 1988. Dynamics of the ice-crushing process. J. Glaciol. 34, 318–326.

Kärnä, T., 1992. A Procedure For Dynamic Soil-Structure-Ice Interaction, in: The 2nd International Offshore and Polar Engineering Conference. International Society of Offshore and Polar Engineers, San Francisco, CA, United states, vol. 2 pp. 764–771.

Kärnä, T., Andersen, H., Gürtner, A., Metrikine, A., Sodhi, D., Loo, M., Kuiper, G., Gibson, R., Fenz, D., Muggeridge, K., Wallenburg, C., Wu, J.-F.-F., Jefferies, M., 2013. Ice- induced vibrations of offshore structures - Looking beyond ISO 19906, in: Proceedings of the International Conference on Port and Ocean Engineering under Arctic Conditions, POAC. Espoo, Finland.

Kärnä, T., Kamesaki, K., Tsukuda, H., 1999. A numerical model for dynamic ice– structure interaction. Comput. Struct. 72, 645–658. https://doi.org/10.1016/S0045-7949(98)00337-X

Kärnä, T., Kolari, K., Jochmann, P., Evers, K.-U., Bi, X., Määttänen, M., Martonen, P., 2003. Tests on Dynamic Ice-Structure Interaction, in: Proceedings of the ASME 2003 22nd International Conference on Offshore Mechcnics and Arctic Engineering. American Society of Mechanical Engineers (ASME), Cancun, Mexico, vol. 3 pp. 823–829. https://doi.org/10.1115/OMAE2003-37397

Kärnä, T., Muhonen, A., 1990. Preliminary results from ice indentation tests using flexible and rigid indentors, in: Proceeding of the 10th IAHR Symposium on Ice. International Association for Hydraulic Research, Espoo, Finland, vol. 3 pp. 261–275.

Kärnä, T., Qu, Y., Yue, Q., 2006. Baltic model of global ice forces on vertical structures, in: Proceeding of the 18th IAHR International Symposium on Ice. International Association for Hydraulic Research, Sapporo, Japan, vol. 2 pp. 253–260.

Kärnä, T., Trunen, R., 1990. A straightforward technique for analyzing structural response to dynamic ice action, in: Proceedings of the ASME 1990 9th International Conference on Ocean, Offshore and Arctic Engineering (OMAE1990). American Society of Mechanical Engineers (ASME), Houston, Texas, vol. IV pp. 135–142.

Kry, P.R., 1978. A Statistical Prediction of Effective Ice Crushing Stresses on Wide Structure, in: Proceedings of the 5th IAHR International Symposium on Ice. International Association for Hydraulic Research, Lulea, Sweden, vol. 1 pp. 33–47.

Løset, S., Shkhinek, K.N., Gudmestad, O., Høyland, K., 2006. Actions from ice on arctic offshore and coastal structures. LAN, St. Petersburg, Russia.

Määttänen, M., 2008. Ice velocity limit to frequency lock-in vibrations, in: Proceedings of the 19th IAHR International Symposium on Ice. vol. 2 pp. 1265–1276.

Määttänen, M., 1983. Dynamic ice-structure interaction during continuous crushing. US Army Corps of Engineers, CRREL.

Määttänen, M., 1981. Laboratory tests for dynamic ice-structure interaction. Eng. Struct. 3, 111–116. https://doi.org/10.1016/0141-0296(81)90037-7

Määttänen, M., 1978. On conditions for the rise of self-excited ice-induced autonomous oscillations in slender marine pile structures. Winter Navigation Research Board.

Määttänen, M., 1977. Ice-force measurements at the Gulf of Bothnia by the instrumented Kemi I lighthouse, in: Proceedings of the 4th International Conference on Port and Ocean Engineering under Arctic Conditions (POAC'77). St. John's, NL, Canada, vol. 2 pp. 730–740.

Määttänen, M., Marjavaara, P., Saarinen, S., Laakso, M., 2011. Ice crushing tests with variable structural flexibility. Cold Reg. Sci. Technol. 67, 120–128. https://doi.org/10.1016/j.coldregions.2011.03.004

Matlock, H., Dawkins, W.P., Panak, J.J., 1969. A model for the prediction of ice-structure interaction, in: Proceedings of the Annual Offshore Technology Conference. Dallas, Texas, vol. 1969-May pp. 687–693.

Michel, B., Toussaint, N., 1977. Mechanisms and Theory of Indentation of Ice Plates. J. Glaciol. 19, 285–300. https://doi.org/10.1017/S002214300002935X

Montgomery, C.J., Gerard, R., Lipsett, A.W., 1980. Dynamic response of bridge piers to ice forces. Can. J. Civ. Eng. 7, 345–356. https://doi.org/10.1139/l80-042

Nandan, H., Younan, A.H., Deng, L., 2011. Ice induced vibration implementation of Maattanen model and development of design supplements, in: Proceedings of the 21st International Conference on Port and Ocean Engineering under Arctic Conditions (POAC'11). Montréal, Canada.

Neill, C.R., 1976. Dynamic ice forces on piers and piles. An assessment of design guidelines in the light of recent research. Can. J. Civ. Eng. 3, 305–341. https://doi.org/10.1139/l76-030

Nordlund, O.P., Kärnä, T., Järvinen, E., 1988. Measurements of ice-induced vibrations of channel markers, in: Proceedings of the 9th IAHR International Symposium on Ice. International Association for Hydraulic Research, vol. 1 pp. 537–548.

O'Rourke, B.J., Jordaan, I.J., Taylor, R., Gürtner, A., 2016a. Experimental investigation of oscillation of loads in ice high-pressure zones, part 2: Double indentor system — Coupling and

synchronization of high-pressure zones. Cold Reg. Sci. Technol. 124, 11–24. https://doi.org/10.1016/j.coldregions.2015.12.002

O'Rourke, B.J., Jordaan, I.J., Taylor, R.S., Gürtner, A., 2016b. Experimental investigation of oscillation of loads in ice high-pressure zones, part 1: Single indentor system. Cold Reg. Sci. Technol. 124, 25–39. https://doi.org/10.1016/j.coldregions.2015.12.005

Palmer, A., Qianjin, Y., Fengwei, G., 2010. Ice-induced vibrations and scaling. Cold Reg. Sci. Technol. 60, 189–192. https://doi.org/10.1016/j.coldregions.2009.11.005

Peyton, H., 1968. Sea ice forces. Ice pressure against structures., Technical Memorandum. National Research Council of Canada, Ottawa, Canada.

Sanderson, T.J.O., 1988. Ice mechanics : risks to offshore structures. London, UK ; Boston : Graham & Trotman, London, UK ; Boston.

Schulson, E.M., Duval, P., 2009. Creep and fracture of ice. Cambridge University Press Cambridge.

Schwarz, J., 1970. The pressure of floating ice-fields on piles, in: Proceedings of the 1st IAHR International Symposium on Ice. International Association for Hydraulic Research, Reykjavik, Iceland, vol. 3 p. 6.3.

Schwarz, J., Jochmann, P., 2001. Ice force measurements within the LOLEIF-project, in: Proceedings of the 16th International Conference on Port and Ocean Engineering under Arctic Conditions (POAC'01). Ottawa, Canada, vol. 2 pp. 669–682.

Sodhi, D., 1994. A Theoretical Model for Ice-structure Interaction, in: Proceedings of the ASME 1994 13th International Conference on Ocean, Offshore and Arctic Engineering (OMAE1994). American Society of Mechanical Engineers (ASME), New York, vol. IV pp. 29–34.

Sodhi, D., 1992. Ice-structure interaction with segmented indentors, in: Proceedings of the 11th IAHR International Symposium on Ice. International Association for Hydraulic Research, Edmonton, Canada, vol. 2 pp. 909–929.

Sodhi, D., 1989. Ice-Structure Interaction During Indentation Tests, in: Ice-Structure Interaction IUTAM/IAHR Symposium, Ice-Structure Interaction. Springer, St. John's, NL, pp. 619–640.

Sodhi, D., 1988. Ice-induced vibration of structures, in: Proceeding of the 9th IAHR International Symposium on Ice. International Association for Hydraulic Research, Sapporo, Japan, vol. 2 pp. 625–657.

Sodhi, D., Chin, S., 1992. Indentation tests using urea ice and segmented indentors, in: Proceedings of the ASME 1992 11th International Conference on Ocean, Offshore and Arctic Engineering (OMAE1992). American Society of Mechanical Engineers (ASME), Calgary, Canada, vol. 4 p. 223.

Sodhi, D., Nakazawa, N., 1988. Results from indentation tests on freshwater ice, in: Proceedings of the 9th IAHR International Symposium on Ice. International Association for Hydraulic Research, Sapporo, Japan, vol. 1 pp. 341–350.

Taylor, R., Browne, T., Jordaan, I., Gürtner, A., 2013. Fracture and damage during dynamic interactions between ice and compliant structures at laboratory scale, in: Proceedings of the ASME

2013 32nd International Conference on Ocean, Offshore and Arctic Engineering (OMAE2013). American Society of Mechanical Engineers (ASME), Nantes, France, vol. 6 .

Taylor, R., Jordaan, I., 2015. Probabilistic fracture mechanics analysis of spalling during edge indentation in ice. Eng. Fract. Mech. 134, 242–266. https://doi.org/10.1016/j.engfracmech.2014.10.021

Taylor, R.S., 2010. Analysis of scale effect in compressive ice failure and implications for design. PhD Thesis, Memorial University of Newfoundland.

Taylor, R.S., Jordaan, I.J., 2011. Pressure-Area Relationships in Compressive Ice Failure: Application to Molikpaq, in: Proceedings of the 21st International Conference on Port and Ocean Engineering under Arctic Conditions (POAC'11). Montréal, Canada.

Taylor, R.S., Richard, M., 2014. Development of a probabilistic ice load model based on empirical descriptions of high pressure zone attributes, in: Proceedings of the ASME 2014 33rd International Conference on Ocean, Offshore and Arctic Engineering (OMAE2014). American Society of Mechanical Engineers (ASME), San Francisco, CA, United states. https://doi.org/10.1115/OMAE2014-24353

Timco, G., Weeks, W.F., 2010. A review of the engineering properties of sea ice. Cold Reg. Sci. Technol. 60, 107–129. https://doi.org/10.1016/j.coldregions.2009.10.003

Timco, G., Wright, B., 2005. Multi-Year Ice Loads on the Molikpaq: May 12, 1986 Event;, in: Proceedings 18th International Conference on Port and Ocean Engineering under Arctic Conditions, POAC '05, May 12, 2005. Postdam, NY, vol. 1 pp. 453–462.

Toyama, Y., Sensu, T., Minami, M., Yashima, N., 1983. Model tests on ice- induced self- excited vibration of cylindrical structures, in: Proceedings of the 7th International Conference on Port and Ocean Engineering under Arctic Conditions (POAC'83). Espoo, Finland, vol. 2 pp. 834–844.

Tsuchiya, M., Kanie, S., Ikejiri, K., Ikejiri, A., Saeki, H., 1985. An experimental study on ice-structure interaction, in: Offshore Technology Conference. Houston, Texas. https://doi.org/10.4043/5055-MS

Withalm, M., Hoffmann, N.P., 2010. Simulation of full-scale ice–structure-interaction by an extended Matlock-model. Cold Reg. Sci. Technol. 60, 130–136. https://doi.org/10.1016/j.coldregions.2009.09.006

Wu, H.C., Chang, K.J., Schwarz, J., 1976. Fracture in the compression of columnar gained ice. Eng. Fract. Mech. 8, 365–370. https://doi.org/10.1016/0013-7944(76)90016-3

Xu, J., Bernt, J.L., 1981. Dynamic response of a jacket platform subjected to ice loads, in: Proceedings of the 6th International Conference on Port and Ocean Engineering under Arctic Conditions (POAC'81). Quebec, Canada, vol. 1 pp. 502–516.

Yue, Q., Bi, X., 2000. Ice-Induced Jacket Structure Vibrations in Bohai Sea. J. Cold Reg. Eng. 14, 81–92. https://doi.org/10.1061/(ASCE)0887-381X(2000)14:2(81)

Yue, Q., Guo, F., Kärnä, T., 2009. Dynamic ice forces of slender vertical structures due to ice crushing. Cold Reg. Sci. Technol. 56, 77–83. https://doi.org/10.1016/j.coldregions.2008.11.008

Yue, Q., Qu, Y., Bi, X., Kärnä, T., 2007. Ice force spectrum on narrow conical structures. Cold Reg. Sci. Technol. 49, 161–169. https://doi.org/10.1016/j.coldregions.2007.02.002

Chapter: 4 Failure Behavior of High-Pressure Zones at Medium-Scale Ice Indentation Tests and the Influence of Test Parameters

Preface

The chapter has been prepared to be submitted as an original journal article. As the primary author, I was responsible for writing the article, performing the experiments and analyzing the results. My co-author Dr. Rocky Taylor provided guidance at different stages of the writing and analysis.

As discussed in the previous chapter, the dynamic ice-structure interaction leading to ice-induced vibrations can be highly sensitive to the ice and structural parameters. The previously performed small-scale indentation tests suggest that the failure behavior of ice and the associated structural response can be highly dependent on interaction speed, ice temperature, indenter size and structural compliance. To identify how these influences can translate to larger scale, a medium-scale ice crushing dynamics test series was carried out. The experimental setup, the test procedure and the results from the test series are presented in this chapter.

Abstract

Results from medium-scale ice crushing dynamic tests are presented in this chapter where confined ice samples were indented using spherical indenters to simulate high-pressure zones (*hpz*s) with areas on the order of 10^3-$10^4 mm^2$. The failure behavior was found to be a combination of continuous extrusion with intermittent spalling, both of which were highly dependent on test parameters. The effect of ice temperature, interactions speed, indenter size and structural compliance on failure behavior were found to be similar with the results obtained from previous small-scale tests suggesting the scale-independence of these contributions on failure behavior. In general, higher dynamics (larger amplitudes and longer duration) associated with failure behavior were observed to be more pronounced for colder ice, smaller interaction area, higher interaction speed, and lower structural compliances.

4.1 Introduction

Extreme forces exerted by ice against fixed offshore structures are a highly important design consideration and in some cases can exceed the 100-year wave force (API, 1995). For sea ice, this force is generally limited by the force required to fail the ice sheets by bending, buckling, crushing or a combination of these. During a nine-month monitoring period in the winter of 1985-86 using Molikpaq, a 90*m* wide caisson retained structure operating in the Beaufort Sea, crushing was found to occur only 1% of the time (Wright and Timco, 1994). However, the highest levels of force were observed in this period, and a small portion of crushing produced a simultaneous failure against the structure leading to ice-induced vibrations. Crushing is often characterized by the extrusion of fine-grained ice particles from the interaction surface and can occur in both ductile and brittle

regimes. In the ductile regime, the extrusion process is often slow, continuous and is associated with extensive damage enhanced creep whereas in the brittle regime the rate of extrusion is very rapid, and this gets interrupted by sudden load drops due to fracture events. Indentation tests are an effective way to study the ice crushing process, and many experimental programs on different scales have been carried out over the years. Depending on the types of tests, the experimental programs can be broadly classified into two categories: (1) Edge indentation of ice sheet; (2) Indentation of ice wall (vertical and conical shapes).

Edge indentations are generally performed by pushing an indenter (usually flat) against an ice sheet in a test basin or in the field (landfast ice). The speed of the indenter, ice thickness, and width of the indenter are some of the common parameters which are varied during tests. The results of these tests have been reported by various authors (Hirayama et al., 1973; Croasdale et al., 1977; Michel and Blanchet, 1983; Timco, 1987; Kärnä and Muhonen, 1990; Sodhi, 1992, 2001; Tuhkuri, 1995; Sodhi et al., 1998) and a comprehensive review about the mechanism was provided by Sodhi (2001). Through a series of 66 tests with varying interaction speed, indenter width, ice thickness, strain rate, and aspect ratio, Timco (1987) found that crushing is the dominant mode of failure in the brittle range and is often accompanied by spalling, radial cracking and circumferential cracking. Based on the results, he proposed a failure mode-map as a function of strain-rate and aspect ratio highlighting the importance of these two parameters on the failure mode.

Tests using a spherical indenter provide valuable insight into the ice crushing process, and the behavior of a single *hpz* can be studied in detail using such tests. Failure within the *hpz*s is influenced by damage processes which typically include microcracking in zones of high shear and low confinement, as well as dynamic recrystallization and localized pressure melting in regions of

high shear and high confinement (Meglis et al., 1999; Melanson et al., 1999; Barrette et al., 2002). Pictures of the indented surface from medium-scale indentation tests at Hobson 's Choice Island (Frederking et al., 1990) showed the evidence of an extensive white layer of crushed material with occasional 'blue' recrystallized zones (Jordaan, 2001). The localized pressure melting and pressure softening within the layer results in a reduction in the load-bearing capacity leading to the extrusion of ice particles from beneath the contact zone. However, such pressure release contributes in reversing the thermodynamic process associated with pressure melting and thus lead to partial recovery of the strength within the layer. This repeating pattern of pressure softening and strength recovery (hardening) has been linked to the cyclic ice loading behavior during dynamic ice-structure interaction (Jordaan, 2001), which can induce frequency lock-in. Observations from the small-scale indentation tests on confined polycrystalline ice specimens showed cyclic loading up to frequency of 250*Hz*, and both indentation speed and structural compliance were found to have a direct relationship on failure frequency (Browne et al., 2013). Short-lived sequences of "lock-in" behavior have also been observed in recent small-scale indentation tests, and thin-section suggests that the depth range of the oscillating deformation cycles during vibration are contained within the crushed layer of ice (O'Rourke et al., 2016b). This observation has important implications since it suggests that under such circumstances, the indenter is continuously in contact with damaged ice. Ice temperature was found to have a significant influence on the failure mode and the microstructure of the crushed layer in that work.

To understand how the observed behaviors can be translated to full-scale interaction, a larger scale indentation program is presented in this chapter. Confined samples of freshwater polycrystalline ice were used for the tests. The ice samples were confined to prevent spalling and allowing pressure softening and extrusion observed during the continuous crushing process. The tests were

performed in the Structures Laboratory of Memorial University and using spherical indenters with nominal contact area ranging from $20cm^2$ – $180cm^2$. The effect of indentation speed, ice temperature, *hpz* area, and structural compliance on the cyclic nature of *hpz* failure behavior has been studied in detail.

4.2 Experimental Setup

4.2.1 Structural frame

Four steel-reinforced concrete pillars located at the Structures Laboratory were used as the core structural frame of the experimental setup. To increase the capacity of the overall system, a steel self-reacting frame with a capacity of 300,000*lb* was built which encapsulated the concrete pillars through an upper and a lower support ring consisting of girders bolted together (Figure 4.1). Additional ring stiffeners were attached with the support rings in the direction of the loading and the upper and lower support rings were connected through four 152*mm* × 152*mm* box beams. Two 100*mm* schedule 80 rail was bolted with the box beams on each side and guide bushes with Teflon sleeves were mounted on them to ensure smooth movement of the indentation system.

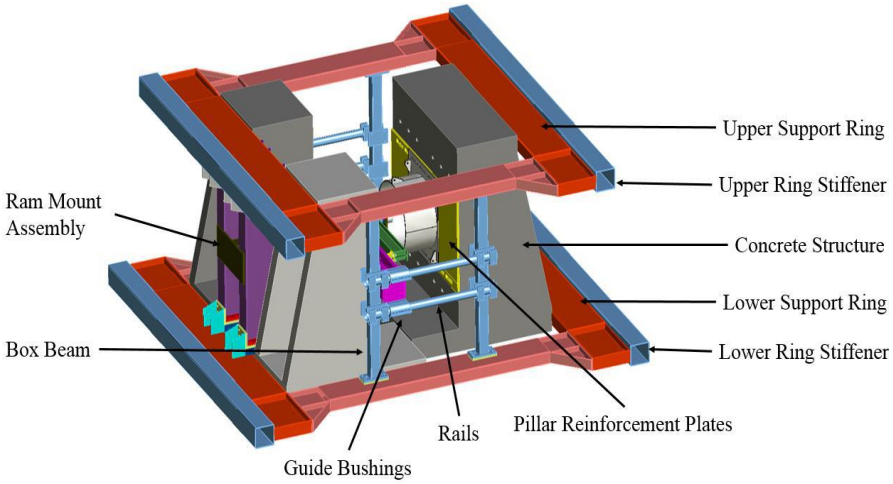

Figure 4.1 CAD drawing of the test apparatus

4.2.2 Indentation system

In this test series an indenter is pushed using a hydraulic system against a single ice specimen mounted on concrete pillars. The hydraulic system for the slow indentation tests consists of an Enerpac GPEx5 series electric pump with a reservoir capacity of 40 litres and an Enerpac CLRG series double acting, high tonnage cylinder. The maximum working pressure for the pump was 10,000*psi* and the flow rate at maximum pressure was 2.0*L/min*. The cylinder had a capacity of 500*ton* with a maximum stroke of 30*cm* and effective area of 730.6cm^2. The maximum speed with this hydraulic system was found to be 2.536*mm/s* which was used for all the slow speed indentation tests. For high speed tests, a Hydraulic Power Unit (HPU) with a flow rate of 11*gal/min* at 2500*psi* was used with a 300*ton* Enerpac CLRG series double acting, high tonnage cylinder. The system resulted in a maximum ram speed of ≈ 16*mm/s* which was used for the high speed tests.

The setup of the indentation system differed slightly depending on the compliance of the specific indenter configuration used in the tests. The complete indentation system and the instrumentations are shown in Figure 4.2. For compliant system 1 & 2, the cylinder was used to push a 3.91*m*

W12×170 mild steel I-beam which supported a parallel ‘compliant’ beam through two flex links made of SAE 4140 alloy steel. A 2.28*m* long 8×21 mild steel I-beam was used as the ‘compliant’ beam for the compliant system 1 and an 8x67 mild steel I-beam of the same length was used for the compliant system 2. The flex links (flange dimensions 127*mm* ×127*mm* ×12.7*mm*) were used to transfer the moment and permit rotation of the compliant beam. The maximum allowable load for the flex links was 444.82*kN* with a maximum deflection of 0.04318*mm*. The indenter was mounted at the center of the beam with a base plate which housed the load cell. Three different sizes indenters were used for the testing (shown in Figure 4.3). The specifications of the indenters are given in Table 4.1.

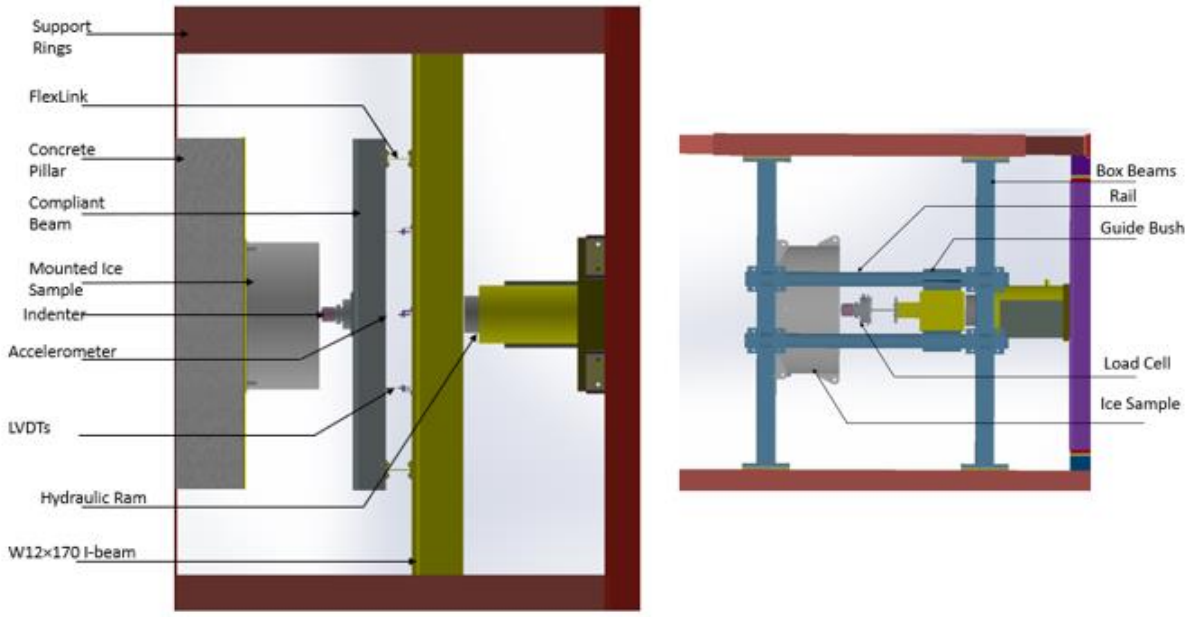

Figure 4.2 Indentation system (a) Top View; (b) Side View (The views are simplified to identify the components clearly)

For compliant system 3, only the W12x170 mild steel I-beam was used and the indenter was directly mounted on it. A 350*mm* long schedule-100 6061 aluminium cylinder attached to two

305*mm* ×305*mm* ×10*mm* aluminium flanges was used as a spacer between the hydraulic cylinder and the beam.

Figure 4.3 Different sizes indenters used in the testing

Table 4.1. Indenter specifications

Diameter (*mm*)	Radius of Curvature (*mm*)	Indenter Height (*mm*)	Nominal Surface Area (m^2)
50	64	90	1.96×10^{-3}
100	127	90	7.85×10^{-3}
150	192	90	17.6×10^{-3}

4.2.3 Instrumentation and data acquisition system

A number of different sensors were used to measure various parameters during the tests. A LPSW-100K Universal Tension & Compression Shear Web Load Cell with a maximum capacity of 445*kN* was placed between the indenter and the base plate to measure the ice load. Three MHR 500 A.C. linear variable displacement transducers (LVDTs) were used to measure the structural deflection of the 'compliant' beams. One LVDT was positioned at the center of the beam and the other two

were placed 560*mm* from the center on each side. The LVDTs were bolted on an aluminium block and clamped to the W12x170 mild steel I-beam using C-clamps (Figure 4.4). These LVDTs had a stroke length of $\pm$12.7*mm*, maximum non-linearity of < $\pm$0.25% and an operating temperature range of -55^{o}C to 150^{o}C. A PCB piezoelectric accelerometer (model 352C33) was also used to measure the acceleration of the 'compliant' beam. The measurement range of the accelerometer was $\pm$50*g* with a sensitivity of 100*mV/g*. A series 330 LVDT was used to measure the distance travelled by the indenter in the ice sample which had a working range of $\pm$25.4*mm*, maximum non-linearity of < $\pm$0.20% and an operating temperature range of -20^{o}C to 80^{o}C. Resistance temperature detectors (RTDs) and a Mastercraft non-contact infrared digital thermometer were used to measure the temperature of the ice samples.

An HBM QuantumX MX840B universal measuring amplifier with 8 connectors was used as the data acquisition system. Using the HBM CATMAN software measurements were recorded at a frequency of 4800*Hz*. All the tests were recorded using GoPro cameras.

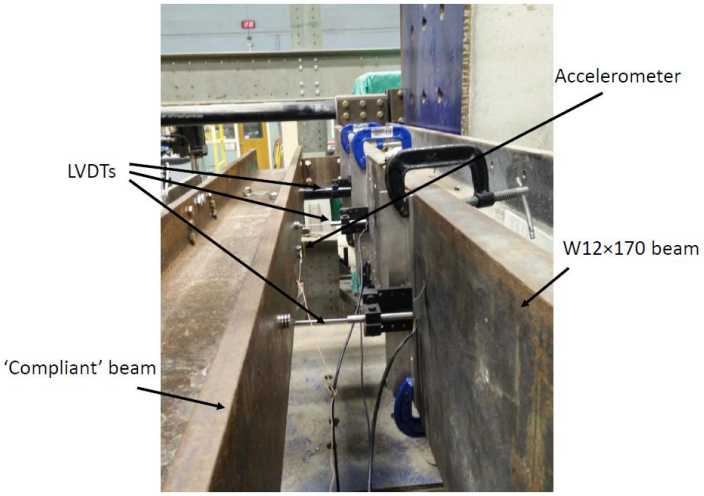

Figure 4.4 Position of the LVDTs and Accelerometer to measure structural response

4.2.4 Ice sample preparation

The cold room facilities at Memorial University and C-CORE were used throughout the project to prepare and store ice samples. Cylindrical ice holders with 1*m* diameter and 50*cm* height were used to prepare confined freshwater polycrystalline ice specimens used for all tests. The sample preparation took place in two stages. During the first stage, 30*cm* of the ice holder was filled with commercially available ice cubes and water chilled at $0^{o}C$.The mixture was stirred thoroughly to remove the air bubbles and was allowed to freeze for multiple days with a Styrofoam cover which insulated the sample from the top and allowed unidirectional ice growth. For the second stage, ice cubes were crushed using a Clawson Model HQ-C Ice Crusher and the crushed ice was sieved using a 2-10*mm* sieve (Figure 4.5). Once the bottom layer of the ice sample was frozen completely, the rest of the ice holder was filled with the sieved ice and chilled water. This allowed a consistent grain size ranging from 2-10*mm* in all ice samples. The final height of the ice samples were approximately 45*cm*. A sample ice specimen is shown in Figure 4.6.

Figure 4.5 Different stages of making ice seeds. (a) Commercially purchased bubble free ice cubes; (b) crushed ice; (c) sieved ice seeds

Figure 4.6 Ice samples used for the tests

4.3 Test Methods

During the tests, the ice sample was transferred from the cold rooms to the Laboratory using a forklift and was mounted on the concrete pillar with the help of a crane. The sample was bolted to the mounting plate and positioned accordingly to allow the indenter to make contact with the ice sample at the center. All of the instrumentation were connected to the data acquisition system using VGA cables prior to installation to reduce the test time. To ensure that ice sample and the indenter have same temperature during testing, the indenter used for a particular test was also stored in the cold room with the sample. However, since the heat transfer of steel is faster than ice, in most cases the indenter was found to have a slightly higher temperature than the ice surface at the time of testing. The non-contact infrared thermometer was used to measure the ice surface temperature just before the test and this temperature was recorded to be ice temperature for that particular test. The RTDs installed into the ice sample were used to confirm the recorded temperature. The hydraulic pump was operated using a remote control which resulted in a constant speed of the ram. The maximum allowed load was set to 70,000*lb* and the maximum displacement of the indenter in

the ice sample was set to 55*mm*. The hydraulic ram was stopped when either of these two limits was reached.

The complete test matrix is presented in Table 4.2.

Table 4.2. Test matrix

Test ID	Indenter Diameter (cm)	Ice Temperature (^0C)	Beam Stiffness (N/m)	Ram Speed (mm/s)
T1_5_16_C1_2.5	5	-16.5	C1 (2.67×10^7)	2.5
T1_5_19_C1_2.5	5	-19.5	C1 (2.67×10^7)	2.5
T1_5_7_C1_2.5	5	-7	C1 (2.67×10^7)	2.5
T1_5_4_C1_2.5	5	-4	C1 (2.67×10^7)	2.5
T1_5_15_C2_2.5	5	-15	C2 (9.61×10^7)	2.5
T1_5_3_C2_2.5	5	-3	C2 (9.61×10^7)	2.5
T1_5_7_C2_2.5	5	-7	C2 (9.61×10^7)	2.5
T1_5_16_C3_2.5	5	-16	C3 (4.64×10^8)	2.5
T1_5_7_C3_2.5	5	-7.5	C3 (4.64×10^8)	2.5
T1_5_3_C2_16	5	-3	C2 (9.61×10^7)	16
T1_5_9_C2_16	5	-9	C2 (9.61×10^7)	16
T1_10_18_C1_2.5	10	-18	C1 (2.67×10^7)	2.5

T1_10_1_C1_2.5	10	-1	C1 (2.67×10^7)	2.5
T1_10_7_C1_2.5	10	-7	C1 (2.67×10^7)	2.5
T1_10_17_C2_2.5	10	-17.5	C2 (9.61×10^7)	2.5
T1_10_6_C2_2.5	10	-6	C2 (9.61×10^7)	2.5
T1_10_2_C2_2.5	10	-2	C2 (9.61×10^7)	2.5
T1_10_15_C3_2.5	10	-15	C3 (4.64×10^8)	2.5
T1_10_6_C3_2.5	10	-6	C3 (4.64×10^8)	2.5
T1_10_5_C2_16	10	-5	C2 (9.61×10^7)	16
T1_10_11_C2_16	10	-11	C2 (9.61×10^7)	16
T1_15_18_C1_2.5	15	-18.5	C1 (2.67×10^7)	2.5
T1_15_6_C1_2.5	15	-6	C1 (2.67×10^7)	2.5
T1_15_6_C2_2.5	15	-6	C2 (9.61×10^7)	2.5
T1_15_8_C2_16	15	-8	C2 (9.61×10^7)	16

4.4 Results & Discussion

4.4.1 Observations during the tests

Most of the tests showed some regular patterns which can be identified as the characteristics of the ice failure process during indentation of the confined ice specimen. Figure 4.7 shows the force,

displacement and acceleration obtained from test T1_10_17_C2_2.5. The ice force shows a periodic ‘sawtooth’ behavior which is observed during intermittent crushing. The first failure event usually generates a lower force due to lower initial confinement for spalls that ran to the free surface. Each load drop is associated with a transient vibration of the beam which damps out quickly. The synchronized displacement of the LVDT suggests that the beam was deflecting as a simply supported beam and its first mode was excited during the associated vibration.

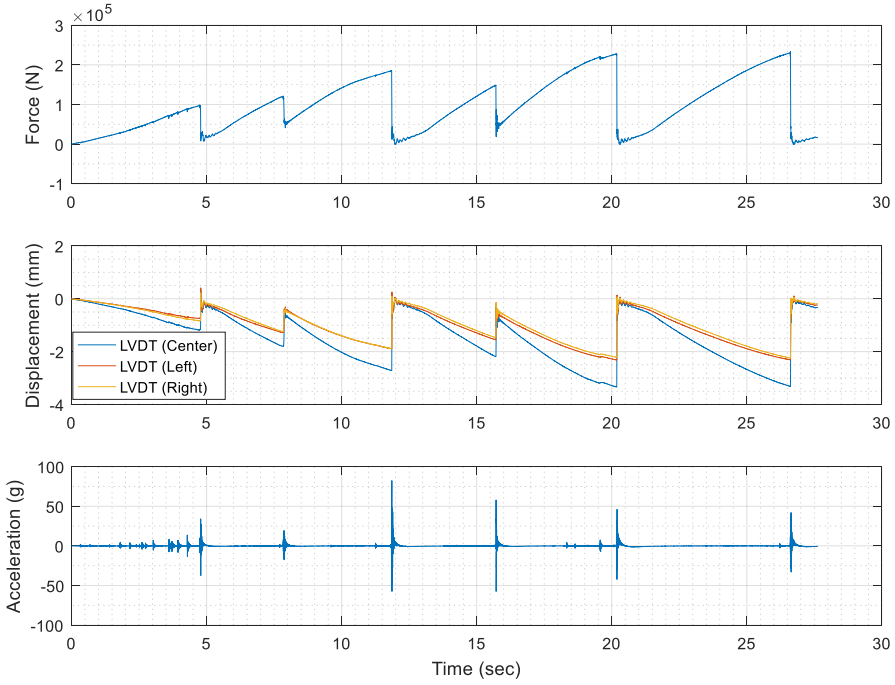

Figure 4.7 Results from T1_10_17_C2_2.5 showing force, displacement and acceleration against time

At the beginning of each ascending part of the loading curve contact area increases as the load accumulates. The load keeps increasing until failure occurs even after the contact area reaches its local maximum value. The failure process was found to be associated with a competition between damage and fracture, the ratio of which is highly influenced by test parameters. Damage refers to the pulverization and extrusion of ice beneath the indenter whereas fracture refers to the

propagation of cracks initiated at the contact zone which results in a removal of larger piece of ice. By synchronizing the video with the obtained data, the effect of the interaction parameters on the ice failure process can be observed. For most of the tests, as the load increases, extrusion of pulverized ice and propagation of cracks occur simultaneously suggesting the initialization of both damage and fracture processes. However, for warmer ice with small indenter size and slow ram speed, the rate of pulverization and extrusion dominates over spalling crack propagation. The loading curve at this point shows a 'smoothed-out' peak usually followed by a dip. After that, the load might increase for a few moments eventually followed by a spall and sharp load drop [see Figure 4.8(a)]. On the other hand, for colder ice, especially with larger interaction areas, cracks develop very quickly and failure is associated with a sharp peak and large load drops [see Figure 4.8(b)].

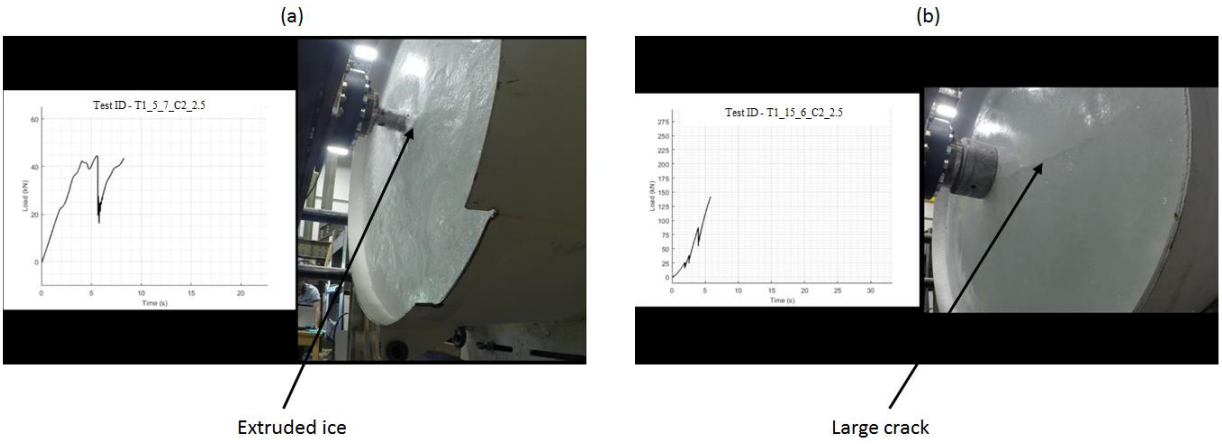

Figure 4.8 Damage and fracture dominated failure in two tests; (a) Test ID: T1_5_7_C2_2.5 showing extrusion process of ice with loading curve; (b) Test ID: T1_15_6_C2_2.5 showing initiation of cracks which results in sharp peak during load drop

During each load drop, a large part of the contact area is usually removed and the indenter surges forward with the energy stored in the beam. Although the total force is less, due to the reduction in the contact area, the pressure in the contact zone becomes very high and the stored energy causes

a rapid pulverization and extrusion process. The rapid extrusion process is often accompanied by pressure melting and dynamic recrystallization (Gagnon and Mølgaard, 1991; Jordaan, 2001). Eventually due to the increase in contact area and the release of strain energy stored in the beam, the process reaches a point where the load of the indenter can be borne by the ice and a new cycle initiates.

4.4.2 Effect of ice temperature

For slow tests (≈ 2.5*mm/s* ram speed), a significant difference in the failure behavior can be observed for all indenter size and compliant system when the ice temperature was above -3^{o}C. Figure 4.9 shows the comparison between tests T1_10_17_C2_2.5, T1_10_6_C2_2.5 and T1_10_2_C2_2.5. The indenter size, ram speed and structural compliance were kept constant for the three tests and the ice temperatures were varied. It is assumed that the nominal indenter area remains constant after the initial full envelopment and the nominal pressure was calculated by dividing the force recorded by the load cell with indenter area. For the tests at -17.5^{o}C and -6 ^{o}C, the pressure-time plot shows similar 'sawtooth' pattern described in the previous section although the peak failure pressure was significantly higher for colder ice for most of the peak pressures (Figure 4.9-Left). It should be noted that in general the peak failure pressure varied significantly within each test and therefore not all peaks of the colder ice were higher than the warmer ice. However, the pressure associated with the first failure event was consistently found to have a significantly higher value for colder ice. Figure 4.9 (Right) shows the average failure frequency (i.e., number of failure events over the interaction period) as a function of ice temperature. It is observed that when the failure is in the brittle domain, the frequency of the 'sawtooth' failure is

not strongly influenced by ice temperature. However, for 'warm' ice the failure frequency is significantly lower.

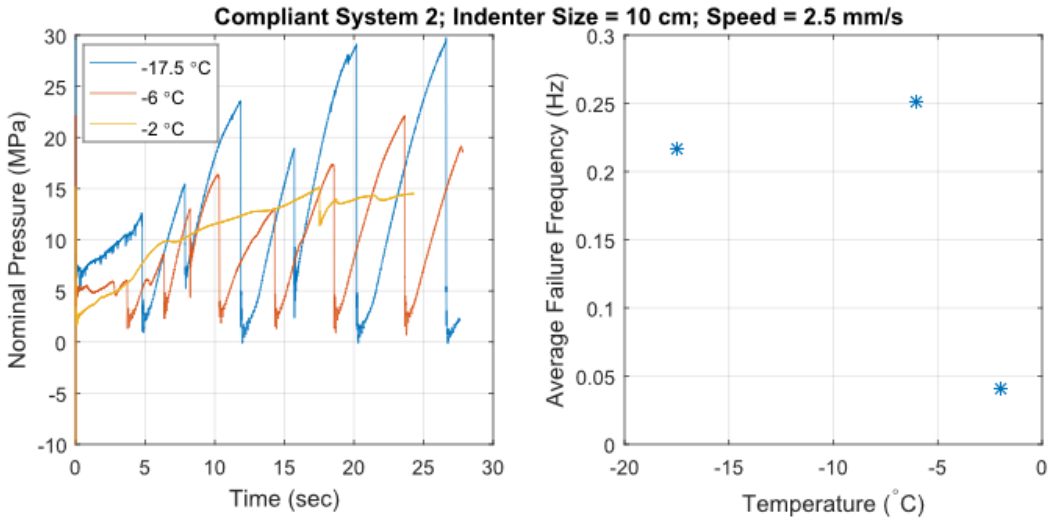

Figure 4.9 Comparison of results for tests T1_10_17_C2_2.5, T1_10_6_C2_2.5, T1_10_2_C2_2.5; (Left) Nominal Pressure plotted against time; (Right) Average failure frequency plotted against ice temperature

Figure 4.10 shows a closer look of the ice failure processes near the indentation area at the end of the tests and the effect of ice temperature at failure behavior. For ice at -2^{o}C the continuous extrusion of highly damaged ice which resulted in the continuous nonlinear pressure-time series can be clearly visible. For 'colder' ice, the failure surface looks very similar suggesting the similarity in the failure processes. However, for ice at -17.5^{o}C, the spall area was much larger compared to ice at -6^{o}C, which is consistent with the observed load drop in Figure 4.9.

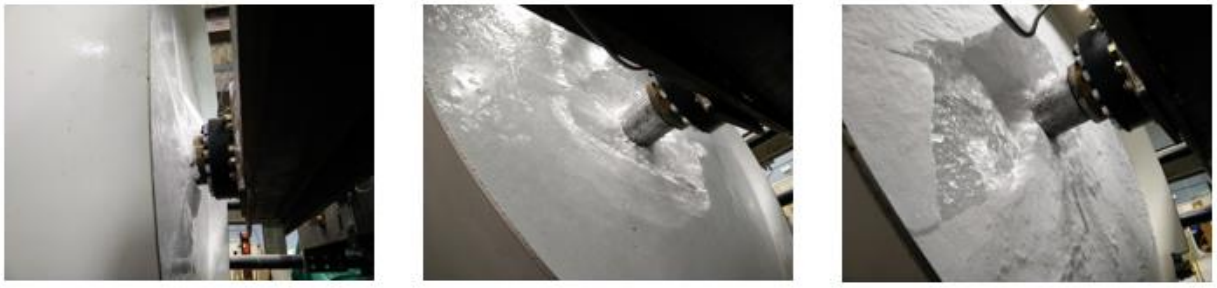

Figure 4.10 Ice failure processes in the indentation area for different temperatures

For high speed tests the failure behavior was slightly different for both the 'warm' ice and 'cold' ice. Figure 4.11 (Left) shows the nominal pressure and beam displacement at the center vs time for tests T1_5_3_C2_16 and T1_5_9_C2_16 where the ice temperatures were -3^{o}C and -9^{o}C respectively. The pressure-time and displacement-time trace shows similar behavior in this case with the failure being a mixture of both continuous extrusion and large load drops. The average failure frequency shows a similar trend to slow speed tests; the failure frequency being considerably high for colder ice (Figure 4.10-Right). The maximum pressure, load drops and maximum displacement were similar in nature; however, the acceleration data shows that the dynamics associated in the two cases were completely different (Figure 4.12). As shown in Figure 4.12, dynamic responses of the beam associated with ice failure were recorded in both cases. For the ice at -3^{o}C, the maximum value ranged only between -0.05g to +0.05g whereas for -9^{o}C the value ranged between -20g to +20g. This has important implication for ice-induced vibration since the results suggest that for colder ice the failure process is sudden and the rapid release of energy can significantly excite the structure. On the other hand although the static deflection of the structure and the maximum load shows a similar magnitude for warmer ice, the load drop involves significant extrusion process which results in a more continuous, 'slow' release of energy,

therefore the process was unable to excite the structure significantly. This observation is consistent with the results presented in the sensitivity study of ice-induced vibration models discussed by Hossain et al. (2018). It is noted here that Bjerkås et al. (2013) reported from their analysis of field measurement data from Norströmsgrund lighthouse that ice-induced vibration were observed to occur more frequently during warmer periods of time in the spring of the year. Further analysis is needed to relate the present work with such observations, since multiple *hpz*s act simultaneously during full-scale interactions and further work is needed to better understand interactions between such *hpz*s over larger scales. Moreover, during the spring months in addition to being warmer, sea ice is at its thickest and is more mobile than during the winter. Since it is known that increases in thickness and drift speed are also expected to increase the likelihood of dynamic interactions, further work is needed to better understand the interplay between temperature, thickness and drift speed in such observations.

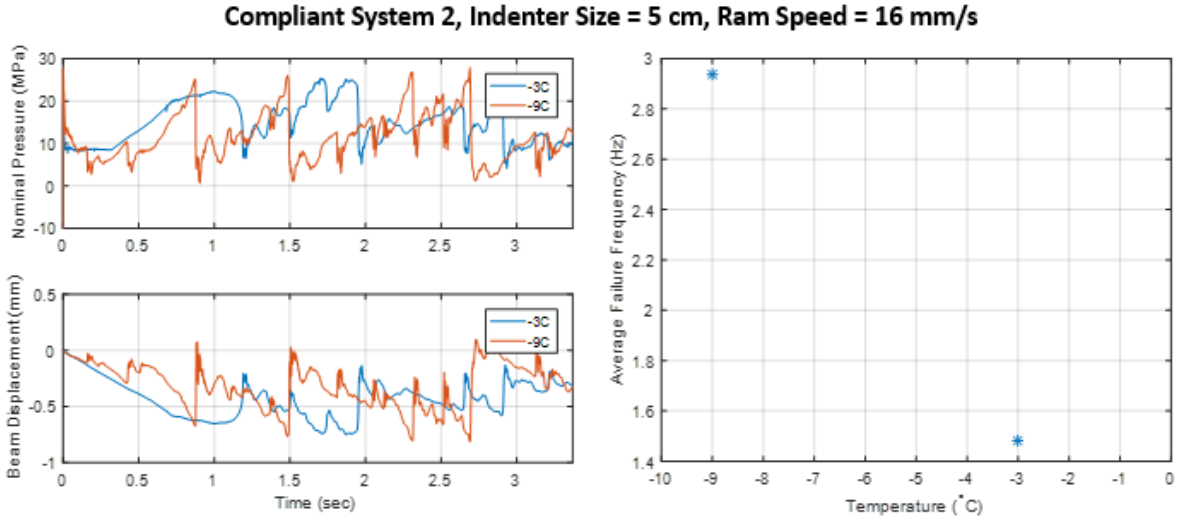

Figure 4.11 Comparison of results for tests T1_5_3_C2_16 and T1_5_9_C2_16 (Left) Nominal Pressure and Beam Displacement at the center plotted against time; (Right) Average failure frequency plotted against ice temperature

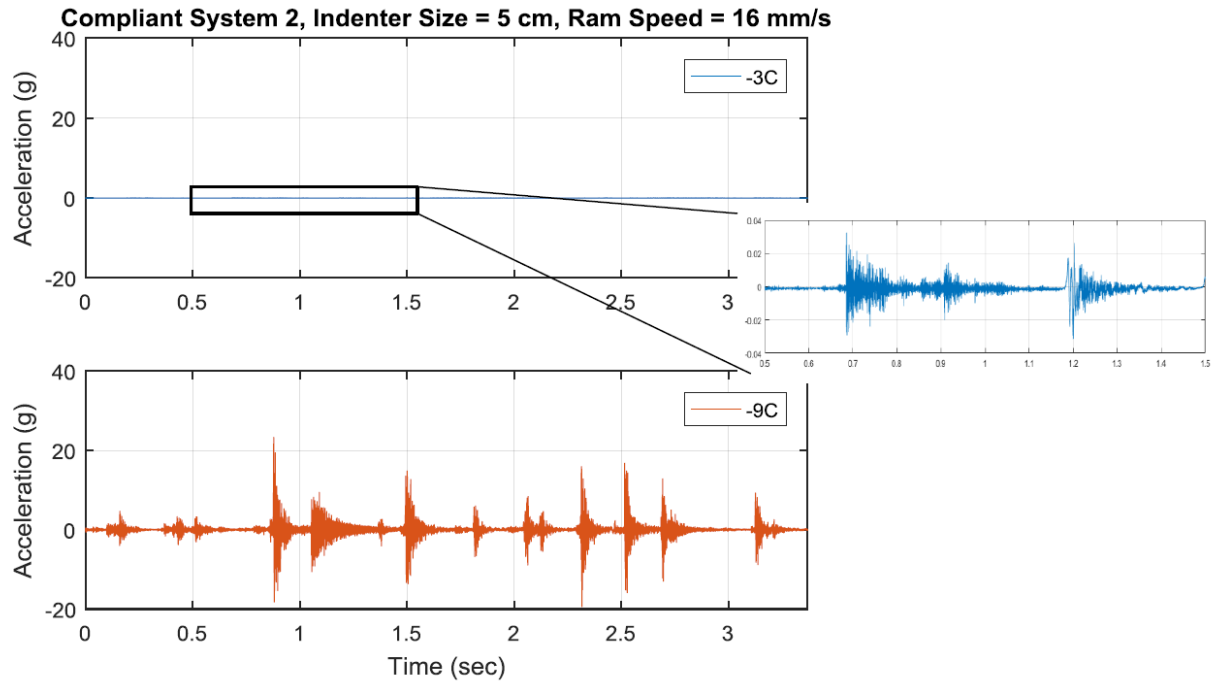

Figure 4.12 Acceleration data from tests T1_5_3_C2_16 and T1_5_9_C2_16 with expanded view of the selected area shown on right

4.4.3 Effect of indentation speed

The tests were performed at two different ram speeds: 2.5*mm/s* and 16*mm/s*. The effect of indentation speed can be seen in Figure 4.13 (Left) where the force was plotted against indentation depth for tests T1_10_6_C2_2.5 and T1_10_5_C2_16. Although the peak failure force was found to be on the same order of magnitude, a number of distinctions in the failure behavior can be identified from the plot. For the slow tests the force increases monotonically until the failure occurs with large pieces of ice being removed and load dropping more than 90%. On the other hand, for fast tests, as the load increases it continues to produce local fractures with smaller ice pieces before a large load drop occurs and larger pieces of ice are removed. For higher rates the existing flaws in the ice get subjected to a more rapidly increasing concentrated stress field (slower dissipative

processes do not have time to relieve local intense stresses) which results in a higher degree of local fracture. Also due to the release of stored energy upon rebound following local fracture events, the cumulative amount of energy stored in the beam is lower for fast tests, which for many cases result in a lower load drop. This has important implication for the development of the damaged layer in the indentation contact zone. If a large amount of energy is stored in the beam during the loading period, the release of this energy upon failure can clear out most of the ice in the damaged layer through extrusion. However, if the energy is not sufficient, part of the damaged layer survives the rebound cycles and continues to grow triggered by the fracture event. Such behavior can result in vibration within the damaged layer as has been observed in small-scale indentation tests (O'Rourke et al., 2016b). The average failure frequency against interaction speed is plotted in Figure 4.13 (Right). As expected, the average failure frequency was consistently found to be significantly higher for fast tests.

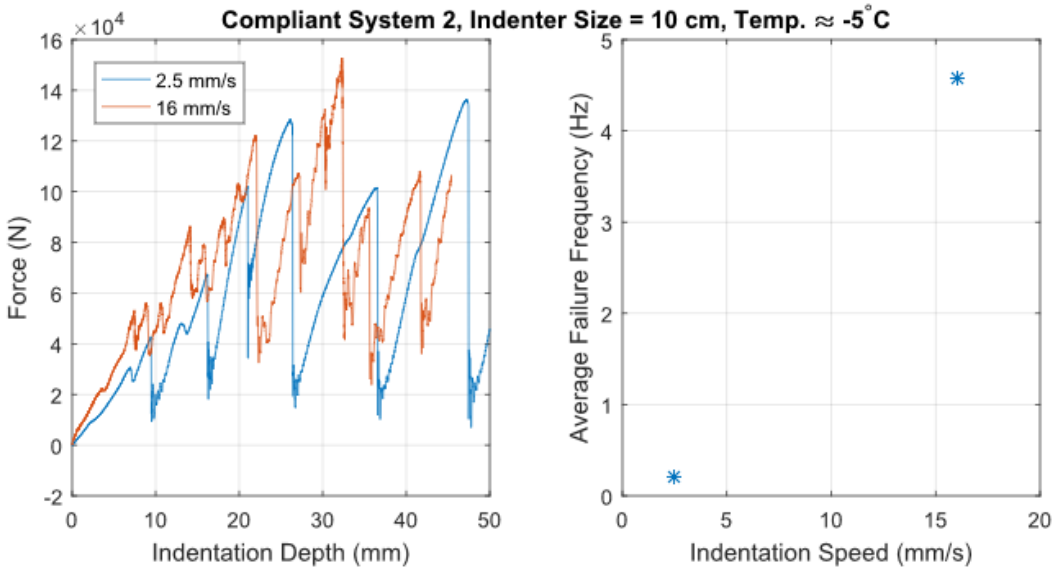

Figure 4.13 Comparison of results for tests T1_10_6_C2_2.5 and T1_10_5_C2_16 (Left) Total Force plotted against time; (Right) Average failure frequency plotted against indentation speed

4.4.4 Effect of indenter size

The ‘pressure-area effect’ or ‘scale-effect’ is a well-known concept in ice research community and refers to the scale dependence of the material during failure (Sanderson, 1988; Masterson et al., 2007). The effect was observed in the test series as the indenter sizes were varied keeping the temperature, structural compliance and ram speed constant. Although the effect was observed in all combinations of test parameters, it was most pronounced with compliant system 1 during slow tests. Figure 4.14 (Left) shows the nominal pressure vs. time for tests T1_5_19_C1_2.5, T1_10_18_C1_2.5, T1_15_18_C1_2.5 and T1_15_18_C1_2.5 where the ram speed was 2.5mm/s and structural compliance was C1 for all tests. The ice temperature varied between -16.5^oC to -19.5^oC and the result shows a clear scale-effect for three indenter sizes. The maximum failure pressure for the 5cm indenter was above 60MPa whereas the maximum failure pressure for the 15cm indenter was just above 10MPa. The frequency of failure was also observed to be somewhat dependent on the indenter size (Figure 4.13-Right); however, such dependency was not found to be very strong.

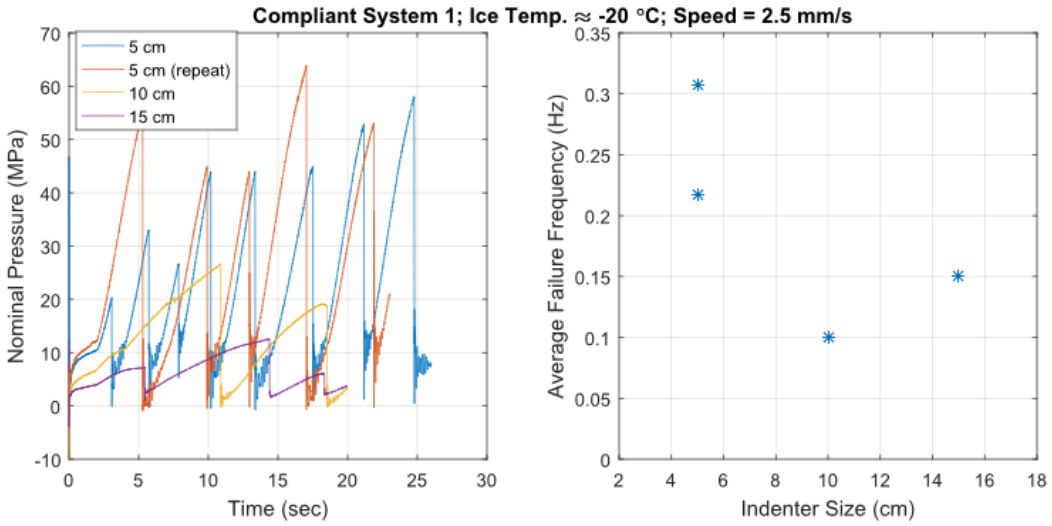

Figure 4.14 Comparison of results for tests T1_5_19_C1_2.5, T1_10_18_C1_2.5, T1_15_18_C1_2.5 and T1_15_18_C1_2.5; (Left) Nominal pressure plotted against time; (Right) Average failure frequency plotted against indenter size

4.4.5 Effect of structural compliance

Three levels of structural compliance were used in this test series with natural frequencies of the beams of 135*Hz*, 145*Hz* and 173*Hz* for C1, C2 and C3 systems respectively. Nominal pressures are plotted against time in Figure 4.15 for tests T1_10_18_C1_2.5, T1_10_17_C2_2.5 and T1_10_15_C3_2.5 for indenter size of 10*cm* and a constant ram speed of 2.5*mm/s*. While there are some variations in ice temperature from test to test, this difference was within $\pm 3^{o}C$. Assuming that compliance is the primary difference between each of the cases, it may be observed that the difference in structural compliance does not have a significant effect on peak failure pressure but it does significantly influence the failure frequency. For compliant system 1, only two major spalling occurs whereas for compliant system 3, seven failure events can be identified. A similar observation was made by Browne et al. (2013) at small-scale where the failure frequency showed linear relationship with structural compliance. The pressure drops following failure were also found to be greater for C1 compared to the other two beams, which can be attributed to the amount

of stored energy in the beam at the point of failure. By comparing the events A, B and C for the three compliant systems with similar peak loads (Figure 4.15), the rebound of the indenter was found to be 0.98*mm* for compliant system 1, 0.71*mm* for complaint system 2 and 0.4*mm* for compliant system 3. From these results it is noted that the extrusion of the damaged layer and associated vibrations within this layer are highly influenced by the rebounding process, which is consistent with observations from small-scale experiments (O'Rourke et al., 2016b). For the most compliant system, given the larger rebound distance which follows a failure event, it is expected that nearly all of the damaged ice would be extruded during the rebound process (e.g. very little of the damaged layer survives the extrusion phase of the oscillation cycle), resulting in the indenter being in contact with much more 'intact' ice at the beginning of the next cycle of loading. On the other hand for the stiffest configuration a lower rebound distance suggests that a more significant part of the damaged layer survives between subsequent 'sawtooth' cycles, highlighting that the ice contacting the indenter at the onset of each loading phase of an oscillation cycle is in a much more damaged state. This has important implications for modelling the behaviour of ice in the contact zone, since it implies that stiffer structures may be less likely to 'reset' the damage layer formation process during each subsequent load cycle, which may give rise to more periodic layer oscillation. By comparison, more compliant structures would extrude most of the damaged ice from the contact zone during each cycle, making such interactions more likely to take on a sawtooth character. Since the behaviour of the ice (e.g. damage rate, fracture behaviour, strain rate dependence and temperature effects) in turn govern the rate and depth of the damaged layer formation, this work further highlights the need for a coupled treatment of dynamics ice-structure interactions.

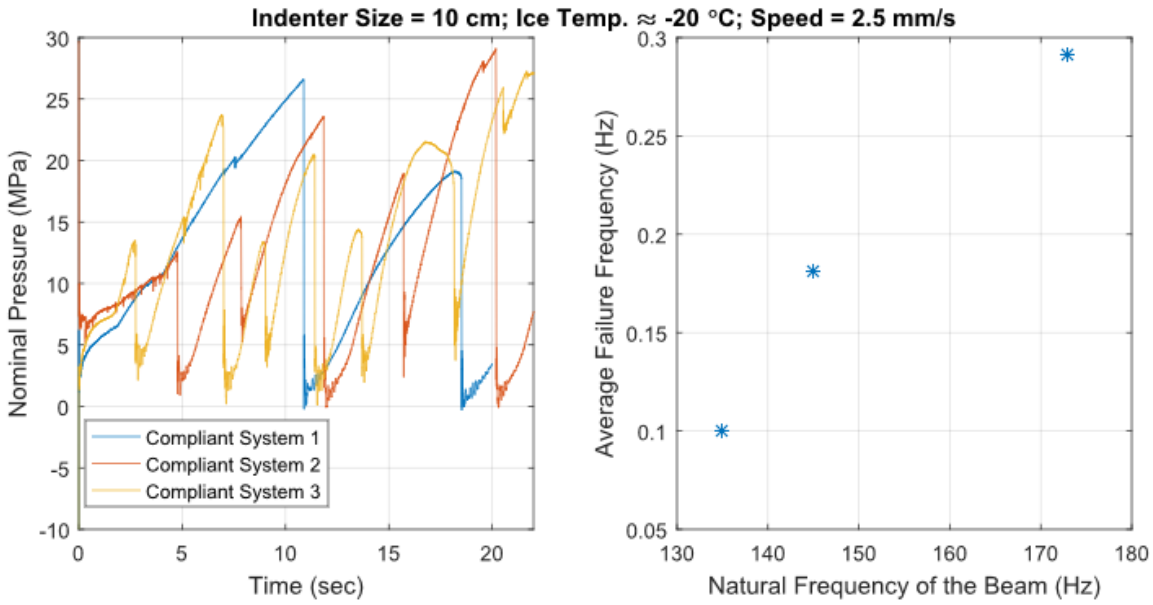

Figure 4.15 Comparison of results for tests T1_10_18_C1_2.5, T1_10_17_C2_2.5 and T1_10_15_C3_2.5; (Left) Nominal Pressure plotted against time; (Right) Average failure frequency plotted against the natural frequency of the beam

4.5 Concluding remarks

This chapter presents results from medium-scale ice crushing dynamics tests which were used to simulate *hpz*s with areas in the order of 10^3-$10^4 mm^2$. The effect of ice temperature, interaction speed, indenter size and structural compliance on failure behavior and associated structural dynamics were observed. The nature of the force-time curve was found to be highly correlated with observed failure behavior which is influenced by a competition between damage and fracture as was described for small-scale tests (e.g. Taylor et al., 2013). In general, for warmer ice and smaller contact area, continuous extrusion with intermittent spalling events was found to dominate failure resulting in a 'smoothed-out' peak pressure. The failure behavior of colder ice and for large interaction area on the other hand was dominated by fracture with sharp peaks and large load drops. Ice temperature was found to have significant effect on failure behavior, with colder ice resulting in higher peak pressure and more dynamic activity. Over the range of rates considered, the

interaction speed did not have a significant effect on the magnitude of peak failure pressures; however, faster tests resulted in a much higher failure frequency for same penetration depth. The well-known 'pressure-area' effect was also observed as the indenter sizes were varied, but the effect was found to be more pronounced in colder ice and for more compliant structures as was also reported in prior analysis (e.g. Taylor and Jordaan, 2015). Results obtained for three levels of structural compliance used suggest that the structural compliance does not have a significant effect on the magnitude of the peak failure pressure but it does highly affect the failure frequency, suggesting that peak pressures are dominated by processes in the ice while frequency is dominated by structural parameters and interaction conditions. Most of the observations presented in the chapter are aligned with the conclusions from small-scale indentation test series performed previously (Gagnon and Mølgaard, 1991; Barrette et al., 2002; Wells et al., 2011; Browne et al., 2013; O'Rourke et al., 2016b) which highlights the consistency in the failure behavior of *hpz*s. Since *hpz*s are a fundamental component of compressive ice failure process, the observed consistency of their failure behavior on multiple scales can be highly beneficial for modelling dynamic ice-structure interaction process. The extension of recent models of non-simultaneous ice failure (Taylor et al., 2019) to include dynamic coupling effects described above is presently underway.

References

API, 1995. Recommended Practice 2N – Planning, Designing and Constructing Structures and Pipelines for Arctic Conditions. Am. Pet. Inst.

Barrette, P., Pond, J., Jordaan, I., 2002. Ice damage and layer formation in small-scale indentation experiments, in: Proceedings of the 16th IAHR International Symposium on Ice. International Association for Hydraulic Research, Dunedin, New Zealand, vol. 3 pp. 246–253.

Bjerkås, M., Lonoy, C., Gurtner, A., 2013. Ice- Induced Vibrations and Effects of Ice Temperature. Int. J. Offshore Polar Eng. 23, 9–14.

Browne, T., Taylor, R., Jordaan, I., Gürtner, A., 2013. Small-scale ice indentation tests with variable structural compliance. Cold Reg. Sci. Technol. 88, 2–9. https://doi.org/10.1016/j.coldregions.2012.12.006

Croasdale, K.R., Morgenstern, N.R., Nuttall, J.B., 1977. Indentation Tests to Investigate Ice Pressures on Vertical Piers. J. Glaciol. 19, 301–312. https://doi.org/10.3189/S0022143000029361

Dempsey, J., Palmer, A., Sodhi, D., 2001. High pressure zone formation during compressive ice failure. Fract. Ice 68, 1961–1974. https://doi.org/10.1016/S0013-7944(01)00033-9

Frederking, R., 2004. Ice pressure variations during indentation, in: Proceeding of the 17th IAHR International Symposium on Ice. International Association for Hydraulic Research, Saint Petersburg, Russia, vol. 2 pp. 307–314.

Frederking, R., Jordaan, I.J., McCallum, J.S., 1990. Field tests of ice indentation at medium scale: Hobson's Choice ice island 1989, in: Proceedings of the 10th IAHR International Symposium on Ice. International Association for Hydraulic Research, Espoo, Finland, vol. 2 pp. 931–944.

Gagnon, R., 2011. An inside look at ice-crushing induced vibration and lock-in, in: Proceedings of the 21st International Conference on Port and Ocean Engineering under Arctic Conditions (POAC'11). Montreal, Canada.

Gagnon, R., Mølgaard, J., 1991. Evidence for pressure melting and heat generation by viscous flow of liquid in indentation and impact experiments on ice. Ann. Glaciol. 15, 254–260. https://doi.org/DOI: 10.3189/1991AoG15-1-254-260

Hirayama, K., Schwarz, J., Wu, H., 1973. Model technique for the investigation of ice forces on structures, in: Proceedings of the 2nd International Conference on Port and Ocean Engineering under Arctic Conditions (POAC'73). vol. 1 pp. 332–344.

Hossain, R., Taylor, R., Moro, L., 2018. An assessment of sensitivity of the self-excited modelling approach for simulating dynamic ice-structure interactions to changes in temperature and scale effects. Ocean Eng. 165, 410–425. https://doi.org/10.1016/j.oceaneng.2018.07.029

Johnston, M.E., Croasdale, K.R., Jordaan, I.J., 1998. Localized pressures during ice-structure interaction: relevance to design criteria. Cold Reg. Sci. Technol. 27, 105–117. https://doi.org/10.1016/S0165-232X(97)00026-8

Jordaan, I.J., 2001. Mechanics of ice-structure interaction. Fract. Ice 68, 1923–1960. https://doi.org/10.1016/S0013-7944(01)00032-7

Kärnä, T., Muhonen, A., 1990. Preliminary results from ice indentation tests using flexible and rigid indentors, in: Proceeding of the 10th IAHR Symposium on Ice. International Association for Hydraulic Research, Espoo, Finland, vol. 3 pp. 261–275.

Kärnä, T., Trunen, R., 1990. A straightforward technique for analyzing structural response to dynamic ice action, in: Proceedings of the ASME 1990 9th International Conference on Ocean, Offshore and Arctic Engineering (OMAE1990). American Society of Mechanical Engineers (ASME), Houston, Texas, vol. IV pp. 135–142.

Masterson, D.M., Frederking, R.M.W., Wright, B., Kärnä, T., Maddock, W.P., 2007. A revised ice pressure-area curve, in: Proceedings of the 19th International Conference on Port and Ocean Engineering under Arctic Conditions (POAC'07). Dalian University of Technology Press, vol. 1 pp. 305–314.

Meglis, I.L., Melanson, P.M., Jordaan, I.J., 1999. Microstructural change in ice: II. Creep behavior under triaxial stress conditions. J. Glaciol. 45, 438–448. https://doi.org/10.3189/S0022143000001295

Melanson, P.M., Meglis, I.L., Jordaan, I.J., Stone, B.M., 1999. Microstructural change in ice: I. Constant-deformation-rate tests under triaxial stress conditions. J. Glaciol. 45, 417–437. https://doi.org/10.3189/S0022143000001271

Michel, B., Blanchet, D., 1983. Indentation of an S 2 Floating Ice Sheet in the Brittle Range. Ann. Glaciol. 4, 180–187.

O'Rourke, B.J., Jordaan, I.J., Taylor, R.S., Gürtner, A., 2016. Experimental investigation of oscillation of loads in ice high-pressure zones, part 1: Single indentor system. Cold Reg. Sci. Technol. 124, 25–39. https://doi.org/10.1016/j.coldregions.2015.12.005

Sanderson, T.J.O., 1988. Ice mechanics : risks to offshore structures. London, UK ; Boston : Graham & Trotman, London, UK ; Boston.

Sodhi, D., 2001. Crushing failure during ice-structure interaction. Fract. Ice 68, 1889–1921. https://doi.org/10.1016/S0013-7944(01)00038-8

Sodhi, D., 1992. Ice-structure interaction with segmented indentors, in: Proceedings of the 11th IAHR International Symposium on Ice. International Association for Hydraulic Research, Edmonton, Canada, vol. 2 pp. 909–929.

Sodhi, D.S., Takeuchi, T., Nakazawa, N., Akagawa, S., Saeki, H., 1998. Medium-scale indentation tests on sea ice at various speeds. Cold Reg. Sci. Technol. 28, 161–182. https://doi.org/10.1016/S0165-232X(98)00017-2

Taylor, R., Browne, T., Jordaan, I., Gürtner, A., 2013. Fracture and damage during dynamic interactions between ice and compliant structures at laboratory scale, in: Proceedings of the ASME 2013 32nd International Conference on Ocean, Offshore and Arctic Engineering (OMAE2013). American Society of Mechanical Engineers (ASME), Nantes, France, vol. 6 .

Taylor, R., Frederking, R., Jordaan, I., 2008. The nature of high pressure zones in compressive ice failure, in: Proceeding the 19th IAHR International Symposium on Ice. International Association for Hydraulic Research, Vancouver, BC, Canada., vol. 2 pp. 1001–1010.

Taylor, R., Jordaan, I., 2015. Probabilistic fracture mechanics analysis of spalling during edge indentation in ice. Eng. Fract. Mech. 134, 242–266. https://doi.org/10.1016/j.engfracmech.2014.10.021

Taylor, R.S., Richard, M., Hossain, R., 2019. A Probabilistic High-Pressure Zone Model for Local and Global Loads During Ice-Structure Interactions. J. Offshore Mech. Arct. Eng. 141. https://doi.org/10.1115/1.4042386

Timco, G., 1987. Indentation and Penetration of Edge-Loaded Freshwater Ice Sheets in the Brittle Range. J. Offshore Mech. Arct. Eng. 109, 287–294.

Tuhkuri, J., 1995. Experimental observations of the brittle failure process of ice and ice-structure contact. Cold Reg. Sci. Technol. 23, 265–278. https://doi.org/10.1016/0165-232X(94)00018-S

Wells, J., Jordaan, I., Derradji-Aouat, A., Taylor, R., 2011. Small-scale laboratory experiments on the indentation failure of polycrystalline ice in compression: Main results and pressure distribution. Cold Reg. Sci. Technol. 65, 314–325. https://doi.org/10.1016/j.coldregions.2010.11.002

Wright, B., Timco, G., 1994. A Review of Ice Forces and Failure Modes on the Molikpaq, in: Proceedings of the 12th IAHR International Symposium on Ice. International Association for Hydraulic Research, Trondheim, Norway, vol. 2 pp. 816–825.

Chapter: 5 Characterization of High-Pressure Zone (hpz) Failure and Linkages with Structural Response during Medium-scale Indentation Tests

Preface

This chapter has been published as an original research article in the Proceedings of the 25th International Conference on Port and Ocean Engineering under Arctic Conditions (POAC'19)[2]. As the primary author, I was responsible for writing the article, performing the experiments and analyzing the results. My co-author Dr. Rocky Taylor provided guidance at different stages of the writing and analysis.

Based on the medium-scale ice crushing dynamics test program described in the previous chapter, the characteristics of the failure behavior of high-pressure zones (*hpz*s) were studied, and the

[2] Hossain, R., Taylor, R., 2019. Characterization of high-pressure zone (hpz) failure and linkages with structural response during medium-scale indentation tests. Proceedings of the 25th International Conference on Port and Ocean Engineering under Arctic Conditions (POAC'19), Delft, The Netherlands, June 9-13, 2019.

effects of ice temperature, indenter size, and structural stiffness on the failure properties were analyzed. To improve the coherence of the thesis and to avoid repetition, a modified version of the paper is presented in this chapter. The section "Introduction" provides the background and motivation of the work presented in this chapter and although the reader of the thesis has already been informed about the background and motivation of the work presented in the thesis in more details in Chapter 1 and 2, the section has been retained here for the completeness of this chapter. The "Experimental Setup" section from the original paper has been removed since a detailed version of the experimental setup has already been presented in section 4.2. An additional sub-section 5.3.4 has been included highlighting the link between the experimental observations and the model development presented in the next chapter.

Abstract

The formation of high-pressure zones (*hpz*s) during compressive ice failure results from a complex mixture of fracture and damage processes that lead to crushing and extrusion. The development of an *hpz* based dynamic ice-structure interaction model requires detailed understanding of these processes, as well modelling of the influence of structural response. In this chapter, results from a recent series of medium-scale indentation tests conducted using spherical indenters to model individual *hpz*s are described. In these experiments, the effects of ice temperature, indenter size and structural stiffness on the failure properties have been analyzed. These tests have been carried out to study links between observed failure behavior of *hpz*s and structural response for a range of temperatures (between $-1^{o}C$ and $-20^{o}C$), with areas on the order of 10^{3}-$10^{4} mm^{2}$ and for structures having three different levels of stiffness (ranging from 2.67×10^{7}- $4.64\times10^{8} N/m$). The average failure pressure was found to be negatively correlated with indenter size, as is expected due to

well-known pressure-area effects in ice. The peak failure pressure was also found to be affected by ice temperature, with colder ice resulting in higher *hpz* pressures. Of particular interest is the observation that the maximum *hpz* loads were found to be insensitive to structural stiffness, while the percentage of force drop was highly dependent on structural compliance. The results have been incorporated into a statistical model of *hpz* failure, which will be integrated into ongoing development of *hpz* based dynamic ice-structure interaction models.

5.1 Introduction

When a drifting ice sheet with sufficient driving force collides with a vertical-sided offshore structure, the localized ice failure process is dominated by spalling and crushing which generates multiple regions of high pressure, termed as high pressure zones (*hpz*s). The non-uniform nature of the contact between the ice sheet and the structure can result in local pressures (e.g. pressures over a structural grillage) which are an order of magnitude higher than the global pressure (acting over the entire nominal interaction area). Medium-scale indentation tests of ice at Pond Inlet, Baffin Island and Hobson's Choice Ice Island shows that the pressure near the center of an interaction area can be significantly higher than the pressure near the edge and the failure may be associated with regular dynamic activity as was shown in the cyclic nature of the 'sawtooth' type load-time trace reported by Frederking et al. (1990) and Kennedy et al. (1994). These observed dynamics have been linked to the development and extrusion of a crushed ice layer at the ice-structure interaction interface. Thin-sections of the crushed layer suggest that the development of this layer occurs due to a complex interplay of a number of different processes such as pressure melting, microcracking, dynamic recrystallization and sintering (Jordaan, 2001). However, the formation of the layer is highly dependent on the interaction parameters such as interaction speed,

ice temperature, indentation area and structural compliance. To study the effects of interaction parameters on the dynamics of *hpz*s and the formation of the associated crushed layer, a number of small-scale indentation test programs have been carried out (Barrette et al., 2002; Wells et al., 2011; Browne et al., 2013; O'Rourke et al., 2016b, 2016a).

During spalling, large pieces of ice near the free surface are removed by fracture, which causes a significant load drop and a reduction in the contact area (Taylor and Jordaan, 2015). The interplay between crushing and spalling is highly influenced by interaction speed, with more spalls occurring as speed increases (Wells et al., 2011). The formation of such spalls is also influenced by the location of *hpz*s since the preferential crack growth during fracture occurs towards free edges (Mackey et al., 2007) and the frequency of spalling is directly proportional to the structural compliance (Browne et al., 2013). The crushing process is also dependent on interaction parameters since temperature plays an important role in microstructural processes in the crushed layer (Barrette et al., 2002; Browne et al., 2013; Taylor et al., 2013). In their two papers, O'Rourke et al. (2016a, 2016b) argued that the periodic formation and extrusion within the crushed layer, as well as the load transmitting mechanism between multiple *hpz*s through structural feedback, could potentially generate conditions for ice-induced vibrations which would be highly dependent on the interplay between different interaction parameters.

At the same time, the well-known pressure-area relationship highlights that ice is a scale-dependent material and to extend observed behavior to full-scale interactions, the dynamic behavior of *hpz*s needs to be studied at a larger scale. The experimental program presented herein has been designed to study the dynamics of *hpz*s with larger areas, on the order of 10^3-$10^4 mm^2$, which is much larger than any previous studies and is approximately the size of individual

*hpz*s during larger scale interaction (Taylor et al., 2019). In this paper, some preliminary results of the medium-scale tests are presented to investigate the sensitivity of *hpz* failure force on ice temperature and structural compliance.

5.2 Overview of the Analyzed Data

5.2.1 Definition of independent *hpz* failure

Continuous indentation was performed in each test until either the maximum load limit (≈70000lb) or the maximum displacement limit of the indenter within the ice (≈50mm) was reached. To identify whether the failure behavior differs significantly with the depth of indentation, Figure 5.1 showing the force vs. depth has been plotted. As may be observed from this figure, for test T1_5_15_C2 the peak force of *hpz* failure is found to be insensitive of indentation depth. A similar trend was observed for other tests as well and therefore, each of these load drops has been interpreted as an independent *hpz* failure event and the rest of the analysis is based on this assumption. It should be noted here that this assumption is only valid since the ratio between the indentation depth and sample diameter is very small (≈ 0.05). For higher ratios between the indentation depth and sample diameter, confinement may have a significant effect on failure strength and should be addressed accordingly.

As discussed by Birajder et al. (2016), for warm ice, especially when the contact area is large, *hpz*s fails due to damage enhanced continuous extrusion. The exact point of such failure is often difficult to interpret and is excluded from the current analysis. In this paper, only test results corresponding to cases where the *hpz*s failed in brittle manner are considered. To maintain a consistent definition of *hpz* failure, events are defined as occurring when the peak of the ascending loading curve drops

more than 50% within 10 subsequent data points ($\approx 2ms$). For example, although event A and B in Figure 5.1 shows a degree of load drop, such events are not considered as an *hpz* failure event.

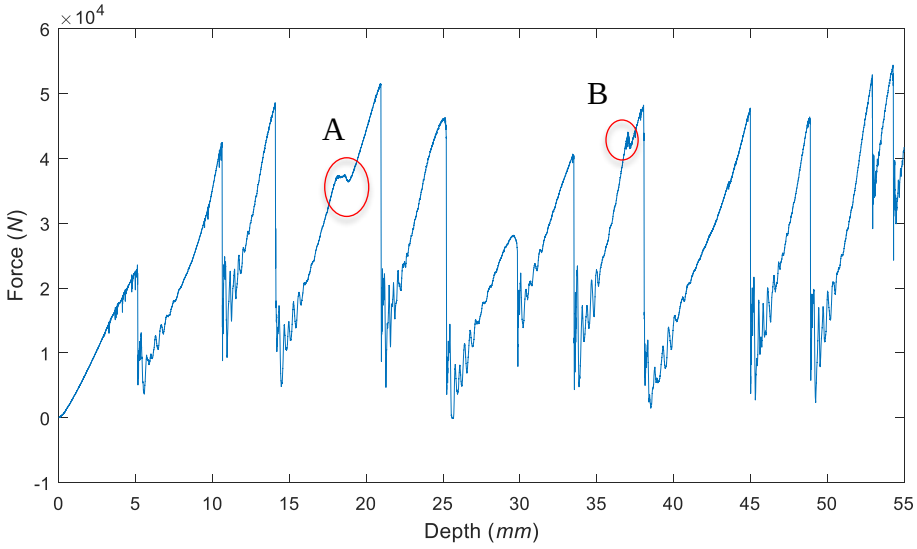

Figure 5.1 Force vs. Indentation Depth plot (Test ID T1_5_15_C2)

5.2.2 Data table

Results from 17 different tests were used for the analysis presented in this paper where indenter size, ice temperature and beam stiffness were the variable parameters. Depending on the test, three sizes of indenters (5cm, 10cm and 15cm) and three level of structural compliance were used. Two target temperatures were set for the ice samples (-5^oC and -20^oC); however, as the tests were not performed in the cold room, the actual temperature of the sample during the tests differed slightly from the target temperature. The full test matrix is presented in Table 5.1

Table 5.1. Data table

Test ID	**Indenter Diameter (*cm*)**	**Ice Temperature (^0C)**	**Beam Stiffness (*N/m*)**	**No. of *hpz* Failure**
T1_5_16_C1	5	-16.5	C1 (2.67×10^7)	5
T1_5_19_C1	5	-19.5	C1 (2.67×10^7)	8
T1_5_7_C1	5	-7	C1 (2.67×10^7)	4
T1_5_4_C1	5	-4	C1 (2.67×10^7)	10
T1_5_15_C2	5	-15	C2 (9.61×10^7)	10
T1_5_7_C2	5	-7	C2 (9.61×10^7)	4
T1_5_16_C3	5	-16	C3 (4.64×10^8)	5
T1_5_7_C3	5	-7.5	C3 (4.64×10^8)	6
T1_10_18_C1	10	-18	C1 (2.67×10^7)	5
T1_10_7_C1	10	-7	C1 (2.67×10^7)	3
T1_10_17_C2	10	-17.5	C2 (9.61×10^7)	5
T1_10_6_C2	10	-6	C2 (9.61×10^7)	7
T1_10_15_C3	10	-15	C3 (4.64×10^8)	7
T1_10_6_C3	10	-6	C3 (4.64×10^8)	5
T1_15_18_C1	15	-18.5	C1 (2.67×10^7)	3
T1_15_6_C1	15	-6	C1 (2.67×10^7)	1
T1_15_6_C2	15	-6	C2 (9.61×10^7)	4

5.3 Results & Discussion

5.3.1 Dependence of average failure pressure on indenter size

The average or nominal failure pressure of an *hpz* was calculated by dividing the maximum force before failure with nominal interaction area. Figure 5.2 shows the mean value of average failure pressure plotted against indenter area with error bars of ±one standard deviation, with no corrections made for differences in temperature or beam stiffness. These results show a strong dependence of failure pressure on interaction area. Such dependence is expected, as is reflected in the "pressure-area" relationship that has been widely discussed in literature (Sanderson, 1988; Masterson et al., 2007).

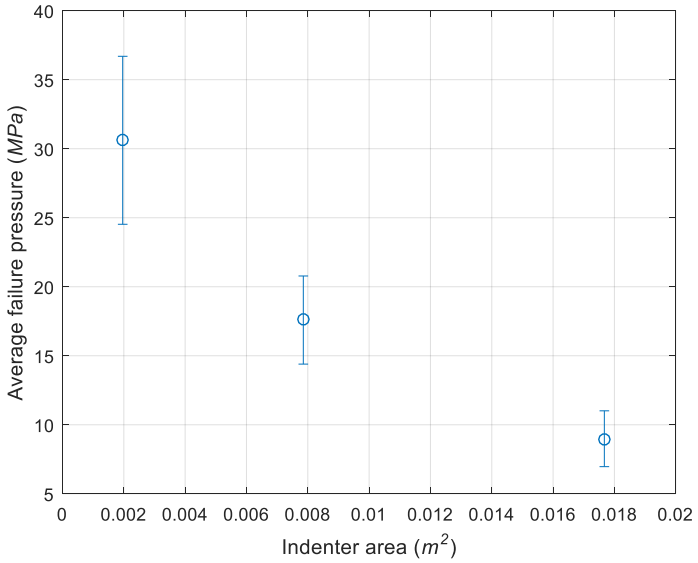

Figure 5.2 Mean of average failure pressure bounded by one standard deviation against indenter area

5.3.2 Effect of ice temperature on average failure pressure

The effect of ice temperature on failure behavior during indentation of freshwater ice has been reported previously by several authors (Browne et al., 2013; Kavanagh et al., 2015; Turner et al., 2015; Birajdar et al., 2016). As the temperature gets closer to the melting point of ice the failure behavior becomes more ductile where the peak load decreases slowly with continuous extrusion. However, in the present analysis only the 'brittle' failures of *hpz*s are being considered since no dynamic activity has been observed during events dominated by ductile ice failure. Figure 5.3 shows the nominal failure pressure as a function of ice temperature. To avoid the influence of scale-effects in this plot, results have been compared for a single indenter size only. The best-fitted line is expressed using the following equation:

$$\sigma_f = -1.17T + 15.99 \quad (5.1)$$

Although a wide scatter is observed in the plot, the best fit line yields a negative slope suggesting that for colder ice, *hpz*s have higher average failure pressure. It is also noted that the range of scatter in the pressure data is larger for colder ice, highlighting the brittle failure behavior of cold ice. Although these results do not exhibit order-of-magnitude differences for the range of temperature considered here, such behavior can have important implication in modelling dynamic ice-structure interaction as has been explored in earlier sensitivity studies by Hossain et al. (2018).

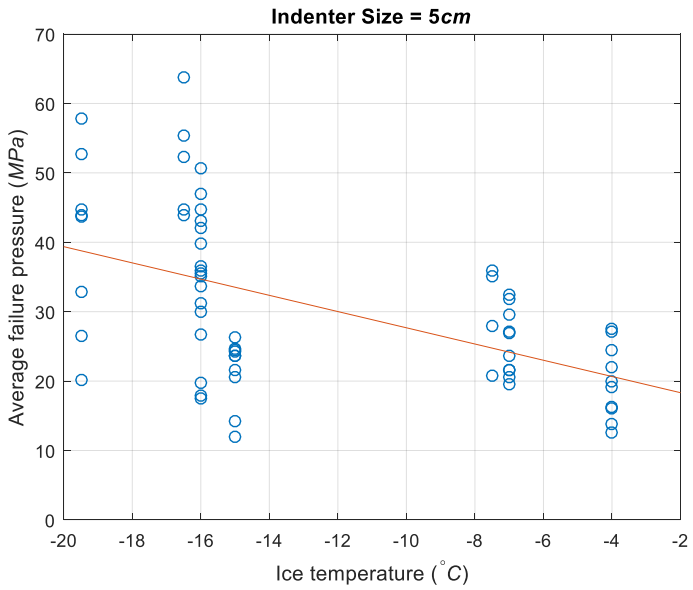

Figure 5.3 Average failure pressure vs. ice temperature for 5*cm* indenter

5.3.3 Effect of structural compliance on peak force and load drop

For the three level of structural compliance used for this test series, the effect of beam stiffness on failure force of *hpz* is shown in Figure 5.4 (mean value with one standard deviation)**.** These results suggest that the magnitude of the failure force is independent of the beam stiffness for the test structures considered, highlighting that the peaks force during an interaction are governed by ice mechanics, not by structural parameters.

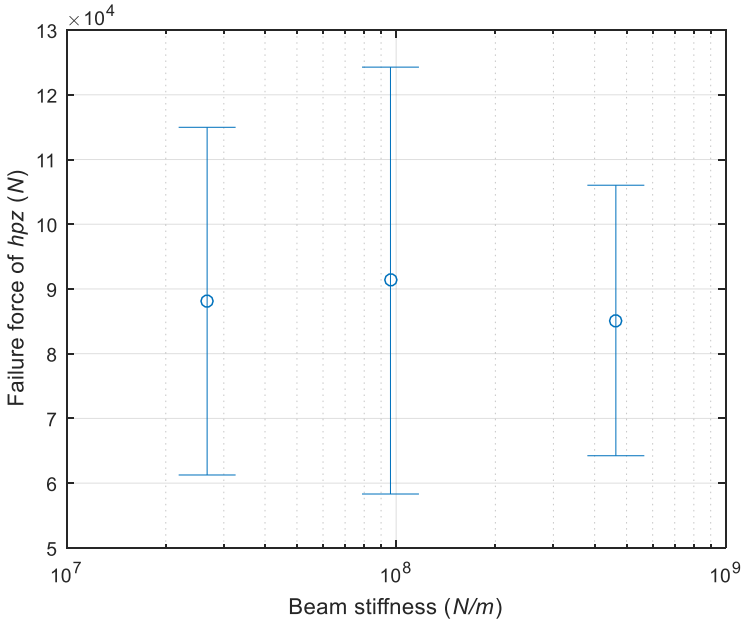

Figure 5.4 Failure force of *hpz* against beam stiffness

After each ice failure event, the indenter springs back due to release of stored elastic energy in the beam following a spalling event, which also results in the rapid extrusion of pulverized ice from the damaged ice layer. Although the depth of this damaged layer depends on the indenter size, ice temperature and loading rate, the extent of the extrusion process following failure was found to depend significantly on the structural compliance. Figure 5.5 shows the percentage of force drop for each different beam stiffness. From this plot, a clear trend may be observed. For the most compliant configuration, the mean percentage of force drop is about 95% suggesting that irrespective of the depth of the crushed layer which forms during the loading cycle, nearly all of the this damaged ice gets extruded upon failure and the next cycle of loading would therefore start with the indenter being in contact with nearly 'intact' ice. On the other hand, the stiffest configuration shows significantly less force drop after failure occurs, suggesting far less damaged ice is removed during a given load cycle and a major portion of the damaged layer survives between subsequent cycles. This observation has important implications since the transient

vibration following the load drops has been linked to vibration within the crushed layer (Jordaan, 2001; O'Rourke et al., 2016a). It should be noted here that the so-called 'intact' ice still exhibits considerable microstructural damage, but the extent of the damage in the ice beneath the indenter at the end of the rebound cycle is expected to be significantly less than is present in the crushed layer beneath the indenter during the upswing phase of the loading cycle.

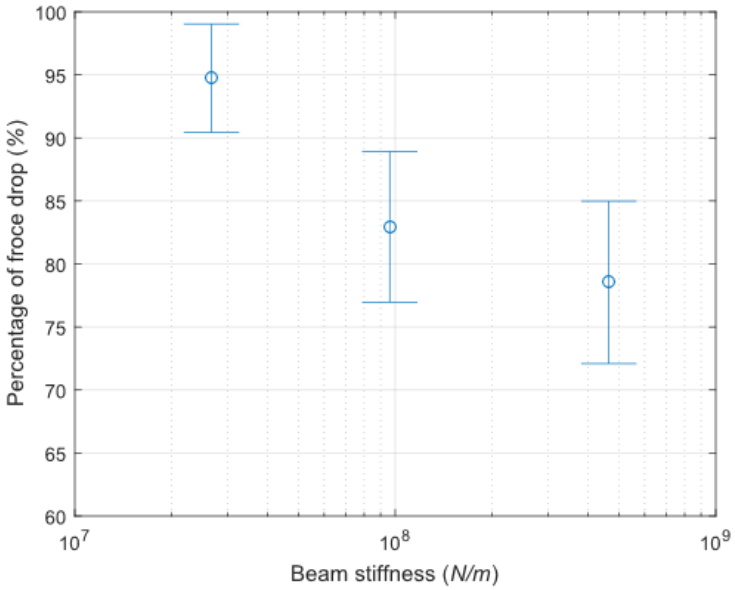

Figure 5.5 Percentage of force drop as a function of beam stiffness. Results showing mean with one standard deviation

5.3.4 Implications for vibration within the damage layer

As discussed in section 4.1 and 2.3.3, the cyclical formation and extrusion of the damaged layer can induce structural vibrations and the discussion presented above has important implications for such processes. Previous small-scale laboratory tests suggest that the layer properties are highly influenced by the interaction parameters and the similar time-traces presented here suggest that such influences are independent of scales. For 'warm' ice under slow loading rate, the damage

layer (regions of microstructurally modified ice) is much thicker than for ‘cold’ ice under fast loading rates.

Figure 5.6 shows the comparison of damage layer under two different test conditions. The schematics are reproduced from the thin-section observations made by Turner et al. (2015). For a 70*mm* diameter indenter, the maximum thickness of the damage layer was found to be higher than 20*mm* for slow loading rate (0.21*mm/s*) and approximately 5*mm* for fast loading rates (21*mm/s*). This suggests that for a certain interaction condition, there is an upper limit for interaction speed, above which the thickness of the damage layer might not be sufficient to sustain cyclical vibration within the damage layer. Small-scale observations also suggest that the thickness of the damage layer is also highly influenced by the temperature of ice.

However, for vibrations within the damage layer to sustain, both the formation and extrusion process of the damage layer are important and although the formation of the damage layer is primarily dominated by the ice parameters, the extrusion process is mostly influenced by the structural compliance, making the structure an ‘active’ component in the overall process. Figure 5.7 shows an expanded view of the indenter displacement after failure events for tests T1_10_18_C1_2.5, T1_10_17_C2_2.5 and T1_10_15_C3_2.5. The complete force-time series of these tests were shown in Figure 4.15. As shown in Figure 5.7, for the most compliant system the structural rebound is more than 1*mm*, whereas for the stiffest configuration the structural rebound is less than 0.5*mm*. This highlights how the structural rebound plays an important role in the extrusion of the crushed layer and affects vibration within the damaged layer. It should be noted here that for the bottom-founded structure in full-scale, the structural compliance is much higher and the higher structural rebound can cause extrusion of much thicker damage layer.

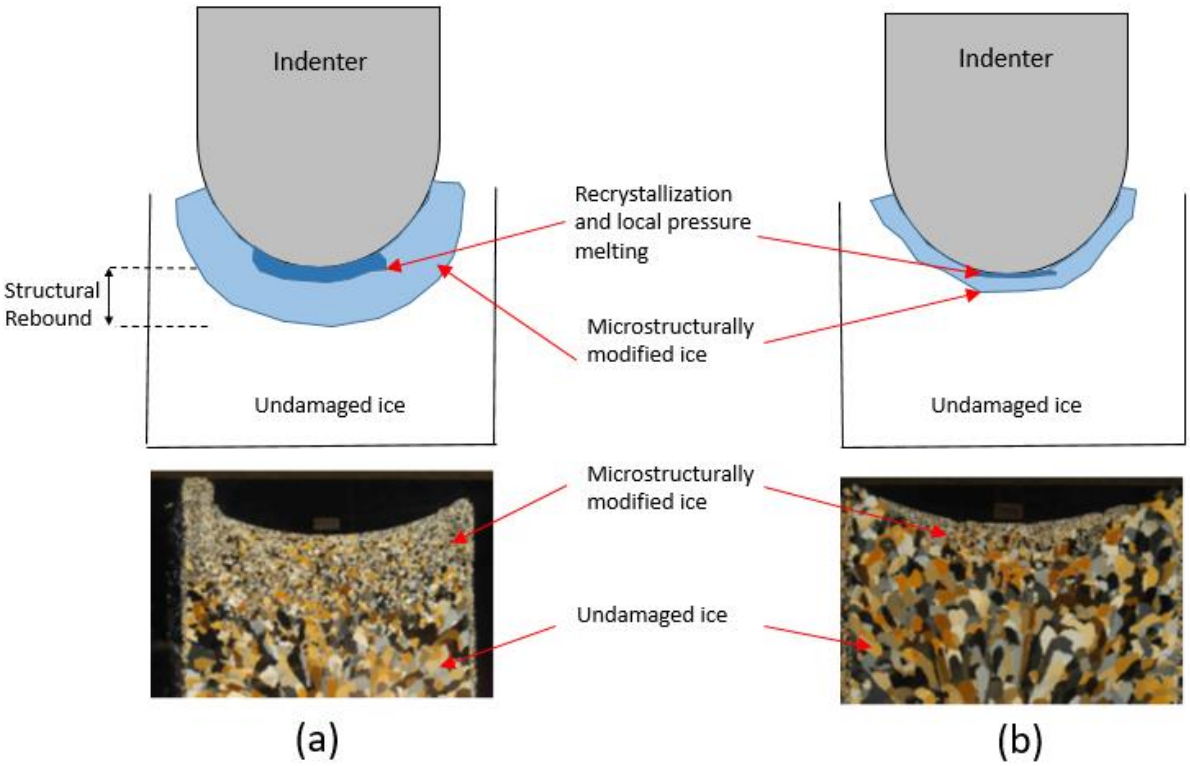

Figure 5.6 Schematic of damage layer for (a) 'warm' ice under slow loading rates; (b) 'cold' ice under fast loading rates. The thin sections are used from the work of Turner (2015)

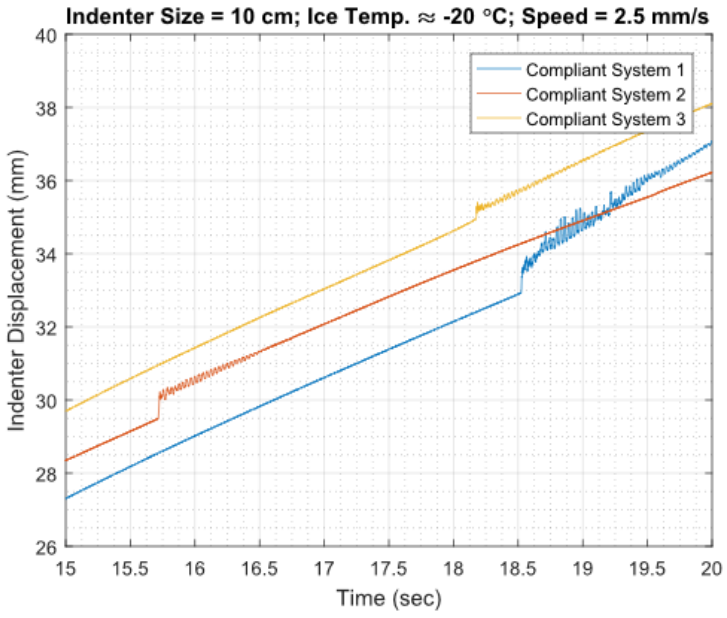

Figure 5.7 Rebound of the structure after failure for different compliant systems

5.4 Conclusions

In this chapter, *hpz* failure behavior has been characterized using results from a series of medium-scale ice crushing dynamics tests for different indenter size, ice temperature and structural stiffness. The *hpz*s studied had areas on the order of 10^3-10^4 mm^2, which is much larger than previous laboratory studies, and are comparable in size with *hpz*s found in other near full-scale datasets. Only brittle type failure has been considered here, where the force-time curve is 'sawtooth' in nature. Each of the load drops was considered as an independent *hpz* failure, and the well-known pressure-area effect was observed for different indenter sizes. Failure pressure was observed to exhibit some dependency on ice temperature, with colder ice having higher average failure pressures. While the different levels of structural stiffness do not seem to have a significant effect on the magnitude of the *hpz* failure force, the extent of the load drop following failure and the associated structural feedback response were found to be highly dependent on the stiffness. Structures that are more compliant were observed to produce larger sload drops (thus producing greater potential feedback response). The feedback response of the structure will have a significant effect on the layer behavior since the extent of the damaged layer which survives each load cycle depends on a complex interplay between the response of the structure and the rate of damage accumulation and layer formation in the ice. This result provides valuable insight into the nature of the interplay between fracture, damage and structural response during dynamic ice-structure interactions.

References

Barrette, P., Pond, J., Jordaan, I., 2002. Ice damage and layer formation in small-scale indentation experiments, in: Proceedings of the 16th IAHR International Symposium on Ice. International Association for Hydraulic Research, Dunedin, New Zealand, vol. 3 pp. 246–253.

Birajdar, P., Taylor, R., Habib, K., Hossain, R., 2016. Analysis of Medium-Scale Laboratory Tests on Ice Crushing Dynamics, in: Arctic Technology Conference. Offshore Technology Conference, St. John's, NL, Canada. https://doi.org/10.4043/27482-MS

Birajdar, P., Taylor, R., Hossain, R., 2017. Analysis of the effect of structural compliance during medium-scale laboratory tests on ice crushing dynamics, in: Proceedings of the 27th International Ocean and Polar Engineering Conference. International Society of Offshore and Polar Engineers, San Francisco, California, USA.

Browne, T., Taylor, R., Jordaan, I., Gürtner, A., 2013. Small-scale ice indentation tests with variable structural compliance. Cold Reg. Sci. Technol. 88, 2–9. https://doi.org/10.1016/j.coldregions.2012.12.006

Frederking, R., Jordaan, I.J., McCallum, J.S., 1990. Field tests of ice indentation at medium scale: Hobson's Choice ice island 1989, in: Proceedings of the 10th IAHR International Symposium on Ice. International Association for Hydraulic Research, Espoo, Finland, vol. 2 pp. 931–944.

Hossain, R., Taylor, R., Moro, L., 2018. An assessment of sensitivity of the self-excited modelling approach for simulating dynamic ice-structure interactions to changes in temperature and scale effects. Ocean Eng. 165, 410–425. https://doi.org/10.1016/j.oceaneng.2018.07.029

Jordaan, I.J., 2001. Mechanics of ice-structure interaction. Fract. Ice 68, 1923–1960. https://doi.org/10.1016/S0013-7944(01)00032-7

Kavanagh, M.B., O'Rourke, B.J., Jordaan, I.J., Taylor, R., 2015. Observations on the Time-Dependent Fracture of Ice; International Conference on Offshore Mechanics and Arctic Engineering, in: Proceedings of the ASME 2015 34th International Conference on Ocean, Offshore and Arctic Engineering (OMAE2015). American Society of Mechanical Engineers (ASME), St. John's, NL, vol. 8 .

Kennedy, K.P., Jordaan, I.J., Maes, M.A., Prodanovic, A., 1994. Dynamic activity in medium-scale ice indentation tests. Cold Reg. Sci. Technol. https://doi.org/10.1016/0165-232X(94)90004-3

Mackey, T., Wells, J., Jordaan, I., Derradji-Aouat, A., 2007. Experiments on the fracture of polycrystalline ice, in: Proceedings of the 19th International Conference on Port and Ocean Engineering under Arctic Conditions (POAC'07). Dalian, China, vol. 1 pp. 339–349.

Masterson, D.M., Frederking, R.M.W., Wright, B., Kärnä, T., Maddock, W.P., 2007. A revised ice pressure-area curve, in: Proceedings of the 19th International Conference on Port and Ocean Engineering under Arctic Conditions (POAC'07). Dalian University of Technology Press, vol. 1 pp. 305–314.

O'Rourke, B.J., Jordaan, I.J., Taylor, R., Gürtner, A., 2016a. Experimental investigation of oscillation of loads in ice high-pressure zones, part 2: Double indentor system — Coupling and synchronization of high-pressure zones. Cold Reg. Sci. Technol. 124, 11–24. https://doi.org/10.1016/j.coldregions.2015.12.002

O'Rourke, B.J., Jordaan, I.J., Taylor, R.S., Gürtner, A., 2016b. Experimental investigation of oscillation of loads in ice high-pressure zones, part 1: Single indentor system. Cold Reg. Sci. Technol. 124, 25–39. https://doi.org/10.1016/j.coldregions.2015.12.005

Sanderson, T.J.O., 1988. Ice mechanics : risks to offshore structures. London, UK ; Boston : Graham & Trotman, London, UK ; Boston.

Taylor, R., Browne, T., Jordaan, I., Gürtner, A., 2013. Fracture and damage during dynamic interactions between ice and compliant structures at laboratory scale, in: Proceedings of the ASME 2013 32nd International Conference on Ocean, Offshore and Arctic Engineering (OMAE2013). American Society of Mechanical Engineers (ASME), Nantes, France, vol. 6 .

Taylor, R., Jordaan, I., 2015. Probabilistic fracture mechanics analysis of spalling during edge indentation in ice. Eng. Fract. Mech. 134, 242–266. https://doi.org/10.1016/j.engfracmech.2014.10.021

Taylor, R.S., Richard, M., Hossain, R., 2019. A Probabilistic High-Pressure Zone Model for Local and Global Loads During Ice-Structure Interactions. J. Offshore Mech. Arct. Eng. 141. https://doi.org/10.1115/1.4042386

Turner, J.D., O'Rourke, B.J., Jordaan, I.J., Taylor, R.S., 2015. Surface Temperature Fluctuations in Ice Indentation Tests; International Conference on Offshore Mechanics and Arctic Engineering, in: Proceedings of the ASME 2015 34th International Conference on Ocean, Offshore and Arctic Engineering (OMAE2015). American Society of Mechanical Engineers (ASME), St. John's, NL, vol. 8 .

Wells, J., Jordaan, I., Derradji-Aouat, A., Taylor, R., 2011. Small-scale laboratory experiments on the indentation failure of polycrystalline ice in compression: Main results and pressure distribution. Cold Reg. Sci. Technol. 65, 314–325. https://doi.org/10.1016/j.coldregions.2010.11.00

Chapter: 6 A Probabilistic High-Pressure Zone Model of Dynamic Ice Structure Interactions and Associated Ice-Induced Vibrations

Preface

The chapter has been prepared to be submitted as an original journal article. As the primary author, I was responsible for writing the article, developing the model, performing the theoretical calculations and simulations, and analyzing the results. My co-authors Dr. Rocky Taylor and Dr. Lorenzo Moro provided guidance at different stages of the writing and analysis.

Based on the experimental observations presented in Chapters 4 and 5, a modelling framework for simulating the dynamic ice-structure interaction is developed and the results are presented here. The section “Introduction” provides the background and motivation of the work presented in this chapter and although the reader of the thesis has already been informed about the background and motivation of the work presented in the thesis in more details in Chapter 1 and 2, the section has been retained here for the completeness of this chapter.

Abstract

During ice-structure interactions that are dominated by ice compressive failure, the majority of the ice loads are transmitted through localized contact regions known as high-pressure zones (*hpz*s). This paper presents a probabilistic modelling framework for dynamic ice-structure interaction based on the mechanics of *hpz*s. Individual *hpz*s are modelled as a nonlinear spring-damper system where the stiffness is modelled as a function of nominal strain, with the degree of softening depending on the average strain-rate. Both spalling and crushing failure mechanisms were assessed in the context of periodical sinusoidal response. For spall dominated failure, the model structure showed presence of frequency lock-in in the speed range of 100-125*mm/s*, beyond which the failure was found to be random in nature with lower amplitude of structural response. The amplitude was also found to be significantly influenced by structural parameters with structural damping having the highest contribution. For pure crushing, an estimated equilibrium layer thickness based on theoretical calculations also showed presence of frequency lock-in. The work highlights the importance of understanding the interplay between these mechanisms, as well as the role of ice conditions and structural parameters on the processes that dominate an interaction.

6.1 Introduction

Design consideration for structures prone to dynamic ice-structure interaction leading to ice-induced vibrations (IIV) require careful assessment of the ice and structural properties and the underlying ice mechanics associated with the failure process. As suggested in the ISO19906 (2010), the dynamic ice-structure interaction leading to IIV can be broadly classified into three categories: namely intermittent crushing, frequency lock-in, and continuous brittle crushing.

Among these three, frequency lock-in has received particular attention, since it produces a sinusoidal-type response of the structure, often close to its natural frequency. The primary challenge for design concerning IIV is identifying how the interplay between different ice and structural parameters can result in a particular mode of vibration, especially frequency lock-in. Since frequency lock-in rarely occurs during a structure's lifetime, the amount of data obtained from full-scale interactions is very limited. Even under the controlled conditions in the laboratory, frequency lock-in is difficult to reproduce, due to the probabilistic fracture behaviour of ice, which makes identifying the conditions for vibration very difficult. This is further complicated by the complex mechanisms involved in crushing failure; the development of the spalls and formation of the damage layer make significant contributions to the overall failure process. As discussed by Jordaan (2001), field test data suggest that the dynamic response of the structure is also associated with the periodic extrusion of the crushed ice from the damaged layer.

Several ice-structure interaction models has been proposed so far to identify the conditions for frequency lock-in. The modeling approaches can be broadly classified into two categories: the forced vibration model and self-excited vibration model. In the forced vibration approach, the source of the alternating ice force has been linked to the failure frequency of the ice. The self-excited vibration approach, on the other hand, considers that the proportional relationship between ice force and the relative velocity is not always positive, and that the structure can vibrate under self-excitation as a result of dynamic instability. Although ice has its own characteristic failure frequency during a particular interaction, such a frequency is highly influenced by interaction parameters, especially the relative velocity between the structure and the ice (Sodhi, 2001). However, the negative proportional relationship between the ice force and the relative velocity is rarely obtained and is itself dependent on the test conditions (Sodhi, 1988). Another critical

consideration in ice-structure interaction is the non-simultaneous nature of the ice failure process across the interaction area due to local contact effects (Kry, 1978). The idea of non-simultaneous failure implies that at any one point in time, different local areas of the failure region can be at different stages of failure, which adds another layer of complexity in the modeling approach.

Nevertheless, over the last 50 years, several authors have proposed different ice-structure interaction models accounting for these effects (Matlock et al., 1969; Määttänen, 1978; Sodhi, 1994; Kärnä et al., 1999; Huang and Liu, 2009; Hendrikse and Metrikine, 2015). The primary difficulty arises when trying to link the model parameters to the fundamentals of ice mechanics such as the dynamics of high-pressure zones (*hpz*s), formation of a damage layer, and the extrusion process. This crucial limitation can be identified as one of the most important reasons for the difficulty in applying these models to unknown conditions (Kärnä et al., 2013). In this chapter, a simple mechanical model is presented based on the dynamics of *hpz*s observed in a wide range of indentation tests. Two failure modes, namely, spalling and crushing are assessed in the context of periodical sinusoidal response of the structure observed during frequency lock-in. The results from the medium-scale ice crushing dynamics tests are used to estimate the *hpz* failure strength and force drop after each failure event. Although the model shows promising results for identifying conditions for frequency lock-in for both spalling and crushing, more analytical and experimental investigations are required for full-scale implementation.

6.2 Model Description

6.2.1 Model idealization

To simulate the observed dynamic ice-structure interaction during indentation tests, a simple *hpz* based mechanical model has been proposed. A schematic of the physical process of the indentation is shown in Figure 6.1. As the hydraulic cylinder moves forward, ice directly beneath the indenter goes through highly microstructural changes. At the same time, cracks that nucleate in the contact zone tend to propagate towards the free surface. The layer of microstructurally modified ice has a certain depth, beyond which is the region of competent ice from which fractures emanate and which exhibits elastic material behaviour.

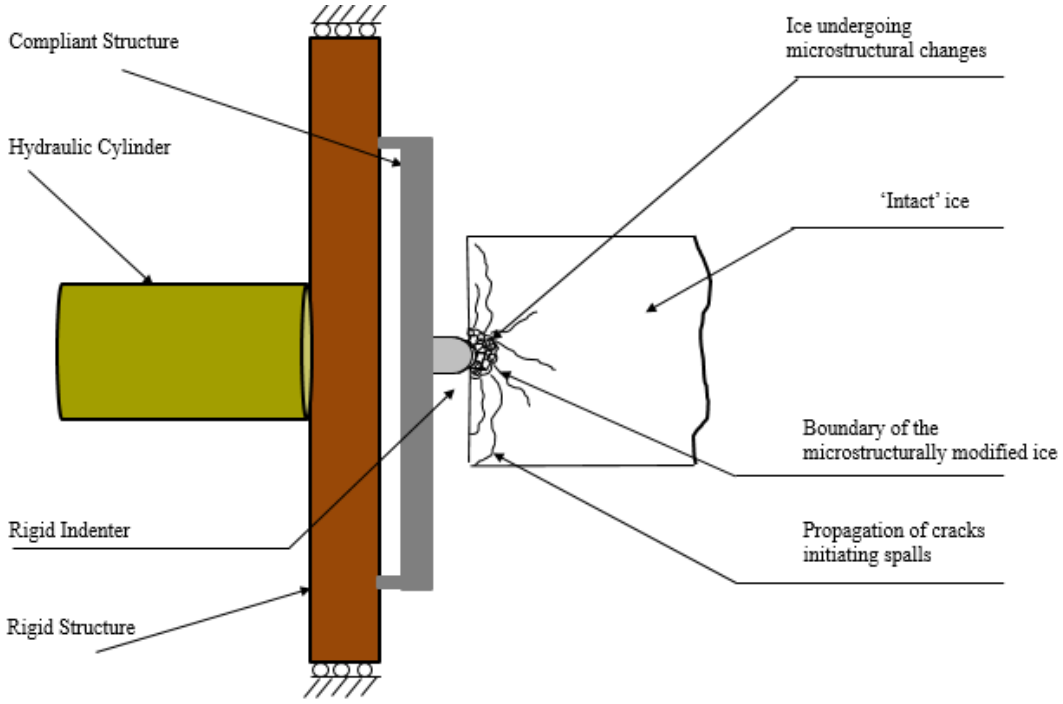

Figure 6.1 Simplified schematic of the ice indentation process

The mechanical representation of the model is shown in Figure 6.2. It is assumed that the hydraulic cylinder moves with a constant speed and that the ice and the indenter never lose contact. The structure has been modelled as a single degree of freedom (SDOF) system and *hpz*s generated beneath the indenter are modelled as massless spring-damper systems with nonlinear spring constants. The behaviour of the intact ice is considered linear viscoelastic. After a failure event, the indenter moves forward due to the elastic energy stored in the structure; however, depending on the failure process, such a rebound can be either instantaneous or continuous. The rebound distance is termed as failure length f_L.

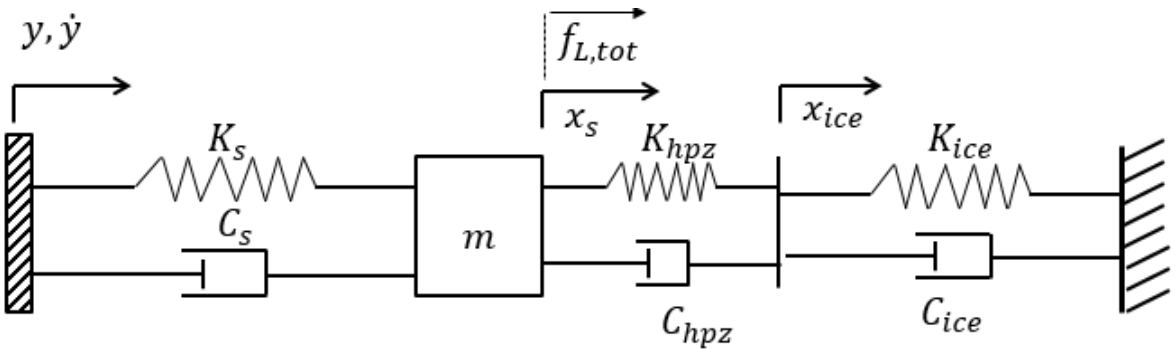

Figure 6.2 Framework of *hpz* based ice-structure interaction model

6.2.2 Equation of motions

The system has 2 degrees of freedom with a singular mass matrix. For time step i, the equations of motion are:

$$m\ddot{x}_{s,i} = K_s\left(y - x_{s,i} - f_{L,tot}\right) + C_s\left(\dot{y} - \dot{x}_{s,i}\right) - K_{hpz,i}\left(x_{s,i} - x_{ice,i}\right) - C_{hpz}\left(\dot{x}_{s,i} - \dot{x}_{ice,i}\right) \quad (6.1)$$

$$C_{hpz}\left(\dot{x}_{s,i} - \dot{x}_{ice,i}\right) + K_{hpz,i}\left(x_{s,i} - x_{ice,i}\right) = K_{ice}x_{ice,i} + C_{ice}\dot{x}_{ice,i} \quad (6.2)$$

The notations are explained below:

K_s = Stiffness of the structure/beam

C_s = Damping coefficient of the structure/beam

m = Mass of the structure/beam

y = Displacement of the hydraulic cylinder

$\dot{y}$ = Speed of the ram (equivalent to ice drift speed)

x_s = Displacement of the indenter

x_{ice} = Displacement of the *hpz* boundary

K_{hpz} = Stiffness of the *hpz*

C_{hpz} = Damping coefficient of the *hpz*

K_{ice} = Stiffness of the ice

C_{ice} = Damping coefficient of the ice

$f_{L,tot}$ = Accumulation of the failure length after each failure event

The structural parameters in eqn. (6.1) and (6.2) can be measured independently. Since the far-field ice behavior is assumed to be linearly viscoelastic, non-linearity in the above model can only originate from the behavior of *hpz.*

Total force measured by the load cell for time step i,

$$F_i = K_s\left(y - x_s - f_{L,tot}\right) + C_s(\dot{y} - \dot{x}_s) + K_{hpz}(x_s - x_{ice}) + C_{hpz}(\dot{x}_s - \dot{x}_{ice}) \quad (6.3)$$

6.2.3 High-pressure zone stiffness

Results from triaxial tests suggest that ice transforms in terms of microstructure and properties if placed under hydrostatic pressure together with shear, and becomes softer with time (Meglis et al., 1999; Melanson et al., 1999). As shown in Figure 6.3, the stiffness of an ice sample under traiaxial loading condition increases with strain up to a certain point and starts decreasing if the strain is increased further. This relationship can be expressed as a 3-parameter power-law equation as follows:

$$K_{hpz} = a\varepsilon^{m}e^{\varepsilon n} \tag{6.4}$$

where a, m and n are parameters dependent on the average strain-rate, the size of *hpz*, boundary conditions and the geometry of interaction. The average strain is calculated as $\varepsilon = \frac{y - f_{L,tot}}{D_i}$ and D_i is calculated as $D_i = \sqrt{\frac{4A_i}{\pi}}$, where A_i is the instantaneous area of the *hpz* and D_i is the instantaneous diameter. For two different strain-rates, the assumed relationship shows good general agreement with the experimental observations (Figure 6.3).

6.2.4 Spalling fracture model

Spalling failure occurs when $\frac{F_i}{A_i}$ exceeds some fracture strength σ_f. Such a failure instantaneously releases the energy stored in the structure, due to the loss in contact area, and the amount of force drop is expressed as:

$$F_{Drop} = F_d F_{peak} \tag{6.5}$$

where F_{peak} is the peak force before failure occurred and F_d is an empirical parameter ranging from 0-1. The failure length due to the elastic rebound of the structure is calculated as:

$$f_L = \frac{F_{Drop}}{K_s} \tag{6.6}$$

The total failure length and the new force are updated as follows:

$$f_{L,tot} = f_{L,tot} + f_L \tag{6.7}$$

$$F_{i,new=}F_{i,old} - F_{Drop} \tag{6.8}$$

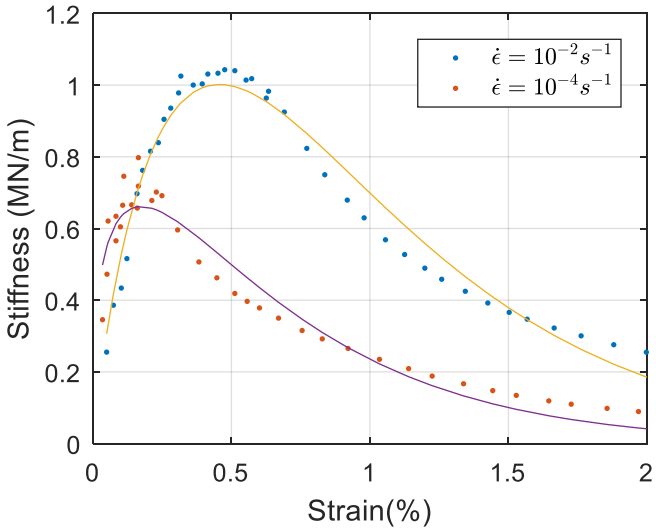

Figure 6.3 Relationship between *hpz* stiffness and nominal strain for two different strain-rates. Experimental data are fitted with the equation 6.3.

6.2.5 Crushing-extrusion model

Under triaxial conditions, the softening process can become very rapid due to runaway processes as localized pressure melting at the boundaries in the highly refined grain structure results in progressive softening of the damaged ice in the highly confined central region of an *hpz*. Once the strain exceeds the value corresponding to the maximum stiffness, pressure softening causes a reduction in *hpz* stiffness, leading to an extrusion of crushed ice particles from beneath the contact zone. However, the release of such pressure contributes to the partial recovery of the stiffness and the cycle of extrusion and hardening can be repeated, as shown in Figure 6.4.

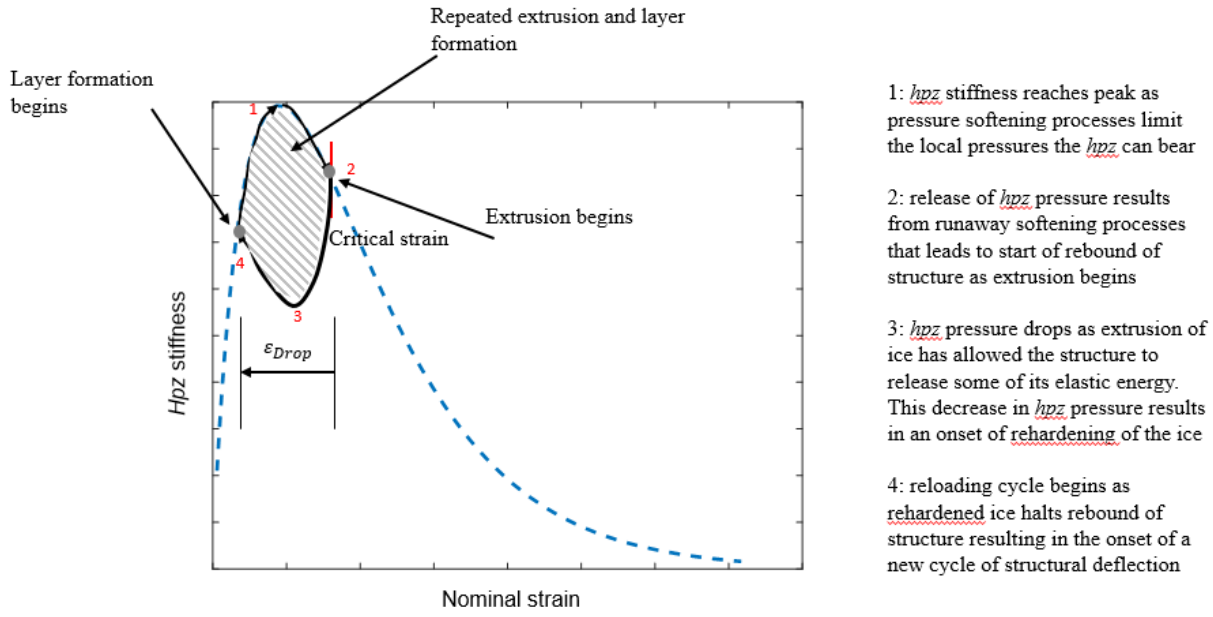

Figure 6.4 Cyclical nature of the crushing process through extrusion and hardening. The physical processes associated with the location of the points are described along the plot

Jordaan and Timco (1988) obtained the expression for extrusion velocity in the direction of indentation by solving the equation of equilibrium during crushing process as follows:

$$v(x) = v_0(1 - \frac{x}{l})(1 + 2\frac{x}{l}) \tag{6.9}$$

where v_0 is the indenter velocity and l is the thickness of the crushed layer.

By replacing $dt = \frac{dx}{v_0}$ and integrating the preceding equation, the expression for failure length during a single crushing-extrusion cycle can be obtained as:

$$f_L = x\left(1 + \frac{x}{2l} - \frac{2x^2}{3l^2}\right) \tag{6.10}$$

The accumulated crushing length is updated using eq. (6.7).

The extrusion of the crushed layer causes a strain reduction within the *hpz*, as shown in Figure 6.4. According to Jordaan (2001), the softening process results in a fast extrusion with particle sliding, which is followed by a layer hardening and sintering process. To model this behaviour, the *hpz* stiffness is assumed to follow a quadratic relationship during the strain drop, as shown in Figure 6.4. Based on observations from these experiments and prior work (e.g. Wells et al., Browne et al, etc.) this assumption is considered to be an accurate representation of the crushing process during *hpz* formation and evolution.

6.3 Model Implementation

6.3.1 Model flowchart

The model implementation process is shown as a flowchart in Figure 6.5. The flowchart begins with defining the structural parameters (stiffness, mass and damping), far-field ice parameters (stiffness and damping), *hpz* damping and the initialization of the variables for simulation period. Eqn. (6.1) and (6.2) are then solved using an explicit numerical time integration scheme with the 4^{th} order Runge-Kutta method. The time integration scheme has been developed as a separate function and the algorithm has been benchmarked against the solution of Kawano et al. (2013) for a 2 DOF system with a singular mass matrix. Once the displacement and velocities are updated for a time-step, the total force, nominal strain and *hpz* stiffness are calculated. The criterion for spalling failure is then tested as described in section 6.2.4 and if the nominal stress becomes higher than the *hpz* strength, the force drop is calculated based on eqn. (6.6) and the force and failure length is updated based on eqn. (6.7) and (6.8).

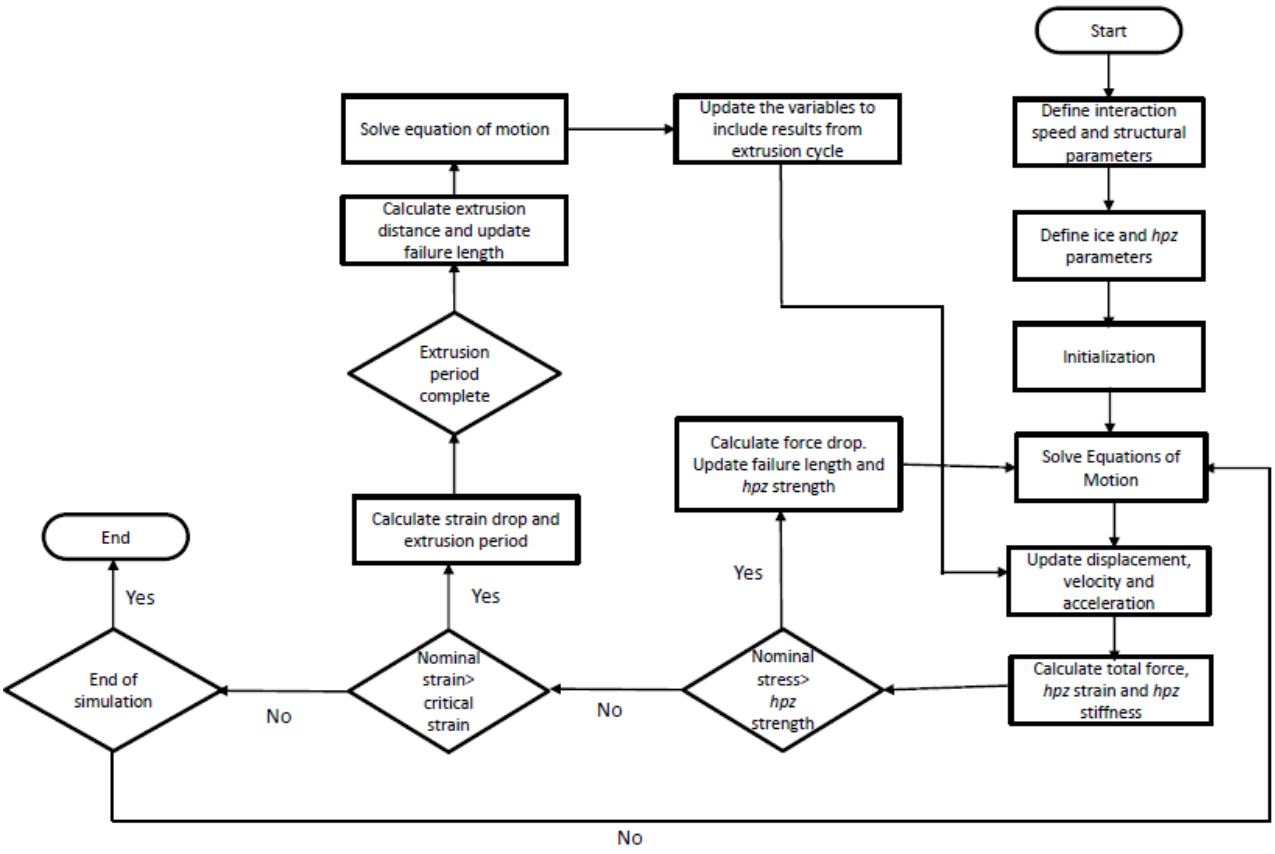

Figure 6.5 Flowchart of model implementation

If the spalling failure criterion is not satisfied the code proceeds to test the crushing-extrusion criterion (nominal strain > critical strain). The critical strain is modelled based on Rist and Murell (1994) which suggests a decrease in failure strain with increasing strain-rate (more details in section 6.3.2.2). The extrusion period is calculated as $\frac{l}{v_0}$ and for this period the failure length is calculated based on eqn. (6.10) and the equations of motions are solved for that period separately. Once the extrusion period is complete, the displacement and velocity is updated in the original program. The program exits when the simulation period is completed.

6.3.2 Parameter estimation

6.3.2.1 Failure pressure

To estimate the failure strength and the force drop coefficient during spalling failure, results from the medium-scale indentation tests discussed in chapter 4 were used. Continuous indentations were performed up to $\approx 55mm$ indentation depth, which resulted in a sawtooth loading pattern in most cases. Since the ratio of the indentation depth to sample diameter is very small, the effect of confinement on failure strength is assumed to be negligible. Hence, each failure event can be considered as an independent failure of the *hpz* (Hossain and Taylor, 2019). Due to the pressure-area effect in ice, the failure strength was found to be highly dependent on indenter area. The mean failure strengths as a function of the nominal indenter area were plotted with a bound of one standard deviation (Figure 6.6). The values were fitted using a power-law relationship and the residuals were modelled using a 3-parameter generalized extreme value distribution. The relationship is as follows:

$$\sigma_f = \alpha_1 A^{\beta_1} + GEV(k, \sigma, \mu) \tag{6.11}$$

with $\alpha_1 = 2.02;\ \beta_1 = -0.44; k = -0.051;\ \sigma = 8.636;\ \mu = -4.624$

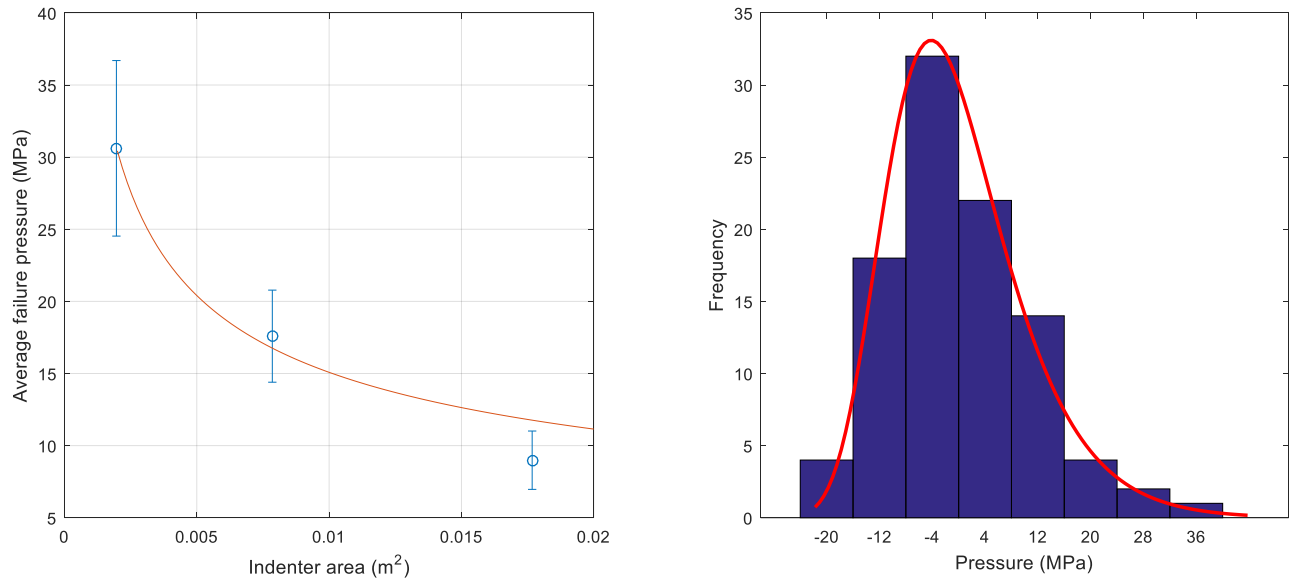

Figure 6.6 Modelling the failure strength as a function of indenter area (left); Residuals are modelled using a generalized extreme value distribution (right)

6.3.2.2 Stress-strain relationship

For a range of strain-rates, the parameters a, m and n in eq. (6.4) are calculated by linear extrapolation from the fitted values of the experimental data shown in Figure 6.3. The critical strain values for crushing failure for the same range of strain-rates are obtained from Rist and Murrell (1994), who performed tri-axial tests under varying strain-rates, ice temperatures and confinement. To be consistent with the results from Melanson et al (1999), tests with a confining pressure of $\approx 20 MPa$ were used in determining the critical strain. It should be noted here that, for the given confining pressure, the failure modes reported by Rist and Murrell (1994) were not exclusively crushing; however, due to the limited tri-axial test results available in the literature, these were identified as the most relevant results for estimating critical strain.

The combination of these two failure criteria is shown in Figure 6.7. Based on the fitted a, m and n values from the experimental data, the stress-strain relationship for a single *hpz* in the range of

$\dot{\varepsilon} = 10^{-4} - 10^{-1}s^{-1}$ was generated (right). Rist and Murrell's data suggest that the critical strain for failure decreases with increasing strain rate, and the stress-strain relationship is shown up to the point of critical strain in each case. However, *hpz* failure can also occur due to failure strength which, is dependent on *hpz* area and randomness of fracture process (left).

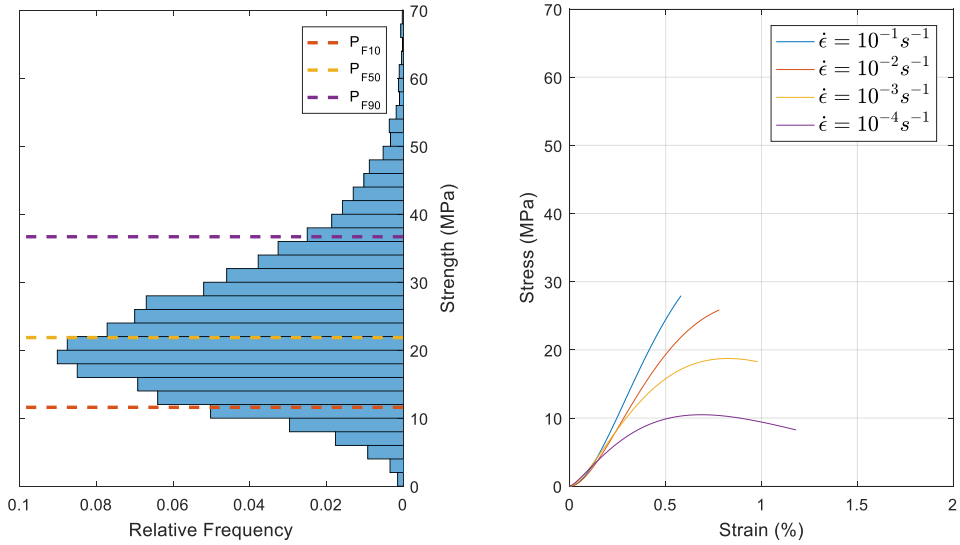

Figure 6.7 Failure criterion of a single *hpz* based on strength (left) and strain (right)

6.3.2.3 Post-failure load reduction

After each spalling event, the elastic energy stored in the beam causes the indenter to surge forward, which leads to a rapid extrusion of crushed ice particles. This causes an instantaneous force drop and the amount of force determines the remaining strength of the *hpz* or the surviving portion of the crushed layer. From the test results, the percentage of force drop was found to be strongly correlated with structural compliance. As shown in Figure 6.8, for the most compliant system, the mean percentage of force drop is almost 95%, whereas for the stiffest system, the value is below 80%. For the current model, the force drop coefficient is modelled using a power law

with the natural logarithm of the beam stiffness, and the residuals are modelled using a 3 parameter generalized extreme value distribution. The relationship is as follows:

$$f_d = \alpha_2(\ln K_s)^{\beta_2} + GEV(k, \sigma, \mu) \quad (6.12)$$

with $\alpha_2 = 3.378 \times 10^3, \beta_2 = -1.2583, k = -0.4377, \sigma = 11.88, \mu = -3.0725$

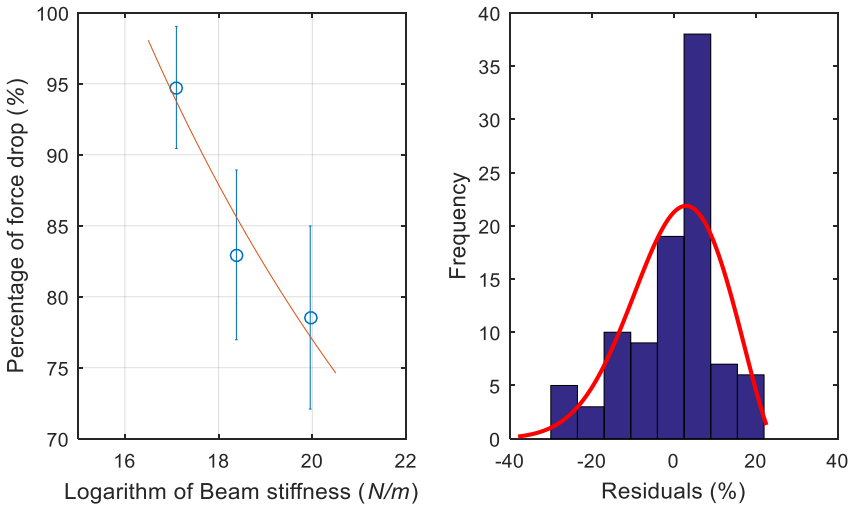

Figure 6.8 Modelling the force drop coefficient as a function of structural compliance. The fitted curve (Left) and the residuals with distribution fitting (right)

6.3.3 Validation of the model with experimental data

To validate the model, results obtained from the simulation are compared with the experimental data. The test case chosen for the comparison has the following parameters:

Table 6.1. Experimental parameters for model validation

Name	Value
Indenter Size	5*cm*
Ice Temperature	-16.5℃
Ram Speed	2.5*mm/s*
Structural Stiffness	$8.84 \times 10^6 N/m$

For the model, the following parameters are used:

Table 6.2. Numerical parameters for model validation

Name	Value
Speed ($\dot{y}$)	$2.5 mm/s$
Stiffness of the Structure (K_s)	$8.84 \times 10^6 N/m$
Mass of the Structure (m)	8956.8 kg
Damping ratio of the Structure (C_s)	0.04
Diameter of the indenter (D_{ind})	$5cm$
Stiffness of ice (K_{ice})	$20 \times 10^6 N/m$
Damping coefficient of ice (C_{ice})	$270 \times 10^3 kg/s$
Damping coefficient of hpz (C_{hpz})	$60 \times 10^3 kg/s$
Constants a, m, n	5.99×10^6, 1.0784, -1.96

The stiffness of the structure was calculated assuming pin-pin boundary conditions for I-beams. The mass of the structure was chosen based on the FFT analysis of the transient response from the experimental data, which suggested that the frequency of the lowest natural mode was about 5 Hz. The damping co-efficient was approximated based on the half-power method using the frequency response function obtained by an impact test. Values for the stiffness and damping coefficients of ice were used from the model of Kärnä and Turunen (1989). The constants a, m, n were determined from the slopes of force-displacement curve for all $5cm$ indenter tests.

Simulation results were compared with experimental data, as shown in Figure 6.9. The failure in this case was primarily dominated by spalling with transient vibration, which decayed very quickly. The figure shows similar levels of peak force for both cases. Since the ratios between the indentation depth and indenter diameter were small, the effects of confinement were not accounted for in the model. As can be observed from the experimental data, the slope of the force-

displacement curve is not constant, but increases over time. A similar behaviour can be observed in the simulation results due to the stiffness-strain relationship mentioned in eqn. (6.3). The spalling frequency was constant due to the high force drop coefficient.

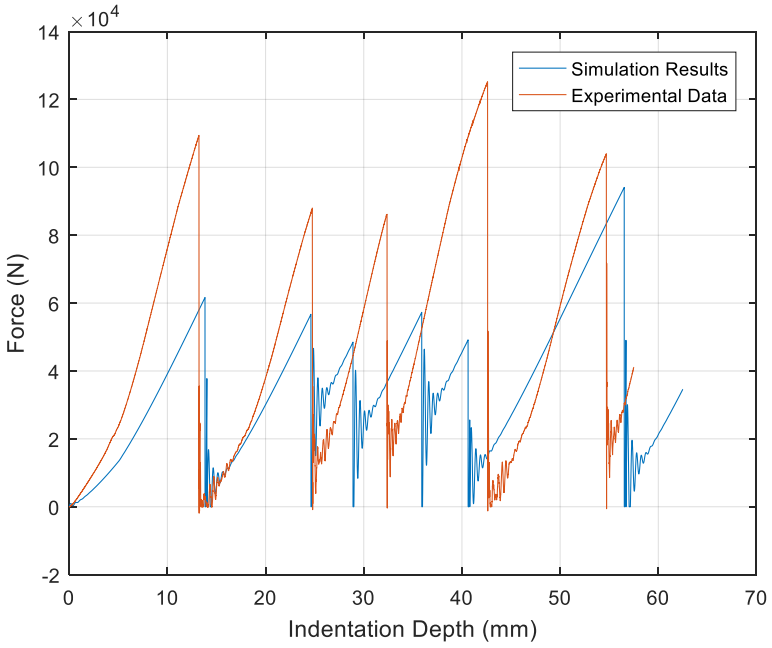

Figure 6.9 Comparison of the simulation results with experimental data

In addition to the time-series comparison, the maximum pressure and average pressure of the experimental data was compared for three validation cases with five simulations for each cases (Figure 6.10). The validation tests compared were T1_5_19_C1_2.5, T1_10_7_C1_2.5 and T1_5_16_C3_2.5 as mentioned in Table 4.2. The plots shows that for maximum pressure and average pressure, results from the simulation is in reasonably well agreement with the experimental observations.

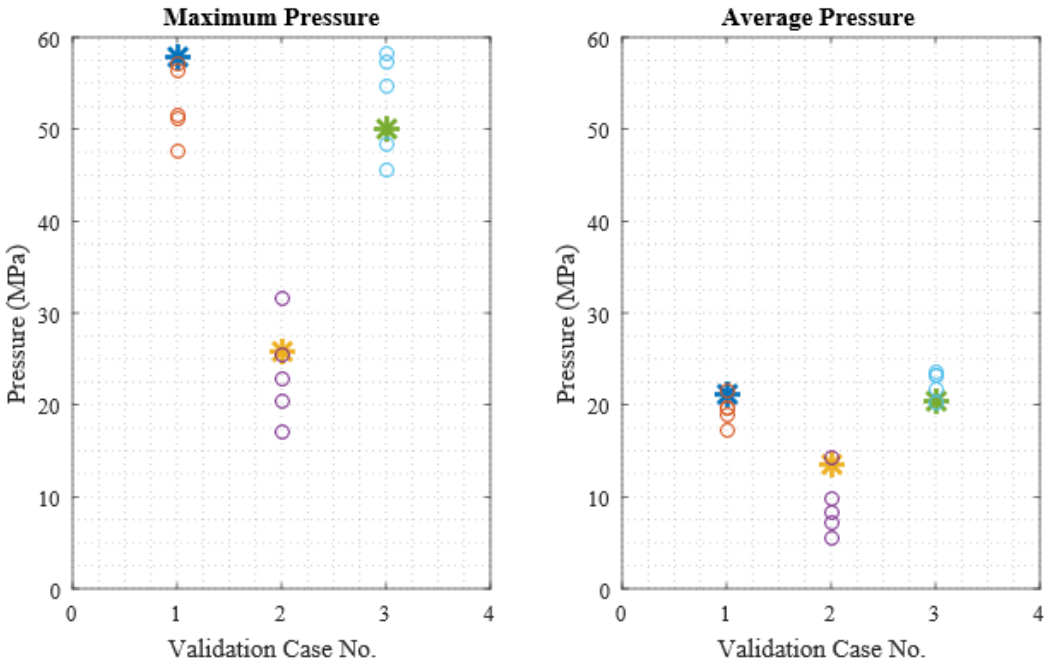

Figure 6.10 Comparison of maximum pressure (Left) and average pressure for experimental data and simulations for three different cases. The experimental data points are marked with '*' whereas the simulation data points are marked as 'o'

6.4 Results and Discussion

6.4.1 Conditions for frequency lock-in

In practice, frequency lock-in rarely occurs in the lifetime of a structure, and even under controlled conditions in the laboratory, it is very difficult to reproduce. Pure crushing events are often interrupted by spalls, which are dominated by the probabilistic fracture mechanics of *hpz* strength. We believe that the interplay among fracture, layer thickness during crushing, interaction speed, and structural configuration all contribute to the conditions for frequency lock-in, and for a certain structural configuration and interaction speed, frequency lock-in can only occur for a certain degree of randomness in ice strength along with certain layer thickness during crushing. Here we considered a certain structural configuration and a certain degree of randomness in *hpz* strength,

based on experimental observation. For these configurations, frequency lock-in was only observed for brief periods when the interaction speed was between 100-125*mm/s* with 5*mm* layer thickness, as shown in Figure 6.11. The structural displacement profile shown here is very similar to the IIV signature obtained for the Norströmsgrund lighthouse for a full-scale lock-in event (Bjerkås et al., 2013). It is obvious that for a different structural configuration with a different degree of randomness in *hpz* strength, the required speed and layer thickness could be considerably different, and for certain configurations, it is possible that the conditions for frequency lock-in would not exist.

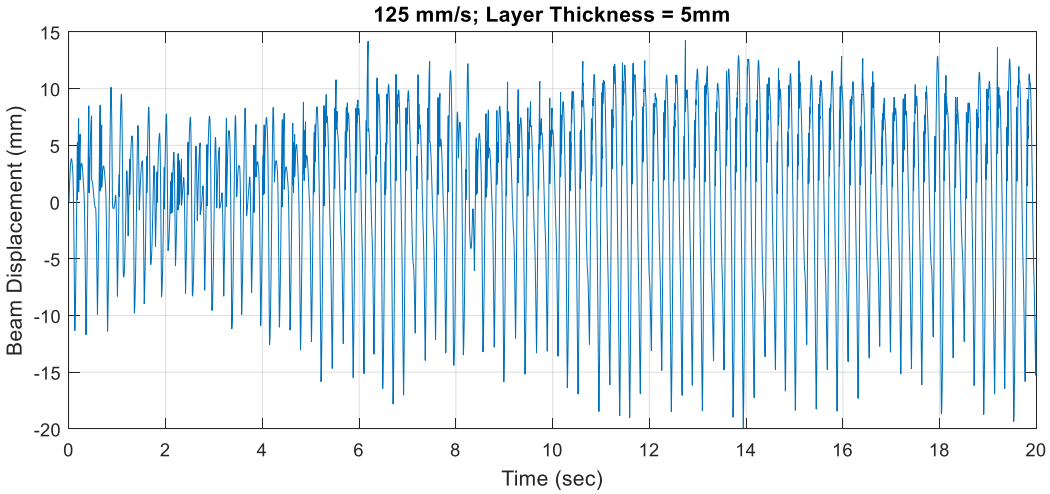

Figure 6.11 Signature of frequency lock in: Interaction speed 125 mm/s, Layer thickness 5mm

In both literature and design guidelines, interaction speed has been identified as the most important factor contributing to the condition of frequency lock-in (Kärnä and Muhonen, 1990; ISO 19906, 2010; O'Rourke et al., 2016a). As the speed increases, the failure mode is considered to move from intermittent crushing to frequency lock-in and then to random crushing, and the structure is considered to be most susceptible to IIV at some intermediate speed range. The simulations performed by the modelling framework also shows a similar behavior. Figure 6.12 shows the effect

of interaction speed on the frequency spectrum of structural displacement for a fixed indentation period. At low speeds, the transient response of the structure similar to the one shown in Figure 6.9 dominates the spectra. As the speed increases, the failure frequency becomes close to the natural frequency of the structure, which results in a significantly higher amplitude. Beyond that speed range, the spectra are dominated by the degree of randomness in failure strength and spreads over a larger frequency range.

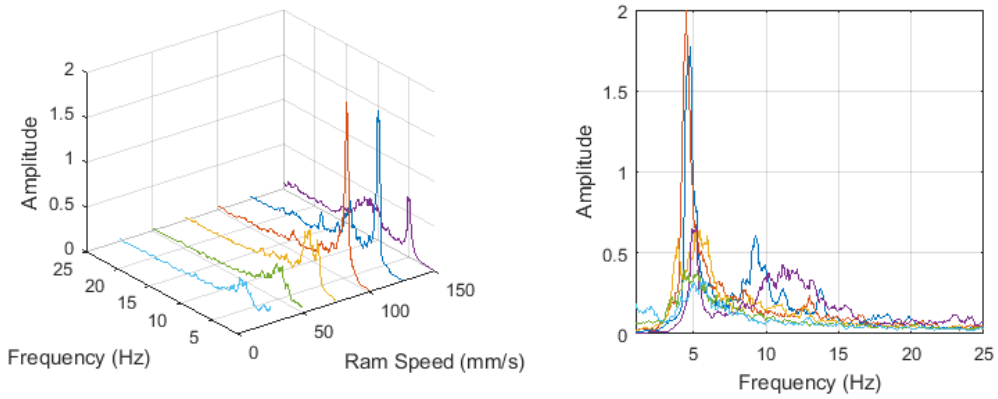

Figure 6.12 Effect of interaction speed on structural displacement response

6.4.2 Interplay between interaction speed and structural parameters

In an ice-structure interaction both ice and the structure plays ‘active’ roles; hence, it is imperative to identify the interplay of ice and structural parameters and their effects on IIV. Using the modelling framework, simulations are performed for a range of interaction speed and structural parameters to identify their effects on the maximum amplitude of structural response. The structural parameters are expressed as ratios of the original parameters mentioned in section 6.3.2 and is termed as ‘factors’.

6.4.2.1 Effect of structural mass

The contour plot of maximum amplitude of the structural response for a range of interaction speed and mass factor is shown in Figure 6.13. The speed was considered to be ranging from 10-150*mm/s* and the mass factor was considered to to be ranging from 0.1-1.5. As mentioned in section 6.4.1, frequency lock-in was found to occur in the speed range of 100-125*mm/s* for the original structural parameters. As expected, the maximum amplitude contour for a mass factor ≈1 was also found to be highest in that speed range and for speeds both side of that range the amplitude decreases. However, the contour also shows clear dependency on the mass factor. For mass factor less than 1, the frequency lock-in regime was found to occur for higher interaction speed.

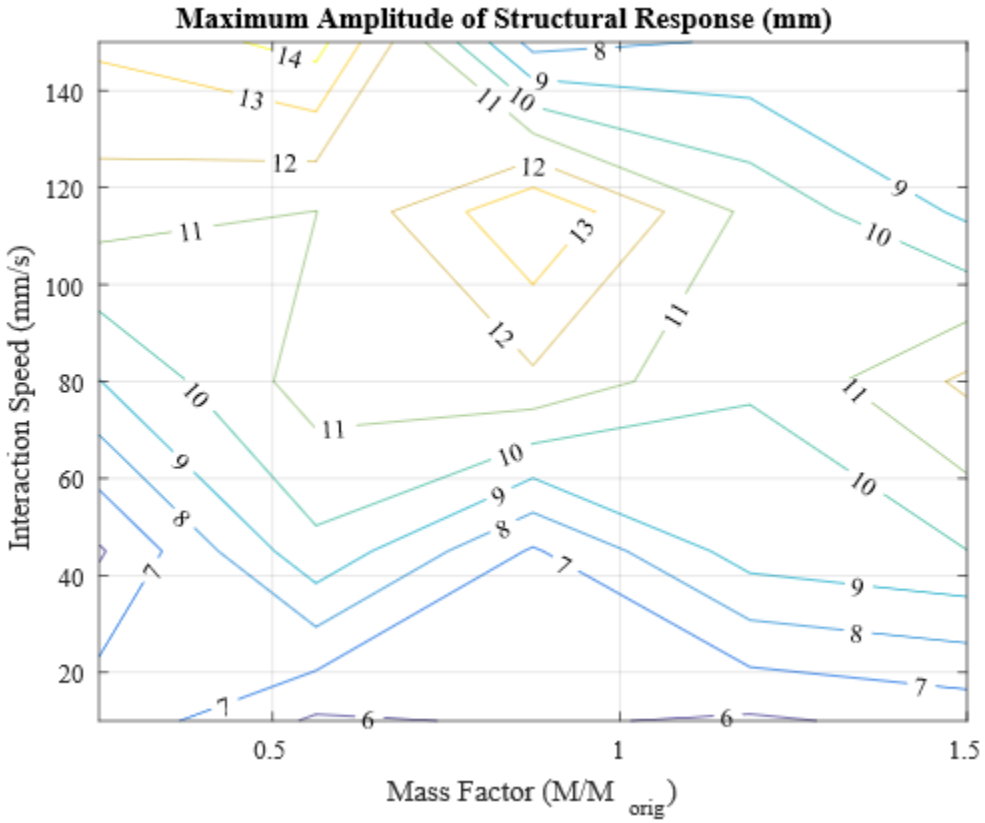

Figure 6.13 Maximum amplitude contour for a range of interaction speed and mass factor

6.4.2.2 Effect of structural damping

As mentioned in the ISO 19906 (2010), structural damping is a key parameter for IIV and the design guideline relies heavily on the choice of a damping co-efficient for mitigating IIV. To identify the interplay between interaction speed and damping co-efficient the maximum amplitude contour of structural response is shown in Figure 6.14. Based on impact test, the damping of the original test structure was found to be 4% of the critical damping. For the frequency lock-in speed range (100-125*mm/s*), the contour plot shows the maximum amplitude to be $\approx 15mm$ in that range. For lower damping co-efficient, the amplitude increases up to $\approx 18mm$; however, above a certain damping ratio, these high amplitudes are not observed, even for higher speeds.

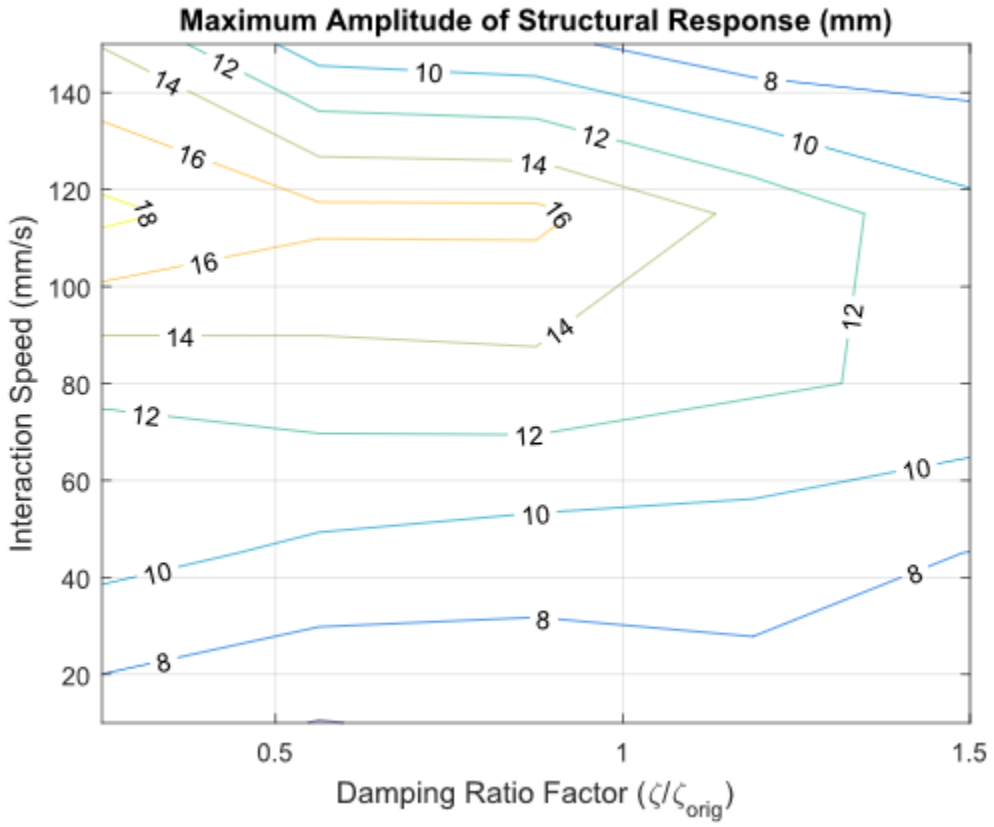

Figure 6.14 Maximum amplitude contour for a range of interaction speed and damping ratio

6.4.2.3 Effect of structural stiffness

The stiffness of the original structure used for model validation was $8.84\times10^{6} N/m$ which was the theoretical stiffness of the beam used in the indentation tests. The effect of structural stiffness on the maximum amplitude of structural response is explored for a range of interaction speeds and the contour plot is shown in Figure 6.15. The higher values are to be concentrated around the speed range of 20-60*mm/s* with lower stiffness factor. Although it is expected that the structural response will be higher for more compliant structure, the results also highlights the important of the interaction speed for a particular structural configuration. For example, for a structure with stiffness factor of 0.25, speed above 50*mm/s*, the failure will be dominated by the randomness in ice strength and that would cause a reduction in structural response.

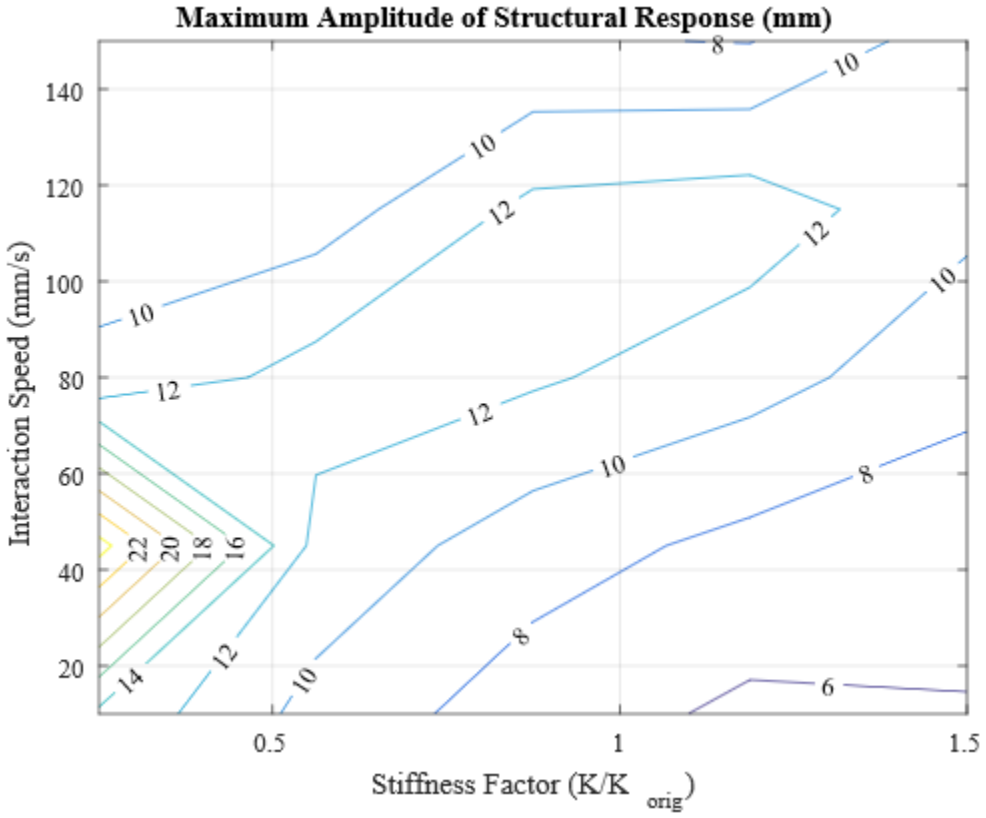

Figure 6.15 Maximum amplitude contour for a range of interaction speed and stiffness factor

6.4.3 Layer thickness equilibrium for IIV in pure crushing

Jordaan (2001) suggested that IIV can occur through repeated cycles of layer formation and extrusion, as shown in the shaded area in Figure 6.4. To model this behaviour and identify a critical layer thickness associated with IIV, it has been assumed that failure in the layer occurs through pure crushing. This is seen as a reasonable approximation, since the compressive state of stress in the layer is expected to supress spalling and probabilistic fracture in this region, and instead, a fracture may be assumed to develop in the adjacent ice surrounding the layer as discussed by Taylor and Jordaan (2015). It is also assumed that layer formation begins when the strain reaches point 1 in Figure 6.4, and extrusion begins when the strain reaches the critical strain for failure (point 2 in Figure 6.4). As discussed by Jordaan and Timco (1988), extrusion begins at an equilibrium layer thickness when the strain energy stored in the system is equal to pulverize and extrude the ice within the layer. Using a similar approach and employing the force model used in the present analysis, the change in force per unit width during an extrusion cycle can be written as:

$$F_{ext} = \frac{1}{D}(K_s \delta_L + (a(\Delta\varepsilon_{ext})^m e^{n\Delta\varepsilon_{ext}})\delta_{hpz}) \qquad (6.13)$$

where

δ_L= Change in failure length (e.g. depth of ice extruded in one cycle) during the extrusion phase

δ_{hpz} = Change in *hpz* displacement in the extrusion phase = $\Delta x_s - \Delta x_{ice}$

$\Delta\varepsilon_{ext}$ = Change in nominal strain during the extrusion phase

D= Diameter of the indenter

A limit cycle for vibration is only possible when the layer is completely extruded in the extrusion phase, and a new layer of the same thickness forms during the hardening phase. For such cases, $\delta_L = \delta_{hpz} = l$, and $\Delta\varepsilon_{ext} = \frac{l}{D}$ where l is the layer thickness.

Equation (6.13) can be re-written as:

$$F_{ext} = \frac{1}{D}\left[K_s l + \left\{\left(\frac{a l^{m+1}}{D^m}\right) e^{\frac{nl}{D}}\right\}\right] \tag{6.14}$$

For 'average' conditions, the equilibrium layer thickness can be calculated on the following basis. If the layer thickness is perturbed by the amount δl, the load changes by an amount:

$$\delta F_{ext} = \frac{\delta F_{ext}}{\delta l}\delta l = \frac{1}{D}\left[K_s + \left\{e^{\frac{nl}{D}}\frac{a l^m}{D^m}(m+1)\right\} + \left\{\left(\frac{a l^{m+1}}{D^m}\right) n e^{\frac{nl}{D}}\right\}\right]\delta l \tag{6.15}$$

The strain energy released is equal to:

$$\frac{F_{ext}\delta F_{ext}}{K_s} = \frac{1}{K_s}\left(\frac{1}{D}\left[K_s l + \left\{\left(\frac{a l^{m+1}}{D^m}\right) e^{\frac{nl}{D}}\right\}\right] \times \frac{1}{D}\left[K_s + \left\{e^{\frac{nl}{D}}\frac{a l^m}{D^m}(m+1)\right\} + \left\{\left(\frac{a l^{m+1}}{D^m}\right) n e^{\frac{nl}{D}}\right\}\right]\delta l\right) \tag{6.16}$$

The equilibrium layer thickness l_m can be obtained by assuming that the energy released by the elastic movement present in eqn. (6.16) is just sufficient to pulverize an additional thickness δl of ice. Any further increase in l_m would cause the load to drop to a level where the strain will not be sufficient to pulverize the ice any further. By considering energy of pulverization per unit volume as γ, the pulverization energy for the perturbation of the layer per unit width would be $\gamma D \delta l$.

Equating this value to eq. (6.16) and solving it numerically, the equilibrium layer thickness l_m can be obtained.

Jordaan and Timco (1988) used γ=0.05 MJ/m^3 for a 9mm thick unconfined ice sheet. For the present analysis, we consider γ=0.3 MJ/m^3. The higher value used here has been chosen to account for the effect of confinement, based on the observation that the failure pressure of a 50mm *hpz* during spherical indentation conditions was found to be 5-6 times higher than the uniaxial compressive strength of ice (Birajdar et al., 2016). For the 15 mm/s indentation speed, the constants a, m and n were calculated and the equilibrium layer thickness was found to be $\approx$ 2mm. A simulation using 2mm layer thickness is shown in Figure 6.16, where a continuous formation and extrusion of a crushed layer with equilibrium layer thickness results in a sinusoidal oscillation of the structure. It is worthwhile noting that, while this average equilibrium layer thickness has been assumed to be a constant for the purpose of the above calculation, in reality, random variations are expected in the layer thickness. Factors such as differences in localized contact geometry, the extent of damage and other material properties contribute to this variation in layer thickness. For any given cycle, if the extrusion depth is smaller than the layer thickness, the result would be a continuous extrusion of crushed ice, since a fixed amount of damaged ice would form in each cycle, but only a portion of it would be removed in the extrusion phase. However, if the extrusion depth is higher than the layer thickness, a structural rebound will occur at the end of extrusion cycle to release the remaining elastic energy stored in the structure.

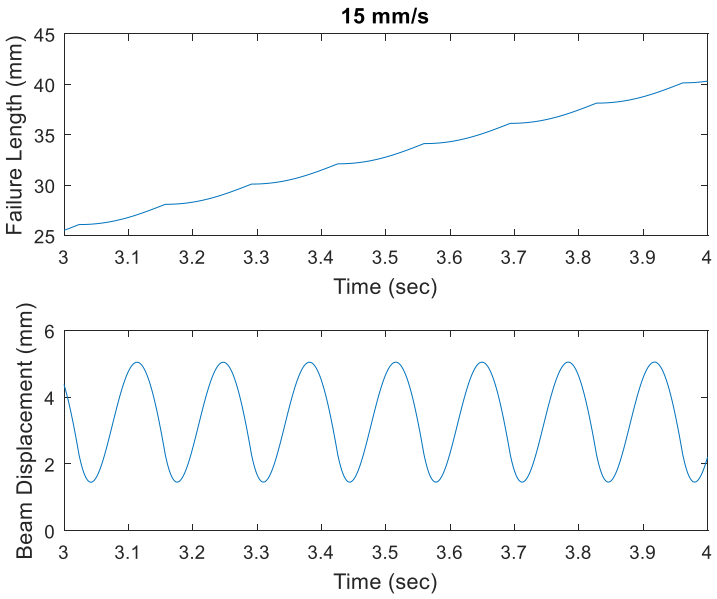

Figure 6.16 Failure length and structural response in pure crushing; Speed = 15 mm/s, Layer thickness = 2mm

6.5 Conclusions

Although ice-induced vibrations (IIV) are fundamental design consideration, full-scale observations suggest that such vibrations occur rarely in the lifetime of a structure. Nevertheless, the consequence of an IIV event can be extremely catastrophic and disruptive, and more understanding is required to address such behaviour, especially regarding the ice mechanics. The design guidelines and previous modelling approaches propose simplified conservative approaches without the incorporation of fundamental components of ice mechanics such as the dynamics of high-pressure zones (*hpz*s). Since the majority of the load during an ice-structure interaction is transmitted through these zones, and their mechanics show similar characteristics over different scales, it is imperative to analyze their roles in the context of dynamic ice-structure interaction leading to ice-induced vibrations. In this paper, a simplified dynamic ice-structure interaction model based on high-pressures zones (*hpz*s) has been presented to evaluate the conditions for IIV.

The stiffness of a single *hpz* is modelled as a function of nominal strain and strain-rate based on the results from triaxial tests. Results from medium-scale crushing tests have been used to model the *hpz* failure strength as a function of *hpz* size and structural feedback as a function of the degree of structural compliance. Preliminary comparison with the experimental data suggests that for similar *hpz* size, interaction speed and indentation depth, the model can reproduce the coupled force-time signature observed in the experiments.

Two distinct failure processes are assessed in the context of periodic sinusoidal response of the structure. First, such responses can result from the vibration within the layer of damaged ice, when the formation of the damaged layer and the extrusion process becomes cyclical during pure crushing. The failure process results in a continuous extrusion, depending on the damage layer thickness, and the failure length can be calculated by integrating the extrusion velocity in the direction of indentation. Since this is a continuous process, the structure also rebounds in a progressive manner. A limit-cycle for continuous vibration can only exist for an equilibrium layer thickness when the structural rebound distance is equal to that layer thickness (energy supplied by the ram is equal to the energy of pulverization and extrusion of crushed ice). Theoretical calculations from previous study were adopted to estimate the equilibrium layer thickness that can result in such vibrations, and the model showed reasonably good agreement with the calculations. The other failure process considered is when the interaction is dominated by spalls with occasional crushing events. Spalling failure causes an instantaneous rebound of the structure, due to the loss of contact area, and the results suggest the force drop to be directly linked to the structural stiffness. Such failure process can result in frequency lock-in of the structure; however, such responses were observed to be highly sensitive to interaction speed and structural parameters. This has been

identified as the primary reason for the infrequent observation of frequency lock-in in full-scale interaction.

The modelling framework presented here is a simplified first-order approximation of dynamic ice-structure interaction; however, the incorporation of fundamental elements of ice mechanics presents a promising step toward a complete framework. The preliminary results highlight the capability of the model to successfully simulate the vibrations within the damaged layer and frequency lock-in under specific conditions, which is similar to the observations in full-scale interaction. However, further refinement of the model is needed based on additional experimental investigation of *hpz* dynamics under controlled condition. The pulverization energy estimated here needs to be investigated for different interaction parameters and linked to the extrusion distance. Experimental investigation to identify the critical strain for *hpz* failure in pure crushing needs to be performed, since the results used in the model involve multiple failure modes. Finally, to simulate the interaction with full-scale structures, the dynamics of multiple *hpz*s and the effect of non-simultaneous failure behaviour need to be incorporated.

References

Barrette, P., Pond, J., Jordaan, I., 2002. Ice damage and layer formation in small-scale indentation experiments, in: Proceedings of the 16th IAHR International Symposium on Ice. International Association for Hydraulic Research, Dunedin, New Zealand, vol. 3 pp. 246–253.

Birajdar, P., Taylor, R., Habib, K., Hossain, R., 2016. Analysis of Medium-Scale Laboratory Tests on Ice Crushing Dynamics, in: Arctic Technology Conference. Offshore Technology Conference, St. John’s, NL, Canada. https://doi.org/10.4043/27482-MS

Bjerkås, M., Alsos, H.S., Meese, A., 2013. Ice induced vibrations-observations of a full scale lock-in event, in: The Twenty-Third International Offshore and Polar Engineering Conference. International Society of Offshore and Polar Engineers, Alaska, USA, pp. 1272–1279.

Browne, T., Taylor, R., Jordaan, I., Gürtner, A., 2013. Small-scale ice indentation tests with variable structural compliance. Cold Reg. Sci. Technol. 88, 2–9. https://doi.org/10.1016/j.coldregions.2012.12.006

Hendrikse, H., Metrikine, A., 2015. Interpretation and prediction of ice induced vibrations based on contact area variation. Int. J. Solids Struct. 75–76, 336–348. https://doi.org/10.1016/j.ijsolstr.2015.08.023

Hossain, R., Taylor, R., 2019. Characterization of high pressure zone (*hpz*) failure and linkages with structural response during medium-scale indentation tests, in: Proceedings of the 25th International Conference on Port and Ocean Engineering under Arctic Conditions (POAC'19).

Huang, G., Liu, P., 2009. A dynamic model for ice-induced vibration of structures. J. Offshore Mech. Arct. Eng. 131, 1–6. https://doi.org/10.1115/1.2979795

ISO 19906, 2010. Petroleum and natural gas industries — Arctic offshore structures. Int. Organ. Stand.

Jordaan, I., Timco, G., 1988. Dynamics of the ice-crushing process. J. Glaciol. 34, 318–326.

Jordaan, I.J., 2001. Mechanics of ice-structure interaction. Fract. Ice 68, 1923–1960. https://doi.org/10.1016/S0013-7944(01)00032-7

Kärnä, T., Andersen, H., Gürtner, A., Metrikine, A., Sodhi, D., Loo, M., Kuiper, G., Gibson, R., Fenz, D., Muggeridge, K., Wallenburg, C., Wu, J.-F., Jefferies, M., 2013. Ice- induced vibrations of offshore structures - Looking beyond ISO 19906, in: Proceedings of the 22nd International Conference on Port and Ocean Engineering under Arctic Conditions, (POAC'13). Espoo, Finland.

Kärnä, T., Kamesaki, K., Tsukuda, H., 1999. A numerical model for dynamic ice– structure interaction. Comput. Struct. 72, 645–658. https://doi.org/10.1016/S0045-7949(98)00337-X

Kärnä, T., Muhonen, A., 1990. Preliminary results from ice indentation tests using flexible and rigid indentors, in: Proceeding of the 10th IAHR Symposium on Ice. International Association for Hydraulic Research, Espoo, Finland, vol. 3 pp. 261–275.

Kärnä, T., Turunen, R., 1989. Dynamic response of narrow structures to ice crushing. Cold Reg. Sci. Technol. http://dx.doi.org/10.1016/S0165-232X(89)80007-2

Kawano, D.T., Morzfeld, M., Ma, F., 2013. The decoupling of second-order linear systems with a singular mass matrix. J. Sound Vib. https://doi.org/https://doi.org/10.1016/j.jsv.2013.08.005

Kry, P.R., 1978. A Statistical Prediction of Effective Ice Crushing Stresses on Wide Structure, in: Proceedings of the 5th IAHR International Symposium on Ice. International Association for Hydraulic Research, Lulea, Sweden, vol. 1 pp. 33–47.

Määttänen, M., 1978. On conditions for the rise of self-excited ice-induced autonomous oscillations in slender marine pile structures. Winter Navigation Research Board.

Mackey, T., Wells, J., Jordaan, I., Derradji-Aouat, A., 2007. Experiments on the fracture of polycrystalline ice, in: Proceedings of the 19th International Conference on Port and Ocean Engineering under Arctic Conditions (POAC'07). Dalian, China, vol. 1 pp. 339–349.

Matlock, H., Dawkins, W.P., Panak, J.J., 1969. A model for the prediction of ice-structure interaction, in: Proceedings of the Annual Offshore Technology Conference. Dallas, Texas, vol. 1969-May pp. 687–693.

Meglis, I.L., Melanson, P.M., Jordaan, I.J., 1999. Microstructural change in ice: II. Creep behavior under triaxial stress conditions. J. Glaciol. 45, 438–448. https://doi.org/10.3189/S0022143000001295

Melanson, P.M., Meglis, I.L., Jordaan, I.J., Stone, B.M., 1999. Microstructural change in ice: I. Constant-deformation-rate tests under triaxial stress conditions. J. Glaciol. 45, 417–437. https://doi.org/10.3189/S0022143000001271

O'Rourke, B.J., Jordaan, I.J., Taylor, R.S., Gürtner, A., 2016. Experimental investigation of oscillation of loads in ice high-pressure zones, part 1: Single indentor system. Cold Reg. Sci. Technol. 124, 25–39. https://doi.org/10.1016/j.coldregions.2015.12.005

Rist, M.A., Murrell, S.A.F., 1994. Ice triaxial deformation and fracture. J. Glaciol. https://doi.org/10.1017/S0022143000007395

Sodhi, D., 1994. A Theoretical Model for Ice-structure Interaction, in: Proceedings of the ASME 1994 13th International Conference on Ocean, Offshore and Arctic Engineering (OMAE1994). American Society of Mechanical Engineers (ASME), New York, vol. IV pp. 29–34.

Sodhi, D., 1988. Ice-induced vibration of structures, in: Proceeding of the 9th IAHR International Symposium on Ice. International Association for Hydraulic Research, Sapporo, Japan, vol. 2 pp. 625–657.

Sodhi, D., 2001. Crushing failure during ice-structure interaction. Fract. Ice 68, 1889–1921. https://doi.org/10.1016/S0013-7944(01)00038-8

Taylor, R., Frederking, R., Jordaan, I., 2008. The nature of high pressure zones in compressive ice failure, in: Proceeding the 19th IAHR International Symposium on Ice. International Association for Hydraulic Research, Vancouver, BC, Canada., vol. 2 pp. 1001–1010.

Taylor, R., Jordaan, I., 2015. Probabilistic fracture mechanics analysis of spalling during edge indentation in ice. Eng. Fract. Mech. 134, 242–266. https://doi.org/10.1016/j.engfracmech.2014.10.021

Timco, G., Wright, B., 2005. Multi-Year Ice Loads on the Molikpaq: May 12, 1986 Event;, in: Proceedings 18th International Conference on Port and Ocean Engineering under Arctic Conditions (POAC ’05). Postdam, NY, vol. 1 pp. 453–462.

Tuhkuri, J., 1995. Experimental observations of the brittle failure process of ice and ice-structure contact. Cold Reg. Sci. Technol. 23, 265–278. https://doi.org/10.1016/0165-232X(94)00018-S

Wells, J., Jordaan, I., Derradji-Aouat, A., Taylor, R., 2011. Small-scale laboratory experiments on the indentation failure of polycrystalline ice in compression: Main results and pressure distribution. Cold Reg. Sci. Technol. 65, 314–325. https://doi.org/10.1016/j.coldregions.2010.11.002

Wright, B., Timco, G., 1994. A Review of Ice Forces and Failure Modes on the Molikpaq, in: Proceedings of the 12th IAHR International Symposium on Ice. International Association for Hydraulic Research, Trondheim, Norway, vol. 2 pp. 816–825.

Xu, J., Bernt, J.L., 1981. Dynamic response of a jacket platform subjected to ice loads, in: Proceedings of the 6th International Conference on Port and Ocean Engineering under Arctic Conditions (POAC'81). Quebec, Canada, vol. 1 pp. 502–516.

Chapter: 7 Conclusions

7.1 Summary

The primary focus of the thesis was to develop a modelling framework of dynamic ice-structure interaction incorporating the mechanics of high-pressure zones (*hpz*s), which are fundamental components of the compressive ice failure process. Emphasis was placed on understanding the effect of scale on *hpz* mechanics through a medium-scale ice crushing dynamics test program. The main contributions of the thesis can be summarized as follows:

- A thorough review of ice-induced vibrations (IIV) events at full-scale, theoretical ice-structure interaction models, mechanics of compressive ice failure and roles of high-pressure zones (*hpz*s), and the dynamics of *hpz*s observed in the indentation test programs were presented (Chapter 2).
- The effect of ice temperature and scale of interaction on the compressive strength vs. stress-rate curve used for the self-excited IIV modelling approach were identified. A qualitative uncertainty analysis considering these effects showed that an increase in ice temperature would require higher ice drift velocity to induce steady-state IIV. For pressure-thickness and pressure-width scale effects, an increase in ice thickness and structure width also showed a higher threshold speed to trigger steady-state IIV and lower dynamic response compared to the predicted response using Peyton's original curve (Chapter 3)
- A medium-scale ice crushing dynamics test program was carried out to study the effects of interaction speed, ice temperature, area of *hpz* and structural compliance on the

dynamics of *hpz* failure. Results suggested that larger amplitudes and longer duration instances of dynamics, associated with failure behavior, are usually more pronounced for colder ice, smaller interaction area, higher interaction speed, and lower structural compliances. (Chapter 4).

- The failure behaviour of *hpz*s were characterized considering the effects of ice temperature, interaction area and the structural compliance. The failure pressure was found to be highly influenced by *hpz* area and the structure compliance was found to be a major contributing factor for the post-failure processes. For structural design, this suggests that when the layer of microstrucrally modified ice is thicker, structure with higher compliance is more susceptible to experience vibration within the damaged layer (Chapter 5).
- A simplified ice-structure interaction model based on the mechanics of *hpz*s observed in the small-scale triaxial tests and medium-scale indentation tests were developed. The model was able to simulate structural response during a frequency lock-in and identified the effects of interaction speed and structural parameters on such response. For a particular structure, frequency lock-in was found to exist for a certain speed range; however, this speed range was found to vary with the natural frequency of the structure. The structural compliance and damping, both were found to influence the maximum amplitude of the structural response (Chapter 6).

7.2 Discussion and Recommendation

The problem of modelling dynamic ice-structure interaction is a complex one, and the primary challenges come from the intricacy of the different processes during compressive ice failure, such as spalling, crushing, extrusion and microstructural modifications. An ice-structure interaction

model incorporating all of these processes is needed, but this is both complex and computationally expensive due to a number of challenges such as: (1) need to develop material modelling approach for ice that can handle both local fracture processes, as well as continuum behaviour (especially processes in highly confined, central region of *hpz*s which limit pressures during interactions); (2) limitations in computational resources given the sub-mm scale of physical processes that need to be modelled and large volumes of ice to simulate for a real interaction scenario (many kms of ice floes per year over the design life), (3) challenges in integrating these different theoretical and probabilistic frameworks. Simplified assumptions are necessary, but also need to account for these processes and identify their roles during ice-structure interaction. High-pressure zones (*hpz*s) are fundamental features of ice-structure interactions dominated by compressive ice failure and the processes associated with *hpz* behaviour are observed to be consistent over a broad range of scales. The interplay of different processes associated with compressive ice failure is observed to play an important role during dynamic ice structure interactions and given the importance of *hpz*s in transmitting the majority of the loads between ice and a structure during an interaction, continued work is needed in modelling *hpz* behaviour. In this work, incorporating additional details of dynamic aspects of *hpz* failure in an ice-structure interaction modelling framework was found to provide new insights into the dynamic interaction process, including the conditions for ice-induced vibrations. Continued work to enhance understanding and modelling of these *hpz* processes is recommended.

The uncertainty analysis presented in Chapter 3 highlighted the sensitivity of response predictions from existing methods to changes in ice properties expected when temperature, rate and scale are taken into account, which have not been accounted for in past methods. Moreover, it showed that even when such effects were accounted for, existing methods do not sufficiently capture the

interaction process, particularly the nature of high pressure zones. This highlighted the importance of developing a new modelling framework and conducting a careful analysis of the influence of interaction parameters at the scale of *hpz* failure process. The medium-scale ice crushing dynamics tests presented in Chapters 4 and 5 clearly demonstrate how ice temperature, *hpz* area, interaction speed and structural compliance influence *hpz* dynamics and associated IIV in the coupled ice-structure system. The characterization of the failure process in terms of crushing and spalling processes focused on visual observations, as well as force, displacement and acceleration responses in the system. These results were compared and found to provide very strong agreement with earlier small scale lab experiments, in which detailed assessments of ice failure and localized fracture and microstructural changes in the ice have been studied in detail. The dependence of dynamic behaviour on ice temperature was shown to be relatively weak for cold ice in the temperature range of $-3^{o}C$ to $-20^{o}C$, however for warm ice (between $0^{o}C$ and $-3^{o}C$) it was observed that ice failure modes transitioned towards damage enhanced creep behaviour, which did significantly alter the nature of interaction dynamics; significant IIV was only observed for colder ice that was dominated by a combination of crushing and spalling; additional testing under more controlled temperature conditions are recommended to provide greater insight into these effects.

The medium-scale ice crushing dynamics tests conducted as part of this research program provides valuable new insights into details of the different failure mechanisms and the influence of test conditions on interaction dynamics for coupled ice-structure systems involving a single *hpz*. To extend this work to full-scale interactions, additional work is needed to account for multiple *hpz*s that occur simultaneously across the interaction area to better understand how individual *hpz*s interact, and the role structural compliance plays in load sharing across these *hpz*s. Extension of

the experimental program to investigate such influences with a modified medium-scale test apparatus is seen as a promising next step to extend this work.

The novel modelling framework presented in Chapter 6 explicitly accounts for the effects of random fracture and continuum pressure-softening associated with microstructural damage processes in *hpz*s using models derived from experiments designed to study these processes in detail. This new approach provides promising results and presents a new direction for dynamic ice-structure interaction modelling. This approach is linked to the underpinning physics responsible for ice compressive failure for a wide range of scales, while also accounting for the interplay between randomness in fracture processes and the potential for cyclic ice crushing due to softening-extrusion-hardening behaviour that can result in oscillations in the layer of damaged ice at the ice-structure interface. Specific areas for continued work include better understanding and modelling of the influence of different interaction parameters on the stiffness-strain curve of individual *hpz*s and additional experimental testing is recommended to help validate and assess uncertainties associated with model coefficients. Refinement of the models of damping behaviour of individual *hpz*s and the far-field ice behaviour is another aspect of the model that could benefit from additional research. Finally, and perhaps most importantly for application in practice, is the need to extend the model to include multiple *hpz*s and to assess the effects of structural compliance on load sharing mechanisms among multiple *hpz*s. Through continued experimental investigation and model refinement, the work presented in this thesis offers promising new directions for modelling full-scale dynamic ice structure interactions that are linked to underpinning physics of ice failure and which can serve as new tools to better inform design practice to help understand and avoid ice-induced structural vibrations.